Whole building control system design and evaluation: Simulation-based assessment

Technical Report · February 2012

CITATIONS
5

READS
1,248

9 authors, including:

Donghun Kim
Purdue University
32 PUBLICATIONS **173** CITATIONS
SEE PROFILE

Pengfei Li
United Technologies Research Center
18 PUBLICATIONS **169** CITATIONS
SEE PROFILE

Satish Narayanan
United Technologies Corporation
75 PUBLICATIONS **1,127** CITATIONS
SEE PROFILE

Eugene M. Cliff
Virginia Polytechnic Institute and State University
225 PUBLICATIONS **1,724** CITATIONS
SEE PROFILE

Whole Building Control System Design and Evaluation: Simulation-Based Assessment

Authors (in alphabetical order):

James E. Braun, Donghun Kim

Purdue University

Miroslav Baric, Pengfei Li, Satish Narayanan, Shui Yuan

United Technologies Research Center

Eugene Cliff, John A. Burns

Virginia Tech

Bill Henshaw

Lawrence Livermore National Lab

Cross-Task Team on Optimal Building Controls Design and Platform

Year 1 Final Report in Support of GPIC Energy Efficient Buildings Hub

Table of Contents

Executive Summary

Building Energy Management Systems (BMS) serve about one-third of the approximately 67 billion ft^2 of commercial floor space in the United States. However, surveys of building operators suggest that only a fraction of possible BMS functionality is utilized in these buildings leading to significant lost opportunities for reducing operating costs through better supervisory controls. Most often, plant and building set-points follow prescribed schedules and are not optimized in response to changing dynamic conditions, including weather, internal loads, occupancy patterns, etc. A number of previous studies have shown potential savings for optimized controls in the range of 10 to 40% of costs to provide cooling. Savings are achieved through system efficiency improvements and changes in the time variation of energy usage in response to dynamic utility rates.

One of the primary obstacles to widespread implementation of optimized controls is the implementation cost. Each building is unique with specific operational, environmental, occupant, and utility factors that require unique engineered solutions. An integrated approach to building controls should consider interactions between sub-systems and components to guarantee performance over the full range of conditions likely to be encountered. The objective should be to guarantee comfort at minimum operational cost. Adaptive and predictive control strategies would follow from these considerations and be based on real-time modeling and utilization of robust sensor and actuator networks. However, in order to achieve cost-effective implementations, the associated control design and implementation must be automated for deployment in a scalable manner.

A cross-task team (from Task 2 and Task 3) of researchers in the GPIC Hub was formed to develop a set of tools and approaches for generating building-specific control algorithms that minimize operational costs while maintaining comfort. The general approach involves the use of model-based predictive control (MPC) with reduced-order models for the building envelope, indoor environment, and plant. The models could be generated from either detailed physical models (e.g., TRNSYS for the building and plant, CFD for the indoor environment) or using measurements from short-term (e.g., two-week) monitoring at the site. The models are utilized in combination with an integral cost function that considers the cost of energy and impacts on comfort. The ultimate goal is to be able to generate the models and cost function with minimal human labor in order to realize a scalable and cost-effective approach.

Progress in the first year has included 1) a literature review of existing tools and models that could be used as part of the envisioned control system design platform, 2) initial formulation of the MPC problem, 3) initial tools to generate reduced-order models for building envelopes from detailed physics-based models along with case study results, 4) initial tools to generate models for indoor environments using CFD along with case study results, and 5) initial case studies to illustrate issues and opportunities for MPC applied to buildings.

Figure 1 depicts an example overall control architecture for implementation of optimal supervisory control. Building control systems are generally organized in a hierarchical manner with supervisory and local-loop layers. The supervisory layer manages the control modes and set-points for device controllers (e.g., AHU, VAV boxes) whereas the local-loop control layer manipulates actuators to maintain specified set-points using single-input single-output (SISO) local (PI) controllers. MPC acts on the supervisory control layer to specify control modes and set-points that minimize an objective function that combines energy costs and comfort impacts and responds to sensor information and forecasts for weather, occupancy, comfort and, and plant performance. In order to take advantage of dynamic (i.e., energy storage) effects, the MPC problem involves minimization of an integral cost function with constraints on comfort and equipment performance and state equations that describe the evolution of energy storage over time. From a supervisory control perspective, the important dynamics occur within the building materials and any specific energy storage device, such as ice or chilled water. The dynamics within the building envelope are highly distributed and cannot be considered using lumped analysis. Furthermore, the thermal comfort within the zones is highly coupled to the envelope states and to the location and design of the comfort delivery devices (e.g., zone air diffusers and returns). Thus, the development of MPC algorithms requires the use of relatively sophisticated models that consider envelope dynamics, spatial comfort variations, equipment performance, etc. It is also of interest to consider interactions between supervisory and feedback control in the development of MPC algorithms. However, practical implementation requires models that can execute rapidly and be generated in a scalable manner with minimal human effort.

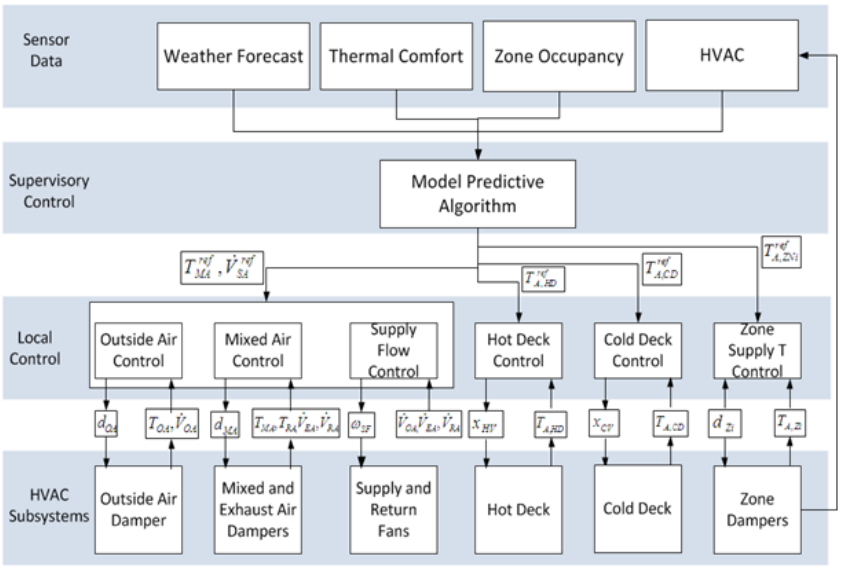

Figure 1. Control system architecture for implementation of MPC

Building energy simulation tools, such as EnergyPlus or TRNSYS, are appropriate for considering the effect of different supervisory control variables on energy use and cost. However, they do not integrate necessary tools for investigating MPC and/or determining

detailed spatial variations of comfort within individual building zones. Also, they are not generally appropriate for analysis of local-loop feedback control because they do not include dynamics of equipment. On the other hand, Modelica and MatLab are general and open platforms that incorporate many tools for investigating dynamic systems and MPC. Both have been widely used within the controls community for design and analysis of feedback control systems. Furthermore, LBNL has developed a library of building and equipment components for Modelica. Ultimately, this could be an appropriate platform for building control system design and analysis. However, the building library is at an early stage of development. For instance, the equipment incorporated within the library for buildings doesn't include appropriate transient effects that would be needed to consider local-loop feedback control. Furthermore, the building envelope models are more detailed than needed for development of optimal control algorithms and yet the model for the indoor air is very simple and doesn't allow consideration of spatial comfort variations.

For the purpose of control system tool development and investigation of MPC, MatLab has been chosen as the platform for this project. Figure 2 depicts the proposed process for development of MPC for building systems that is currently under investigation. The current approach involves the use of detailed physical models for the building envelope that capture both transient and spatial variations for each zone. These models are used to develop reduced-order models that are more amenable to implementation within an MPC. The plant that provides cooling and heating for the individual building zones is currently treated with quasi-static models. The use of quasi-static plant models allows the use of off-line methods for determining optimal plant modes and set-points. Optimal modes and setpoints can then be mapped along with the associated minimum power consumption in terms of the primary plant boundary conditions, such as total cooling requirement and ambient drybulb and wetbulb temperatures. The reduced-order building envelope and indoor air models are coupled with the plant within an MPC implementation to provide a tractable methodology for determining optimal supervisory control in response to driving functions as depicted in Figure 1.

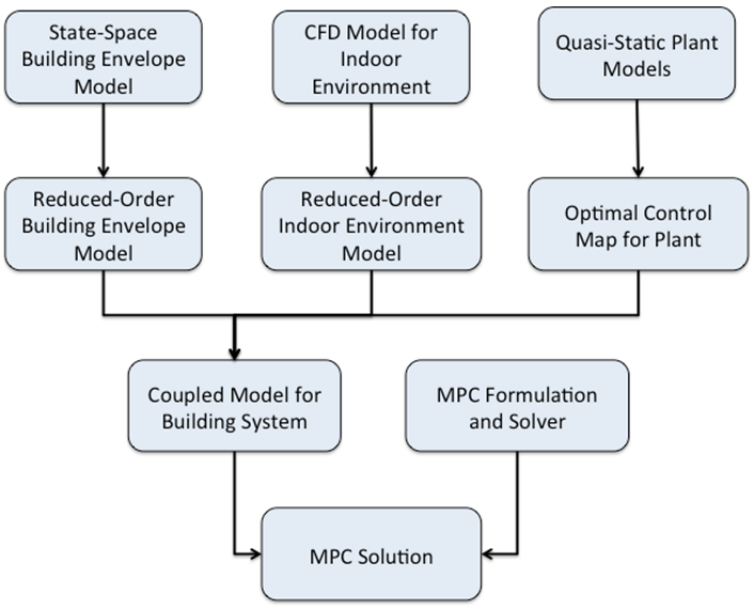

Figure 2. Proposed flow chart for control system development

The approach being developed for generating reduced-order models for the building envelope and internal partitions involves the use of a detailed state-space model that considers one-dimensional transient condition within wall materials, solar radiation through windows, linearized radiation exchange between internal surfaces, and the ability to separate individual walls into sub-sections and to specify multiple coupled zones. The linearized state-space representation of the building system has the following form.

$$\dot{\vec{T}} = \tilde{A}\vec{T} + \tilde{B}\vec{u}$$
$$\vec{y} = \tilde{C}\vec{T}$$

where the vector T includes temperatures of all discretized wall nodes and local zone temperatures in contact with interior wall surfaces, the vector u includes inputs that act directly on the zone temperatures (e.g., convective internal gains), and the vector y contains the outputs of interest (e.g., zone sensible cooling requirements).

A detailed multi-zone model based on this state-space representation has been implemented within MatLab to enable construction of reduced-order building models. The main assumption involved in constructing reduced-order building models is constant heat transfer coefficients. Various algorithms for building lower order models have been investigated but the "square-root method for Balanced Truncation Model Reduction" is currently being applied to the state-space representations. Different case studies have been considered that include multi-layer, multi-zone buildings with windows and reduced-order model results have been compared with results from TRNSYS. Figure 3 shows sample comparisons for a single-zone case study where zone temperature is predicted in response to time-varying driving conditions. The detailed and

reduced-order state-space models provide nearly identical predictions and agree very well with results from TRNSYS. The number of states was reduced from 103 for original state-space model to 8 for the reduced-order representation.

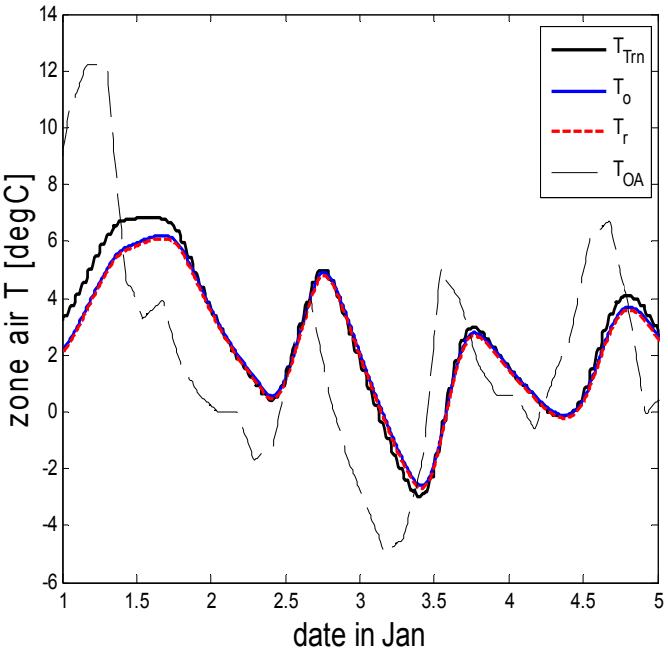

Figure 3. Example comparison of predicted floating zone temperatures for TRNSYS (T_{Trn}), original state-space (T_o), and reduced-order (T_r) models (T_{OA} is outdoor temperature)

As previously noted, the building-energy model is decomposed into building-envelope and indoor-air sub-systems. The indoor-air model is based on Computational Fluid Dynamics (CFD) and model-order reduction. A data-driven approach is used for the model-order reduction wherein time-accurate simulations of step-like changes to wall-surface temperatures are used to produce heat-load time-histories. The heat-load data are used to construct the Markov parameters of the wall-temperature to heat-load system. The resulting high-order transfer function is optimally approximated by a low-order system of specified order.

The initial application for reduced-order indoor environment modeling is the Purdue Living Laboratory Radiant Room. A sketch of the facility, which is expected to be available in the Spring 2013, is shown in Figure 4. The horizontal lines on the walls, as well as the lines on the floor serve to partition the surfaces for purposes of specifying boundary temperatures with the various surface segments assigned numeric labels {1,2,...,19}. The south wall has a large window area that leads to relatively large surface temperature variations within the space when the sun is shining. In addition, this space will have radiant chilled beam panels on the ceiling and a radiant floor. These features enable the study of factors that could cause significant spatial

variations in comfort conditions for occupants and make this an interesting case study for considering MPC with both energy and comfort performance criteria.

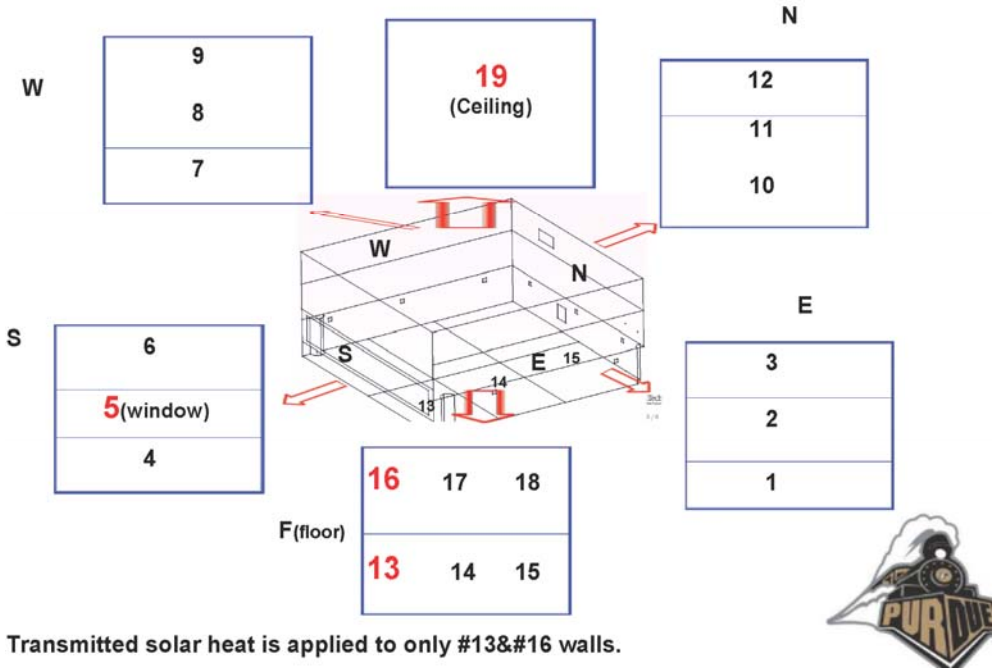

Figure 4. Purdue Living Laboratory (LL) with wall zones

A reduced-model for the coupled velocity-temperature-moisture dynamics was determined directly from simulations (measurements). The simulation data for this problem were produced by a FLUENT simulation and coupled velocity-temperature-humidity dynamics were simulated on a grid with n≈200,000 nodes. The inputs to the FLUENT simulation included:

1. the flow-rate on the inlets (all the same),
2. the temperature of the inlet air,
3. the water-vapor mass fraction of the inlet air, and
4. energy and water-vapor source disturbances in an occupied region around the table.

The monitored outputs were

1. the water-vapor mass fraction in the occupied region,
2. the temperature at a sensor location on the wall, and
3. the temperature in the occupied region.

Each input was subjected to a step-like change from an initial steady value and then the outputs were sampled to produce a reduced-order model. The final reduced-order model is of order r = 50. The reduced-order model was then executed using the same step-like change input used for the FLUENT simulation and reduced-order outputs were compared with the original data. The

results for some representative input/output combinations are shown in Figure 5. The reduced-model obtained directly from measurements does a very good job of matching the full-order simulation.

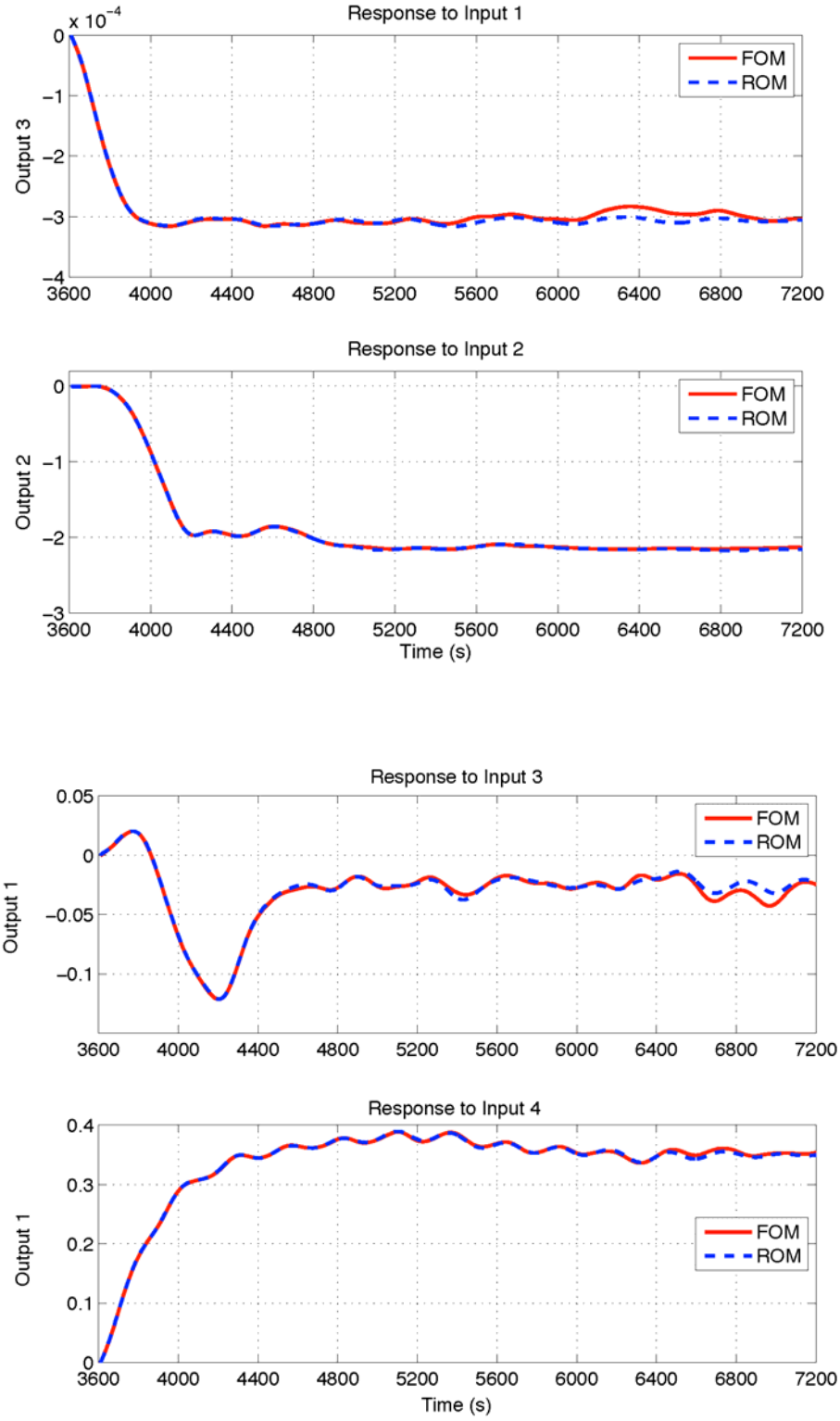

Figure 5. Example time domain responses for different set inputs

The reduced-order building envelope and indoor air models have not yet been coupled. However, in order to make progress in developing the overall tool chain, two representative MPC simulation case studies were carried out. One case study is based on the Purdue Living Laboratory (depicted in Figure 4) with a fully-mixed indoor air temperature assumption and the second case study was performed for Building 14 at the Navy Ship Yard.

Figure 6 depicts the MPC problem for the living laboratory case study. The MPC controller provides set points to the local controller of the HVAC system based on the zone air temperature, mean radiant temperature and predictions of weather data and internal sources. In order to simplify the problem, the building and plant system were decoupled. A model for a chilled water system with cooling towers was coupled to an air handling unit model to represent the cooling plant. Dynamics of the plant were neglected and an optimal plant control map was developed in terms of cooling load and ambient conditions. The map for optimal cooling plant performance was incorporated within a cost function that considers energy costs and occupant comfort. The MPC problem involved determining the trajectory of zone ventilation cooling rates (Q_{vent}) over a 24-hour time horizon that minimizes the integral cost of energy while maintaining the comfort conditions (measured using percent people dissatisfied (PPD) within acceptable bounds. PPD was determined using a comfort model that uses zone air and mean radiant temperature as inputs. The reduced-order model of the LL zone (depicted in Figure 4) was used to determine the comfort conditions in terms of Q_{vent} and ambient boundary conditions.

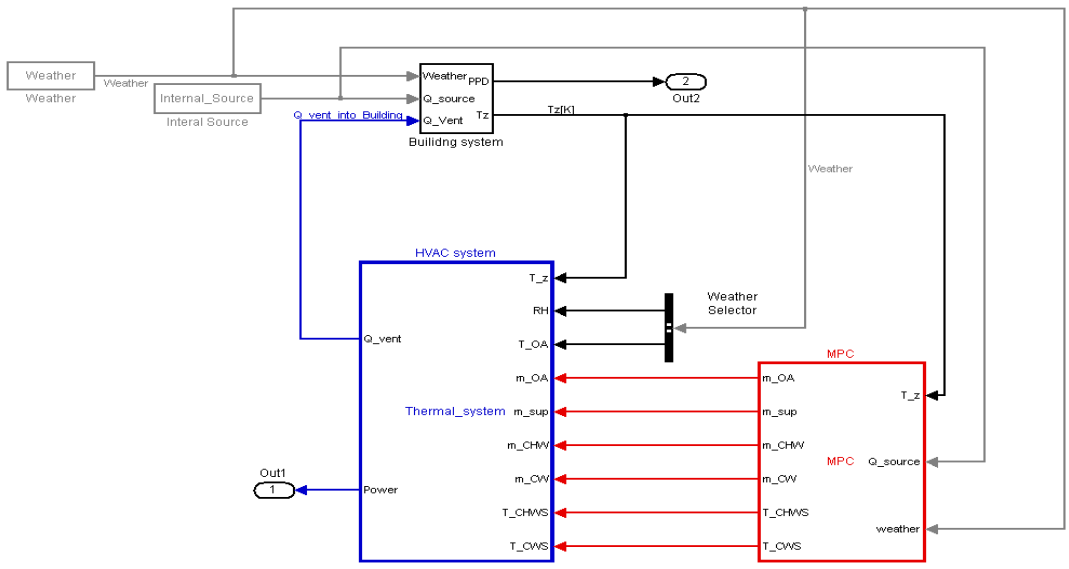

Figure 6. MPC formulation for living laboratory case study

At this point, solutions to this MPC problem have been achieved using successive quadratic programming and some sample results have been generated. Figure 7 shows sample results for cooling on a hot summer day for a case with 2-to-1 on-peak to off-peak electric rates (co-incident

with the occupancy period from 7 am to 6 pm). The MPC performs pre-cooling of the zone near the end of the un-occupied period and then the zone temperature rises quickly at the beginning of occupancy in order to maintain PPD at the upper end of its constraint of 10% throughout the occupied period. This is the energy optimal solution in the absence of any demand charges. The PPD constraint is relaxed to 30% during the unoccupied period and the MPC responds quickly to this change at the end of occupancy. Another interesting point is that the optimal zone air temperature peaks at the beginning of the occupied period and goes down during occupancy. This result would not occur if only zone air temperature were considered for thermal comfort. When PPD is used to evaluate comfort, then the optimal zone air temperature set-points can be set higher since the inside surface temperature is cool at the beginning of occupancy. The higher zone air temperature set-point implies the possibility of achieving energy savings using a PPD model for comfort in MPC as compared with constraining control solely based on zone air temperature. Evaluation of the cost savings potential for MPC in this application will be considered in the next year.

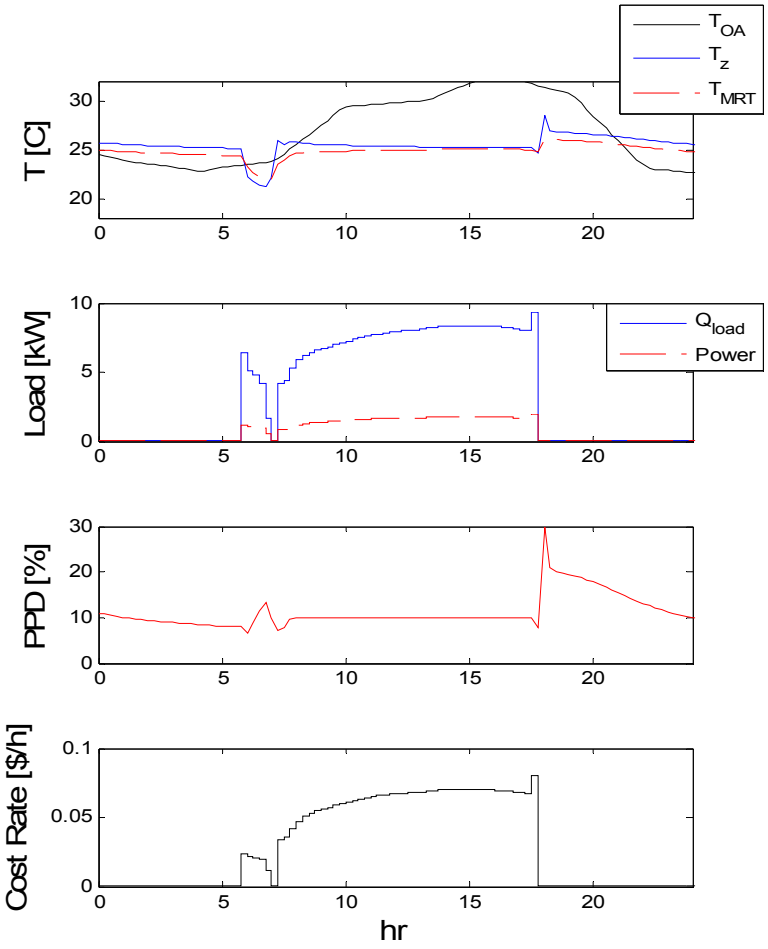

Figure 7. Sample MPC results for Purdue Living Laboratory (July 22, optimal values for zone temperature set-point, AHU cooling load, plant power, percent people dis-satisfied, and cost)

A more complicated and complete case study was carried out using a detailed energy model of Building 14 located in the Philadelphia Navy Yard. A TRNSYS model was developed that consists of two parts - building envelope and the HVAC system with control logic. The dynamics are considered for the envelope but neglected for the HVAC system. The building was modeled using four separate uncoupled zones. Supervisory control at the level of each AHU was considered as well as coordinated supervisory control of the chiller plant. On the AHU level the controller looks ahead for 3 hours to decide on optimal values of the temperature and inflow of the supply air in order to maintain the zone temperatures in a prescribed comfort interval. Simultaneously, the controller computes the optimal values for the chilled and cooling water temperature that maximize the coefficient of performance of the chiller plant while satisfying the current load. Air-side economizer operation was not considered in the current case study.

For the MPC, simple linear ARX models were identified for each zone to represent their input–output response for short-term predictions of building loads. Figure 8 shows sample 3-hour ahead predictions of zone temperature compared to TRNSYS results for a single zone with zone subjected to time varying inputs. Simple quadratic relations were used to map the chiller plant performance.

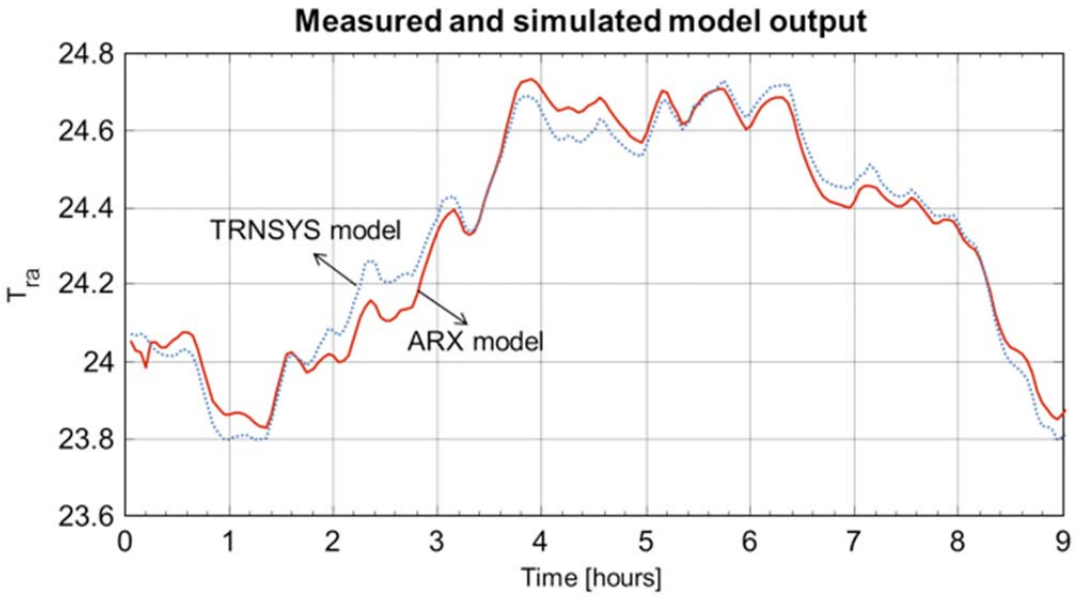

Figure 8. Simulated response of the ARX model of the building 14 NS wing and the actual return air temperature for the validation data set

Figure 9 depicts the architecture for the MPC case study with individual MPC algorithms for each thermal zone. At each time instance the local zone controller receives measurements of the return air temperature T_{ra} and outside ambient temperature T_{oa}, and computes optimal values for the supply air temperature reference (T_{sa}^{sp}) and the reference for the supply air mass flow rate

ϕ_{sa}^{sp}. In addition, optimal values for the chilled water temperature T_{chw}^{zone} and T_{chw}^{zone} are computed.

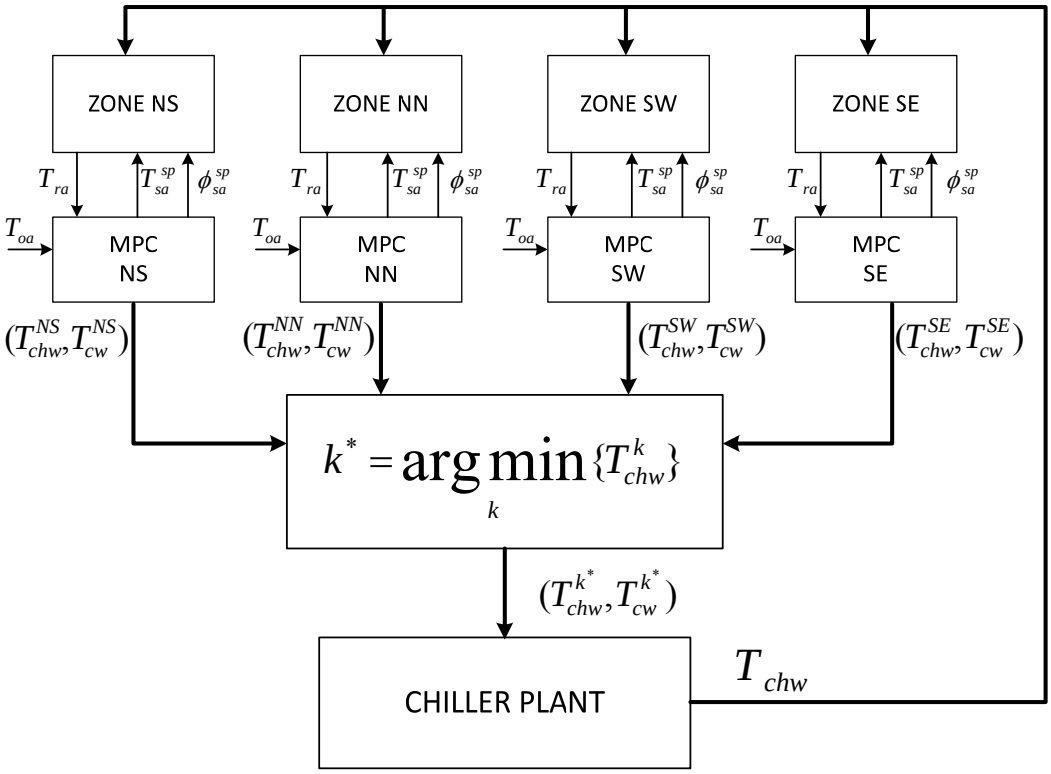

Figure 9. Multi–zone control architecture for building 14 case study

Figure 10 shows a comparison of energy consumption for the baseline control and the MPC control when control variables are optimized at both the AHU and chiller plant level. The savings are nearly 15% and are only a portion of the potential for MPC. This case study only employed a 3-hour ahead time horizon for set-point optimization. Greater savings would be expected for longer time horizons that could take more advantage of energy storage in the building thermal mass. In addition, free cooling associated with economizer operation was not considered and could lead to more significant savings. These issues will be investigated in the next year.

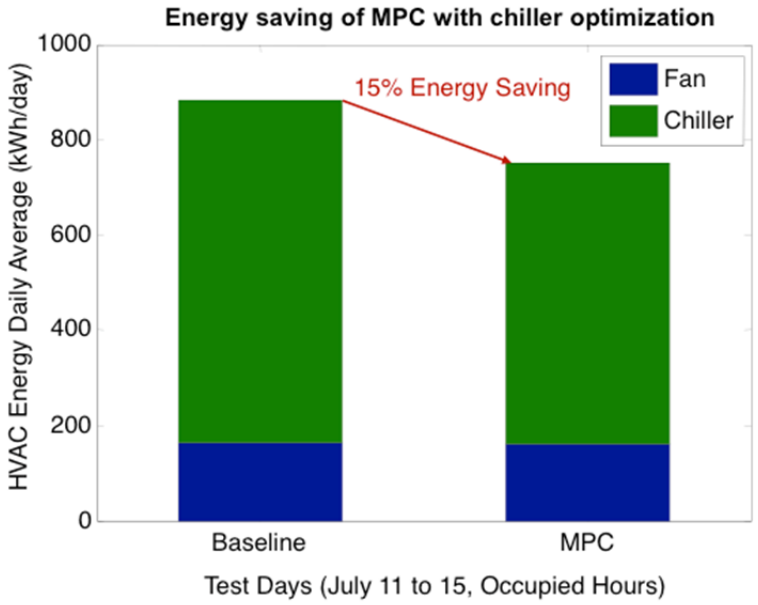

Figure 10. Potential energy savings for MPC with chiller plant optimization

This collaborative effort will continue in the next year and will involve further development and application of the tools developed in year 1. Approaches for generating reduced-order building and indoor air models need to be generalized and further validated. Coupling of the building and indoor air models will be carried out and integrated within MPC framework for the Purdue Living Laboratories, including rooms that have radiant and air comfort delivery. Inverse modeling approaches will be investigated for both the Living Laboratories and Building 101. Finally, the benefits and implementation requirements for MPC will be evaluated for both the Purdue Living Laboratories and Building 101.

1. Introduction

Robust operation of buildings is critical to achieving and maintaining energy efficiency and high performance building environments. Current design practices ignore dynamic and uncertain operational load characteristics, including seasonal variations in lighting requirements, temperature control, and occupancy patterns, focus on peak load demands rather than on strategies for dynamic load shifting, for example, results in over- or under-sizing system components with detrimental effects on cost and utilization efficiency. The failure to integrate controls that can adapt to changing usage within building automation systems prevents them from achieving optimal performance. Furthermore, each building is unique with specific operational, environmental and occupant factors that are not easily predicted. An integrated approach to building controls should consider interactions between sub-systems and components to guarantee performance over the full range of environmental conditions and occupant factors likely to be encountered. Adaptive and predictive control strategies would follow from these considerations and be based on real-time modeling and utilization of robust sensor and actuator networks. Energy efficiency gains of 10-20% in existing and new buildings are feasible when utilizing dynamic knowledge of the plant loads and environmental disturbances[1]. While the performance benefits of advanced control strategies are promising, the associated control design and implementation must be automated for deployment in a scalable and cost effective manner.

The following are specific barriers to implementation being tackled in the current project:

- In current practice extraction of control algorithms for software and hardware implementation is manual requiring tuning during commissioning and occupancy phases.
- Current software implementations require exhaustive field testing and tuning.
- Current control architectures are inherently Single-Input, Single Output feedback loops (typically PID type) that ignore variables associated with sub-system coupling, and do not utilize prediction. Fixed parameters are used that are not optimized and do not adapt to indoor and outdoor changes, resulting in low performance and instabilities.
- Models or representations are not available for use in real-time control implementation that accurately capture the sub-system couplings in the building needed for dynamic energy and comfort performance optimization
- Relevant variables are not all available from measurements. This includes external (weather-driven) and internal (occupancy-driven) loads, and thermal and airflow states.

To overcome the above the project will deliver:

- High level control algorithms to generate optimal set points for lower level controllers, accounting for outdoor and indoor disturbances with uncertain thermal loads.

[1] Ma, Y., Borrelli, F., Hencey, B., Coffey, B., Bengea, S., Packard, A., Wetter, M., Haves, P., "Model Predictive Control for the Operation of Building Cooling Systems", To appear in Proceedings of IEEE American Control Conference, 2010, Baltimore, Maryland.

- Adaptive control algorithms that can adapt and optimize performance with changing environmental and building usage conditions. Model-predictive controls to compensate loads in a predictive fashion while respecting state and actuation constraints
- Reduced-order models which capture the relevant physics and dynamics of the building sub-systems and the indoor environment and are suitable for advanced supervisory and terminal control design. The models will be easily replicable and scalable to multiple building configurations and locations, reducing the effort required for control design and optimization.
- Model-based estimators to estimate and predict the future evolution of the relevant states (including external and internal loads)

A cross-task team (from Task 2 and Task 3) of researchers in the GPIC Hub was formed to address the above challenges with the following specific objectives:

- Review existing tools for dynamic modeling and control for building systems
- Develop a simulation framework for control system design and evaluation
- Develop and evaluate reduced-order modeling approaches for the building envelope and indoor environment which are suitable for control design and implementation
- Formulate a model-based predictive control approach
- Develop case studies for assessing the benefits of optimized controls for buildings

2. Existing Models for Control System Design for Buildings

2.1 Overview and Limitations of Energy Simulation Programs for Control System Design

Commercial buildings utilize complex systems for comfort conditioning that often have a large number of subsystems and components having non-linear interactions that make it difficult to accurately analyze and evaluate control system design. Nonetheless, there are significant opportunities for optimizing control setpoints and modes of operation in response to dynamic forcing functions and utility rate incentives. Accurate but computationally efficient building and plant models are needed in order to realize the full potential for control optimization.

There are a number of simulation tools available for estimating the energy consumption of buildings. In fact, about 400 building software tools are summarized on the Department of Energy (DOE) homepages[1]. These tools range from simple spreadsheets to sophisticated programs that integrate different aspects of building performance such as CFD analysis for Indoor Air Quality (IAQ) analysis and control toolkits[2]. However, most existing building software programs focus on calculations necessary for building and HVAC system design and retrofit analysis and are not appropriate for studying advanced control algorithms to optimize building performance.

There is generally a two-level hierarchy for building control systems that includes local and supervisory control[2]. Local control is implemented in a low-level controller that manipulates an actuator to maintain a given control set-point or follows a command for a mode change. Single-input, single-output (SISO) proportional-integral (PI) control is most commonly employed for feedback control of set-points in local controllers for HVAC equipment. Sequencing control defines the order and conditions associated with switching equipment ON and OFF. Sequencing controllers are typically used for chillers, cooling towers, fans and pumps. Energy simulation programs, such as eQuest, EnergyPlus, and TRNSYS often assume perfect feedback control and don't consider the short-term dynamics associated with equipment. More general-purpose programs, such as MatLab and Modelica, have sophisticated tools for analyzing dynamic systems with feedback control and have been widely used for this purpose in many industries. Furthermore, Lawrence Berkeley National Laboratories (LBNL) is developing a library of building system models for Modelica. However, most of the equipment models in the current library neglect or only consider very simple equipment dynamics.

Supervisory controllers provide set-points and operational modes for local controllers based on higher-level logic or control algorithms. Optimal supervisory control is typically not implemented in buildings because of the complexities and costs associated with engineering site-specific solutions. Although there is potential to automate the process of developing optimized site-specific supervisory control algorithms using system simulation as part of the design process, the available tools are not fully developed for this purpose. Energy simulation programs, such as EnergyPlus and TRNSYS lack the general tools for solving optimal control problems.

General simulation platforms, such as MATLAB and Modelica, have sophisticated tools that can be used for designing and testing of advanced controllers. Furthermore, there have been some developments of libraries for building systems for both the Modelica and MATLAB programming environments. LBNL is developing a building library for Modelica termed the Modelica Buildings Library, whereas a tool called SIMBAD[4] has been developed based on the MATLAB platform and includes a library of building system components. Recently there is a movement to integrate couple building simulation tools for the purpose of investigating advanced design and control features. For example, the Building Controls Virtual Test Bed (BCVTB) is being developed by LBNL that allows coupling between Matlab/Simulink, EnergyPlus, Modelica, Radiance etc. in order to take advantage of the unique models and outputs of each tool[5].

No tools have emerged that provide a scalable solution for generating site-specific and optimized controls. However, the DOE is supporting the development of the Modelica Buildings Library for this purpose so the following section provides an overview of this platform and library.

2.2 Overview and Assessment of the Modelica Buildings Library

2.2.1 Overview of Modelica Buildings Library

Modelica is an object-oriented equation based programming language that was developed for the purpose of simulation and analysis of highly complex dynamic systems. This platform is particularly useful for simulating hybrid differential algebraic equations (DAE) that are systems of difference, differential equations with algebraic constraints. Modelica uses a special algorithm, called the Tarjans algorithm, that performs a transformation of the system of equations to block lower triangular (BLT) form and reduces the equations symbolically by finding the strongly connected components. The algorithm enables efficient solution of sparse equation systems by reducing the variables and the numbers of equations. This language is promising tool for modeling and analysis of complex building and HVAC systems that require thousands of algebraic and nonlinear or linear differential equations.

Modelica includes the following important features[6].

- Modelica is an equation-based language rather than being based on input-output relationships. This acausal modeling facilitates the use and re-use of the basic building blocks, component, and subsystem models for a variety of purposes.
- Modelica can contain and connect multi-disciplinary models covering electronics, mechanics, thermodynamics, hydraulics, and control fields.
- Modelica is an object-oriented language that enables reuse of components and evolution of models.
- Modelica has a graphical input language similar to TRNSYS, Simulink or Labview, that facilitates model development for complex large-scale physical systems.

The building library developed by LBNL[7] based on the Modelica platform includes the following packages[5,7,9].

Airflow: This package calculates air flow rate and contaminant transport between different rooms and between the exterior environment and a room. The approach for calculating air flow rate is taken from CONTAM where the driving force is the pressure difference and the flow is regulated by flow restrictor.

Boundary Conditions: This package contains models for reading weather data, such as TMY3 and converting solar radiation data to radiation on tilted surfaces.

Controls: This package contains models for local controllers such as a PID controller and setpoint scheduling.

Fluid: This package includes models for HVAC components.

Heat transfer: This includes basic models for conduction, convection, radiosity, internal sources, and windows.

Rooms: The room package contains a building envelope model that can be integrated with the Airflow package to consider building dynamics coupled to the indoor environment, including infiltration or air flow rate between different rooms caused by pressure difference. Coupling with the Fluid and Airflow packages allows construction of an entire representation of a building and HVAC system.

Utilities: This contains psychrometric calculations, models for human comfort including Predicted Mean Vote (PMV) and Percent People Dissatisfied (PPD) and interfaces to the Building Controls Virtual Test Bed (BCVTB), which enables coupling to other tools such as Energyplus, Matlab/Simulink, and Radiance[3].

Table 2.1 provides a list of different HVAC models within the Fluid Package of the Modelica Buildings Library that are described briefly in subsequent paragraphs to provide a sense of the level of detailed considered.

Table 2.1. Fluid package for Modelica Buildings Library

Name	Description
Actuators	Actuator such as valves and dampers
Boilers	Fuel-fired or electric boiler models
Chillers	Electric chiller models
Delays	Pure time delay
FixedResistances	Fixed flow resistances (pipes, diffusers etc.)
HeatExchangers	Heat exchangers
MassExchangers	Mass exchangers
MixingVolumes	Mixing volumes
Movers	Fans and pumps
Sensors	Sensors
Sources	Boundary condition models
Storage	Thermal energy storage devices
Utilities	Utility functions
Types	Type definitions
BaseClasses	Base classes for Buildings.Fluid
Interfaces	Interfaces for fluid models

Buildings.Fluids.Actuators

The actuator model is used for air dampers and water flow valves and is based on a flow coefficient[7] representation.

$$\phi = \frac{C_v(y)}{C_v(y=1)}$$

where ϕ is the flow coefficient defined as flow rate at the current actuator position, y, divided by the flow rate at $y=1$. Linear, quick opening and equal percentage valves are modeled.

Buildings.Fluids.Boiler

A quasi-steady boiler model allows for a variable efficiency according to the following equation.

$$\dot{Q} = \dot{Q}_0 \frac{\eta(y,T)}{\eta(y=1,T_0)} y$$

where $\dot{Q}$ is a heat transfer rate from the boiler to a working fluid, η is a boiler efficiency that is a function of load fraction, y, and the boiler temperatures. For dynamic simulation, a lumped

method is utilized that is based on the energy balance $\dot{U} = \dot{Q} + \dot{H}_{flow}$ where the net heat transfer from the boiler, $\dot{Q}$, is calculated using the quasi-efficiency efficiency model.

Buildings.Fluids.Chiller

Three quasi-steady chiller models are available in the library that are termed Carnot, ElectricReformulatedEIR and ElectriEIR model. The last two models are regression models based on DOE-2.1[8] and can also be found in EnergyPlus. These models compute power consumption using chilled water supply setpoint temperature, condenser water supply temperature or the outdoor air dry-bulb temperature for air–cooled equipment, partial load ratio, nominal capacity and nominal power. They can also incorporate a time delay using a first-order differential equation with a specific time constant, τ .

Buildings.Fluids.HeatExchangers

Models for heat exchangers include cooling coils, cooling towers and radiators as shown in the list of Table 2.2.

Table 2.2. HeatExchanger package for Modelica Buildings Library

Name	Description
Boreholes	Ground borehole heat exchangers
CoolingTowers	Cooling towers
Radiators	Radiators models for hydronic space heating systems
ConstantEffectiveness	Heat exchanger with constant effectiveness
DryEffectivenessNTU	Heat exchanger with effectiveness - NTU relation and no moisture condensation
DryCoilCounterFlow	Counterflow coil with discretization along the flow paths and without humidity condensation
WetCoilCounterFlow	Counterflow coil with discretization along the flow paths and humidity condensation
DryCoilDiscretized	Coil with discretization along the flow paths and no humidity condensation
WetCoilDiscretized	Coil with discretization along the flow paths and humidity condensation
HeaterCoolerPrescribed	Heater or cooler with prescribed heat flow rate

The cooling tower model is based on regression applied to a York cooling tower and uses range temperature, wet bulb temperature, water to air flow rate ratio as inputs to calculate an approach temperature. Fan power to meet the required range temperature of water is calculated using the fan affinity law as

$$\frac{\dot{P}}{\dot{P}_0} = \left(\frac{\dot{m}_{air}}{\dot{m}_{air,0}}\right)^3$$

The library heat exchanger models "Buildings.Fluid.HeatExchangers.DryCoilDiscretized" and "Buildings.Fluid.HeatExchangers.WetCoilDiscretized" are cooling coil models that contain dynamics based on a finite volume representation. In this approach, individual pipes are decomposed into a number of segments along the coolant flow direction. A heat exchanger row is constructed from a group of pipes that are on perpendicular plane forms, called a register. A number of the registers can be arranged to construct a heat exchanger.

Buildings.Fluid.Movers

This package contains models for fans and pumps. The same models are used for fans or pumps. The models use performance curves that compute pressure rise, electrical power draw and efficiency as a function of the volume flow rate and speed.

Table 2.3 Movers Package for Modelica Buildings Library

Name	Description
FlowMachine_Nrpm	Fan or pump with ideally controlled speed Nrpm as input signal
FlowMachine_dp	Fan or pump with ideally controlled head dp as input signal
FlowMachine_m_flow	Fan or pump with ideally controlled mass flow rate as input signal
FlowMachinePolynomial	Fan or pump with head and efficiency declared by a non-dimensional polynomial

2.2.2 Assessment of the Current Modelica Buildings Library

The Modelica Buildings Library can be used to simulate energy and dynamic performance of building systems for the purpose of investigating alternative controls. The library includes a large number of HVAC components and is continually expanded and improved. Most of the equipment models are based on quasi-steady representations with the ability to add dynamics using two different approaches[10].

- "Lumped" models: These are based on physical principles such as mass, momentum and heat balance equation applied to a fluid control volume. They can be applied to discretized control volumes to enable relatively detailed analysis.

- "Filter" models: This approach is based on adding a simple time constant to a steady-state model in order to introduce simple dynamic behavior. The use of the term filter comes from a first order dynamic system that filters high frequency input signals.

Most of the HVAC equipment model (fans, pumps, chillers, heat exchangers and boilers) in the Modelica buildings library include dynamic options based on filter and/or lumped representations. As previously described, the detailed heat exchanger models incorporate

multiple lumped volumes that accommodate dynamic spatial variations along the fluid flow direction.

Modelica utilizes solvers that are appropriate for stiff problems that include dynamics at multiple time scales, as occurs for building systems where both local and supervisory control are of interest. Modelica uses symbolic manipulation and index reduction and can effectively handle thousands of differential algebraic equations. As a result, the Modelica buildings library is a promising platform for delivering site-specific and optimized controls in the future. However, there are limitations of the current library that should be noted.

In particular, most of the equipment models in the Modelica Buildings Library were developed assuming quasi-steady behavior with simple dynamics added using the "filter" modeling approach. This includes the models for fans, pumps, chillers and boilers. Although the dynamic response to a step input may be reasonable, a simple filter model will eliminate high frequencies and can not capture important transient features such as overshoot[10]. Most HVAC equipment has distributed dynamic elements and a single dynamic parameter is not sufficient to describe its transient characteristics. For example, refrigerant transients associated with a chiller are dominated by the time delay associated with refrigerant phase change and transport that occurs within and between the evaporator and condenser. The physics associated with these processes cannot be adequately represented using a simple filter model.

Detailed dynamic models for heat exchangers are found in the library, which are based on a finite volume method (FVM). However, the models are restricted to the unmixed-unmixed type of heat exchanger and the dynamics do not consider the effect of heat exchanger material.

Generally, the equipment models within the current Modelica Buildings Library require specification of the nominal performance of the equipment and don't utilize geometrical and other detailed physical parameters. For instance, the epsilon-NTU heat exchanger model requires specification of a nominal heat transfer rate, mass flow rates, inlet temperatures and pressure differences on both sides and this information is used to estimate performance parameters (e.g., NTU). The accuracy of this type of model in extrapolating to other conditions may be limited.

For study of supervisory control strategies, detailed dynamic behavior may be of limited interest in assessing overall energy performance. In fact, detailed dynamic models would be a computational burden for this case and probably not warranted. So the simplified and computationally efficient dynamic modeling approaches in the Modelica Buildings Library are probably suitable for development and assessment of optimal supervisory control. However, many of the dynamic models within the library may not be appropriate to study performance issues related to local controllers, such as disturbance rejection, insensitivity to noise or command following, etc. In this case, more detailed dynamic models should be considered. Furthermore, the library currently does not include tools for assessing the control performance or

stability analysis of local controllers, such as computation of eigenvalues, zeros, or frequency response plots.

2.3 Overview of Published Transient Models for Building Components and Systems

The literature contains descriptions of relevant dynamic models that could be part of a future platform, such as the Modelica Buildings Library, for design of building control systems. This section provides a brief overview of relevant dynamic models in the literature. For the development and assessment of supervisory controls, the dynamic effects of some components may be negligible or treated with simple dynamic models that already exist within Modelica, e.g. pipes, ducts and actuators. The focus of the literature review is on dynamic models for components having more significant and complex dynamics such as chillers, heat pumps, heat exchangers and cooling towers. Some reviews have been previously published[10,14] and were a source for this brief review.

There have been a number of developments of transient models for vapor compression equipment that have been published in the literature. Several of the models are based on a dynamic model of two-phase flow in heat exchangers that was developed by Wedekind et al[16]. This model is based on a moving boundary formulation that tracks the boundaries between single and two-phase sections. Within the two-phase section, a system mean void fraction is developed. The model also decouples energy and momentum equations.

Dhar and Soedel[17] present one of the first models of a complete vapor compression refrigeration system. This model of a window air conditioner was built from first principles using the moving boundary approach in the heat exchangers. Two-phase refrigerant in the heat exchangers is treated as a coupled pair of lumps representing the liquid and vapor phases that exchange mass internally and heat externally. The model also accounts for refrigerant dissolution in the oil of the hermetic, reciprocating compressor. Despite using fairly simple representations, all major transients are well captured.

A model from Chi and Didion[18] is among the few that works with the transient form of the momentum equation. Their model of an air-to-air heat pump system, is built on a moving boundary lumped parameter formulation. The start-up transients when operating the model in cooling mode are analyzed. All the components, including the heat exchanger fans and the motor shaft are included. The dynamics of all components are captured, including the momentum of air flowing across the heat exchangers and rotational inertia of the motor shaft.

MacArthur[20] presents one of the earliest of models that moves away from the lumped parameter approach towards a distributed formulation using a finite-difference approach in the heat exchangers. McArthur and Grald[21] used similar formulations for the system components with the space-time dependent conservation equations simplified by assuming one-dimensional flow in both heat exchangers. The two-phase region in the condenser is treated as homogenous whereas

in the evaporator the liquid and vapor phases are modeled separately. The earlier work (MacArthur[20]) uses a simpler version of the heat exchanger formulation in that, the pressure response of the heat exchangers is de-coupled from the thermal response by the imposition of uniform flow velocities along the heat exchanger length. This yielded inaccurate mass distribution predictions and the issue is addressed in McArthur and Grald[21] where the mass balance is coupled to the energy balance and allowed to dictate the pressure response.

Sami et al[22] used a lumped parameter approach to model the system components where the dynamics were relevant. Multiple component configurations are modeled including shell and tube condenser and evaporator, air-cooled condenser, direct expansion evaporator, capillary tube and thermostatic expansion valve. The heat exchangers are modeled using a drift-flux model that consists of separating the vapor and liquid phases and coupling the mass and energy balances of the individual phases through the evaporation or condensation mass and energy exchange. This model is built to allow cooling and heating cycle operation of the system. Validation of the model is provided for the start-up performance of a liquid chiller. Sami et al[22] used a model of hermetically sealed reciprocating compressors taken from Yasuda et al[23] and enhanced by including oil dissolution in the refrigerant. The earlier work produced a complete system model, on lines similar to Dhar and Soedel[17], except that the condenser modeled is a shell-and-tube construction instead of air-cooled. The object of this model is to capture what are termed small transients. These include transients caused by feedback control and by instability triggered by poor valve setting. Sami and Dahmani[26] expanded on the model of Sami et al[22] to include finite differencing within the drift-flux model. This model was used to study alternatives to HCFC-22 for heat pumps, including R-407a, R-507 and NARM-502.

A number of models have been developed and used for studying control issues with vapor compression equipment. Nyers and Stoyan[24] focused on dry evaporators and built a moving boundary formulation using finite differencing within each phase to study the evaporator's behavior under step jump, exponential saturation, and periodic oscillation of the temperature and flow rate of the secondary fluid, compressor speed, condenser pressure, and throttle coefficient. Vargas and Parise[25] used a simplified component level lumped parameter formulation applied to a variable-speed heat pump to study improvements in cyclic energy efficiency for alternative forms of closed-loop control. He et al[27,28] utilized the moving boundary approach to develop a dynamic model for a vapor compression air conditioning system for the purpose of studying the effect of multivariable control. The model was used to study multivariable variable feedback control for better disturbance rejection and transient response compared to conventional single-input-single-output (SISO) control. Williatzen et al [29] employed lumped parameter moving boundary formulations for dynamic two-phase heat exchanger model and developed an algorithm that switches between appropriate sets of equations depending on the combination of phases that are present. The model was applied to studying PID control.

Bendapudi and Braun[30] developed a detailed dynamic model for vapor compression centrifugal liquid chillers that uses the finite-volume approach for shell-and-tube heat exchangers. The

paper considered numerical issues such as mesh dependence, integration order, and step size and provided guidance for balancing accuracy and computational requirements. The model was validated using data from a 90-ton R-134a centrifugal chiller. Bendapudi and Braun[31] considered the same chiller as a case study for comparing finite-volume (FV) and the moving-boundary (MB) methods. The FV formulation was found to be more robust through start-up and all load-change transients. The MB method can handle all load-change transients but start-up stability is more sensitive to compressor and expansion valve formulations. The MB formulation also executes about three times faster than the FV while maintaining nearly identical accuracy. With the homogenous two-phase assumption, charge prediction is seen to be less accurate in the MB approach.

There have been numerous developments of models for heat exchanger dynamics in the absence of dehumidification. Some initial developments of Gartner and Harrison[32] focused on the transient behavior of cross-flow heat exchangers and involved solutions to partial differential equations describing energy storage in the primary fluid (air), heat exchanger material, and secondary fluid (water) with the assumption of steady flow for both flow streams. The solutions were presented in terms of transfer functions that relate outlet air and water temperatures to variations of inlet air and water temperatures under the condition of constant fluid flow rates. The validity of the model was demonstrated through comparisons with transient experimental data. This model has been the basis for many other transient heat exchanger models, including models described by Gartner and Harrison[33], Gartner and Daane[34], Tamm[35], Tamm and Green[36], Bhargava et al[37], and Jawadi[38]. Jawadi simplified the modeling by neglecting transients associated with air.

Only a small number of transient models have been developed for cooling and dehumidifying coils. Clark[39] and Ding et al[40] developed simplified models for cooling coils but only performed comparisons with experimental data for dry conditions. The Clark model is based on a time constant applied to quasi-steady log-mean-enthalpy-difference (LMHD) approach. Similarly, the Ding et al model applies a single lumped capacity to a quasi-steady representation. Zhou and Braun[41] developed a finite-volume model that employs both air-side and water-side effectiveness relations that allow each row of a cooling coil to be accurately treated using a single control volume. The model was shown to provide predictions that agree very well with a detailed reference model but showed some significant differences in comparison to the models of Clark and Ding et al. Zhou and Braun[42] performed a detailed and extensive experimental validation of the simplified model of Zhou and Braun[41] over a wide range of dynamic operating conditions including wet and dry coils. The model provides very accurate dynamic and steady-state predictions.

Li et al[43] developed a Modelica implementation of a cooling coil model. To construct an accurate and computationally efficient model, reformulation was made to the heat exchanger model in the Air Conditioning Library[44] and the Lewis relation was applied to calculate the condensed flow rate for the dehumidifying process. Model results were compared with experimental data

obtained from two different coils collected by Zhou[45] and the computation time was also compared with Zhou's model.

Li et al[46] developed a dynamic model for a typical mechanical draft counter-flow wet cooling tower. The simulation model was implemented in Modelica with Dymola Version 6.1 and the TLK/Ift Library. The heat and mass transfer direction is assumed to be normal to the flow to separate water and air flow. A finite volume method is then applied to each fluid. The mass transfer coefficient and the heat transfer coefficient were determined using overall NTU for mass transfer (ASHRAE[47]; Braun et al[48]; Kröger[49]) and the Lewis relation. Experimental results from Simpson and Sherwood[50] were used to verify the steady state predictions of the model.

2.4 References

1. Department of Energy Building Energy Software Tools Directory, http://www.eere.energy.gov/
2. M. Trčka, L.M. Hensen, "Overview of HVAC system simulation", *Automation in Construction*, 19, 93–99, 2010
3. Homepage of Building Controls Virtual Test Bed, https://simulationresearch.lbl.gov/bcvtb
4. P. Riederer, "Matlab/Simulink for building and HVAC simulation - State of the Art", *9th International IBPSA Conference*, Montreal, Canada, 2005
5. M. Wetter, W. Zuo, T.S. Nouidui. "Recent developments of the modelica buildings library for building heating, ventilation and air-conditioning systems", *8th International Modelica Conference*, Dresden, Germany, 2011
6. P. Fritzson, "Principles of object-oriented modeling and simulation with modelica 2.1", Wiley-IEEE Press, 2004
7. M. Wetter, "Modelica library for building heating,ventilation and air-conditioning systems", *7th Modelica Conference*, Como, Italy, 2009
8. M. Hydeman, K.L. Gillespie. "Tools and techniques to calibrate electric chiller component models", *ASHRAE Transactions*, AC-02-9-1, 2002
9. Homepage of Modelica Library for Building Energy and Control Systems http://simulationresearch.lbl.gov/modelica
10. J. Bourdouxhe, J. Leburn, "*Refererence guide for dynamic models of hvac equipment*", American Society of Heating, Refrigerating and Air-Conditioning Engineers Inc., 1998
11. X. Zhou, "Dynamic modeling of chilled water cooling coils" PhD thesis, Purdue university, 2005
12. S. Bendapudi, J. E. Braun, "Development and evaluation of modeling approaches for transient in centrifugal chillers", PhD thesis, Purdue university, 2004
13. S. Wang" Dynamic simulation of a building central chilling system and evaluation of emcs on-line control strategies", *Building and Environment*, Vol. 33, No. 1, pp. I-20, 1998

14. S. Bendapudi, J.E. Braun, "A review of literature on dynamic models of vapor compression equipment". ASHRAE Research project 1043-RP, 2002

15. S. Bendapudi, J.E. Braun "A review of literature on dynamic models of vapor compression equipment". ASHRAE Research Project 1043-RP, 2002

16. G.L. Wedekind, B.L. Bhatt, B.T. Beck, , "A system mean void fraction model for predicting various transient phenomena associated with two phase evaporating and condensing flows.", *International Journal of Multiphase Flow*, Vol. 4, pp. 97-114, 1978

17. M. Dhar , W. Soedel, "Transient analysis of a vapor compression refrigeration system.", *XV International Congress of Refrigeration*, Venice, 1979

18. J. Chi, D.A. Didion, "A simulation model of the transient performance of a heat pump", *International Journal of Refrigeration*, Vol. 5, No. 3, pp. 176-184, 1982

19. Y. Yasuda, S. Touber, C.H.M. Machielsen, "Simulation model of a vapor compression refrigeration system", *ASHRAE Transactions* Paper No. 2787, pp. 408-425, 1982

20. J.W. MacArthur, "Transient heat pump behavior: a theoretical investigation", *International Journal of Refrigeration*, Vol. 7, No. 2, pp. 123-132, 1984

21. J.W. MacArthur, E.W. Grald, "Prediction of cyclic heat pump performance with a fully distributed model and a comparison with experimental data", *ASHRAE Transactions*, Vol. 93, Part 2, 1987

22. S.M. Sami, T. Duong, Y. Mercadier, N. Galanis, "Prediction of the transient response of heat pumps", *ASHRAE Transactions*, Vol. 93, pg. 471, 1987

23. R.R. Johnson, Y. Mohammed-zadeh, J.A. Edwards, P. Safemazandarani, "Experimental evaluation of three ground-coupled heat pump systems", *ASHRAE Transactions*, Vol. 94, Part 1, 1988

24. J. Nyers, G, Stoyan, "Analysis of the dynamic model of the dry evaporator of heat pumps and refrigerators", *Bull. Of Applied Mathematics*, Vol. 683 (LIV), pp. 279-285, 1990

25. J.V.C. Vargas, J.A.R. Parise, "Simulation in transient regime of a heat pump with closed-loop and on-off control", International Journal of Refrigeration, Vol. 18, No. 4, pp. 235-243, 1995

26. S.M. Sami, A. Dahmani, "Numerical prediction of dynamic performance of vapor compression heat pump using new hfc alternatives to hcfc-22", *Journal of Applied Thermal Engineering*, Vol. 16, Nos. 8/9 pp. 691-705, 1996

27. X. He, S. Liu, H.H. Asada, "Modeling of vapor compression cycles for multivariable feedback control of HVAC systems", *ASME Journal of Dynamic Systems, Measurement and Control*, Vol. 119, No. 2, 1997

28. X. He, S. Liu, H.H. Asada, " Multivariable feedback design for regulating vapor compression cycles", *American Control Conference*, 4331 - 4335 vol.6, 1995

29. M. Williatzen, N.B.O.L. Petit, L. Ploug-Sorensen, "A general dynamic simulation model for evaporators and condenser in refrigeration: Part 1 – moving boundary formulation of two-phase flows with heat exchange", *International Journal of Refrigeration*, Vol. 21, No. 5, pp. 398-403, 1998

30. S. Bendapudi, J.E. Braun, E.A. Groll, "Dynamic model of a centrifugal chiller system - model development, numerical study and validation," *ASHRAE Transactions*, Vol. 111, Pt. 1, pp. 132-148, 2005.

31. S. Bendapudi, J.E. Braun, E.A. Groll, "A comparison of moving boundary and finite volume formulations for transients in centrifugal chillers," *International Journal of Refrigeration*, Vol. 31, No. 8, Pages 1437-1452, 2008.
32. J.R. Gartner, H.L. Harrison. "Frequency response transfer function for a tube in crossflow", *ASHRAE Transactions*, 69: 323-330, 1963
33. J.R. Gartner, H.L. Harrison. "dynamic characteristics of water-to-air crossflow heat exchangers", *ASHRAE Transactions*, 71: 212-224, 1965
34. Gartner, J.R., and L.E. Daane. "Dynamic response relations for a serpentine crossflow heat exchanger with water velocity disturbance", *ASHRAE Transactions*, 75(2): 53-68, 1969
35. H. Tamm, "Dynamic response relations for multi-row crossflow heat exchangers", *ASHRAE Transactions*, 75(1): 69-80, 1969
36. H. Tamm, G.H. Green. "Experimental multi-row crossflow heat exchanger dynamics", *ASHRAE Transactions*, 79(2): 9-18, 1973
37. S.C. Bhargava, F.C. McQuiston, L.D. Zirkl, "Transfer functions for crossflow multi-row heat exchangers", *ASHRAE Transactions*, 81(2): 294-314, 1975
38. Z. Jawadi, "A Simple transient heating coil model. analysis of time dependent thermal systems", Winter Annual Meeting of ASME: 63-69, 1988
39. D.R. Clark, "Type 12: cooling or dehumidifying coil, hvacsim+ reference manual", National Bureau of Standards: 63-68, 1985
40. X. Ding, J.P. Eppe, J. Lebrun, M. Wasacz, "cooling coil model to be used in transient and /or wet regimes. theoretical analysis and experimental validation", *Third International Conference on System Simulation in Building*, Liège, Belgium: 405-441, 1990
41. X. Zhou and J.E. Braun, "A simplified dynamic model for chilled water cooling and dehumidifying coils – Part 1: Development," *HVAC&R Research*, Vol. 13, No. 5, Pages 785-804, 2007.
42. X. Zhou and J.E. Braun, "A simplified dynamic model for chilled water cooling and dehumidifying coils – Part 2: Experimental validation," *HVAC&R Research*, Vol. 13, No. 5, Pages 805-817, 2007.
43. P. Li, Y. Li, J.E. Seem, "Modelica based dynamic modeling and self-optimizing control of water-cooled centrifugal chiller system", *Purdue Compressor Engineering, Refrigeration and Air Conditioning and High Performance Buildings Conferences*, 2010
44. Modelon, AB. 2007b. Air Conditioning Library User's Manual Version
45. X. Zhou, "Dynamic modeling of chilled water cooling coils", PhD thesis, Purdue University, 2005
46. X. Li, Y. Li, J.E. Seem, "Dynamic modeling of mechanical draft counter-flow wet cooling tower with Modelica", *International Refrigeration and Air Conditioning Conference*. Paper 1094, 2010
47. ASHRAE Equipment Guide, American Society of Heating, Refrigerating, and Air-Conditioning Engineers Inc. Atlanta, GA, 1983
48. J.E. Braun, S.A. Klein, J.W. Mitchell, "Effectiveness models for cooling towers and cooling coils", *ASHRAE Transactions*, Vol. 95(2), pp. 164-174, 1989
49. D.G. Kröger, "Air-cooled heat exchangers and cooling towers - thermal flow performance

evaluation", D. G., 2004

50. W. M. Simpson, T. K. Sherwood, "Performance of Small Mechanical Draft Cooling Towers", *Refrigerating Engineering*, vol. 52, no. 6: p. 535-543, 574-576, 1946

3. Modeling and Control System Design Approach

For the purpose of control system tool development and investigation of MPC, MatLab has been chosen as the platform for this project. Figure 3.1 depicts the proposed process for development of MPC for building systems that is currently under investigation. The current approach involves the use of detailed physical models for the building envelope that capture both transient and spatial variations for each zone. These models are used to develop reduced-order models that are more amenable to implementation within an MPC. The plant that provides cooling and heating for the individual building zones is currently treated with quasi-static models. The use of quasi-static plant models allows the use of off-line methods for determining optimal plant modes and set-points. Optimal modes and setpoints can then be mapped along with the associated minimum power consumption in terms of the primary plant boundary conditions, such as total cooling requirement and ambient drybulb and wetbulb temperatures. The reduced-order building envelope and indoor air models are coupled with the plant within an MPC implementation to provide a tractable methodology for determining optimal supervisory control in response to driving functions. The MPC involves minimizing a cost function that is the integrated energy cost of providing comfort conditions over a 24-hour moving horizon. Comfort can be treated as either a constraint or within the cost function using productivity penalty.

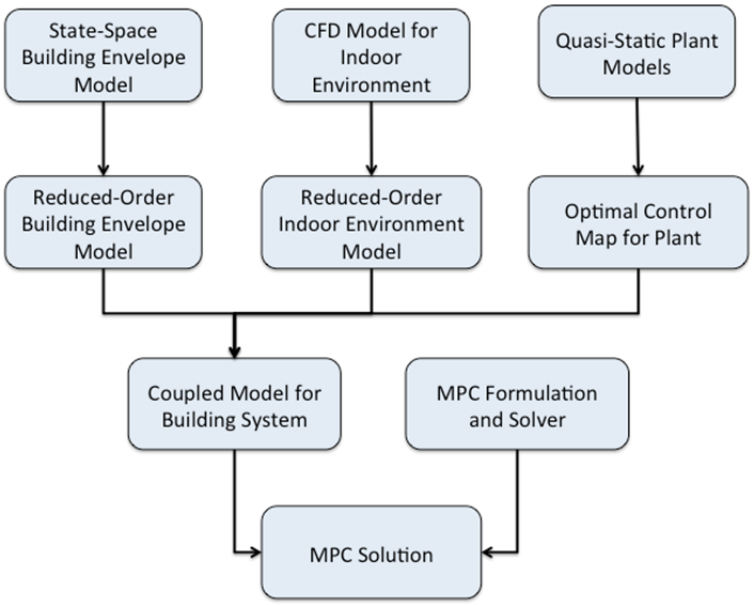

Figure 3.1. Proposed flow chart for control system development

Computationally efficient coupling between the reduced order building and envelope models is a particular challenging problem. For this purpose it is convenient to decompose the model into systems for the building-envelope and for the indoor-air. The basic idea for the decomposition is shown in Figure 3.2.

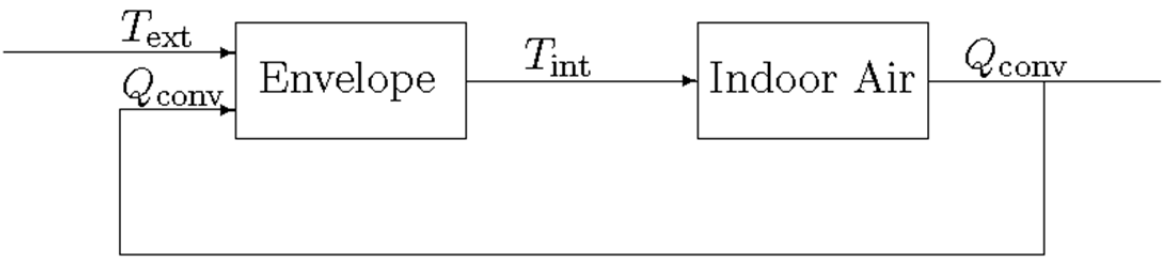

Figure 3.2. Coupling between building envelope and indoor air models

The *Envelope* is modeled by a system of ordinary differential equations that describe the evolution of the temperatures on interior surface(s) (T_{int}); it includes conductive and radiative transfer mechanisms. The *Indoor-Air* models the dynamics of the interior air flow. As indicated in Figure 3.2, wall surface temperatures (T_{int}) are *inputs* to this model and resulting wall heat loads (Q_{conv}) are *outputs*. Other features, such as solar loads for the *Envelope* and/or cooling for the *Indoor-Air* can be readily included.

To set the stage for the later work, we now consider the *Standard Model* in this cascade framework. In standard practice the heat load on a wall segment would be modeled as

$$Q_i(t) = (h\,A)_i(T_i(t) - T_z(t)),\ \text{i} = 1, \ldots, \text{m}, \tag{3.1}$$

where T_z is the zone (air) temperature, and $(h\,A)_i$ represent the film coefficient and area of the i^{th} segment. In the case of a single zone the evolution of T_z is described by

$$M_i(t)\frac{dT_z(t)}{dt} = \sum_{k=1}^{m} Q_k(t) + Q_{ext}(t) \tag{3.2}$$

where M is the thermal capacitance of the room air (J/K) and Q_{ext} accounts for any other thermal loads.

If we identify the inputs (u) with the segment temperatures T, and the outputs (y) with the segment loads (Q), then the system (3.1, 3.2) is a linear time-invariant (LTI) system and in the usual first-order system form (A,B,C,D) we can identify

$$C = \begin{bmatrix} (hA)_1 \\ (hA)_2 \\ \vdots \\ (hA)_m \end{bmatrix},\ \text{D} = \begin{bmatrix} (hA)_1 & 0 & \cdots & 0 \\ 0 & (hA)_2 & \cdots & 0 \\ \vdots & \vdots & \ddots & \vdots \\ 0 & 0 & 0 & (hA)_m \end{bmatrix}$$

$$A = -\sum_{k=1}^{m} \frac{(hA)_k}{M} \text{ (a scalar), and } B = \frac{C^T}{M} \tag{3.3}$$

Note that (3.33) does not account for the $(m + 1)^{st}$ input (Q_{ext}).

The transfer function from the inputs (wall-segment temperatures *T*) to the outputs (wall-segment loads *Q*) is given by

$$H^{std}(s) = \frac{-CC^T}{(M\ s + \sum (hA)_k)} + D,$$

where the arrays (*C*,*D*) depend on the wall-segment *convective parameters* (*hA*) as given in display (3.3). Note that the transfer function H^{std} is not strictly proper ($D \neq 0$).

4. Model Order Reduction for the Building Envelope

4.1 Introduction

The application of Model Predictive Control (MPC) to buildings could have high computational requirements depending on the number of control variables, the time horizon for the optimization, the discretization for control decisions and model solution, and the complexity of the models. Reducing model complexity and computation requirements while retaining prediction accuracy is the goal when considering reduced-order building modeling.

In general, models for control can be grouped into two types: forward and data-driven models. Forward models start from first principles such as conservation equations of mass, energy and momentum. They can be highly accurate but may have a high computational burden especially for control purposes. On the other hand, data-driven models rely on experimental data or simulation results from a physical model to train an empirical or black-box model and can sometimes yield unrealistic and non-physical results[1], especially when employed outside of the range where they were trained. One of the most important and difficult problems in the system identification procedure is choosing the "best" model among a set of candidate models. It necessarily requires "model validation" to choose the "best" model. As much as 80% of the effort is spent on this step.

The main purpose of the study described here is to develop a general methodology for converting the complex thermal network of a multi-zone building into a compact reduced-order state-space representation that will more readily enable implementation and assessment of advanced control concepts.

The complexities of heat transfer phenomena through glazings and long wavelength exchanges among walls make the representation difficult. In the detailed reference model used to determine a reduced-order model, the net radiosity method for long-wave interaction and a simple window model are adopted to construct a general form which includes heat transfer through windows, long-wave interaction among surfaces, conduction through walls, distributed thermal capacitance within walls, conductive heat transfer between the rooms and so on. After constructing a state-space representation for the reference model, a model-order reduction method is applied to the forward model to construct a reduced-order model.

4.2 Nomenclature

Nz = number of zones (or rooms)

Nw = number of walls in a zone (or a room)

$nnod$ = number of nodes in a wall

Nc = number of nodes to construct multi-zone model

$\vec{T} \in R^{Nz \cdot Nw \cdot nnod + Nconn + Nz}$ = set of all temperatures nodes of walls and zone air in multiple zones,

$$\vec{T} = \left[\vec{T}_W^T,\ \vec{T}_Z^T \right]^T$$

$\vec{T}_W \in R^{Nz \cdot Nw \cdot nnod + Nconn}$ = set of all temperatures nodes of walls in multiple zones,

$$\vec{T}_W = \left[\ (\vec{T}_w^1)^T \ \ .. \ \ (\vec{T}_w^{Nz})^T \ \ (\vec{T}_C)^T \ \right]$$

$\vec{T}_Z \in R^{Nz}$ = set of all zone air temperatures nodes in multiple zones

$\vec{T}_w^I \in R^{Nw(I) \cdot nnod}$ = set of all node temperatures of walls and windows in Ith zone

$$\vec{T}_w = \left[\ \vec{T}_1^T \ \vec{T}_2^T \ . \ . \ \vec{T}_n^T \ \right]$$

$\vec{T}_C \in R^{Nc}$ = set of all temperatures nodes to construct multi-zone model

$\vec{T}_j \in R^{Nw}$ = set of all jth temperature nodes of walls in a single zone, $\vec{T}_j = \left[\ T_j^1 \ \ T_j^2 \ \ .. \ \ T_j^{Nw} \ \right]^T$

T_j^i = temperature at jth node in ith wall

ρ_j^i = density at jth node in ith wall

w_j^i = width of control volume of jth node in ith wall [m]

$k^L|_j^i$ = thermal conductivity at left surface of the jth node in ith wall

$w^L|_j^i$ - distance from the "j-1"th node to the jth node in ith wall [m]

q_{LWR} = net long wavelength radiation exchange with environment [W/m^2]

q_{SWR} = short wavelength solar irradiation [W/m^2]

q_{SWR}^w = short wavelength solar irradiation onto a window [W/m^2]

q_{gen} = energy source term [W/m^2]

$(\vec{q})_i$ = ith component of a vector $\vec{q}$

$h_{cv,in}$ = convective heat transfer coefficient at an internal wall [W/m^{2}K]

$h_{cv,ex}$ = convective heat transfer coefficient at the outside surface of a wall[W/m^{2}K]

$q_{net,rad}$ = net radiative heat flux out of an internal surface [W/m^2]

$\overline{T}$ = mean temperature [K]

δ_{ij} = Kronecker delta

$\tilde{A}_{ij}$ = (i,j) components of a matrix $\tilde{A}$

$\tilde{I}$ = identity matrix

h_o^i = external radiative source term acting on ith surface [W/m^{2}K]

HTC = heat transfer coefficient [W/m^2-K]

ρ^I = Ith zone air density [kg/m^3]

C_V^I = Ith zone air thermal capacity (constant volume specific heat) [J/kg-K]

V^I = Ith zone air volume [m^3]

T_z^I = Ith zone air temperature [K]

$\dot{Q}$ = heat flow rate [W]

$\dot{m}_{IJ}$ = mass flow exchange rate between Ith zone air and Jth zone air [kg/s]

$h_{cv,in}^{i(I)}$ = internal convective HTC at ith interior wall of Ith zone [W/m^2-K],

$$\hat{h}_{cv,in}^I = \left[0 \quad 0 \quad .. \quad (\vec{h}_{cv,in}^I)^T \right]^T \in R^{Nw(I)\cdot nnod}$$

4.3 Detailed Multi-Surface, Multi-Zone Model Formulation

The terminology of a zone that is used in this section is assigned to a unit or module of the thermal network of a room that is shown in Figure 4.1. A multi-zone representation is a group of thermal network units. The state-space model of a building system starts from a module (network unit) and extends to constructing more complex multi-zone models. A detailed formulation is described in this section. Some of the important assumptions used to construct the network unit are

- The temperature of each surface or surface segment is uniform within its cross section.
- A room is well mixed.
- Each wall emits or reflects diffusely and is gray and opaque.
- Air is a non-participating media with respect to radiation.
- Heat transfer is one-dimensional.
- Conduction between the window and window frame is neglected (1-D assumption).

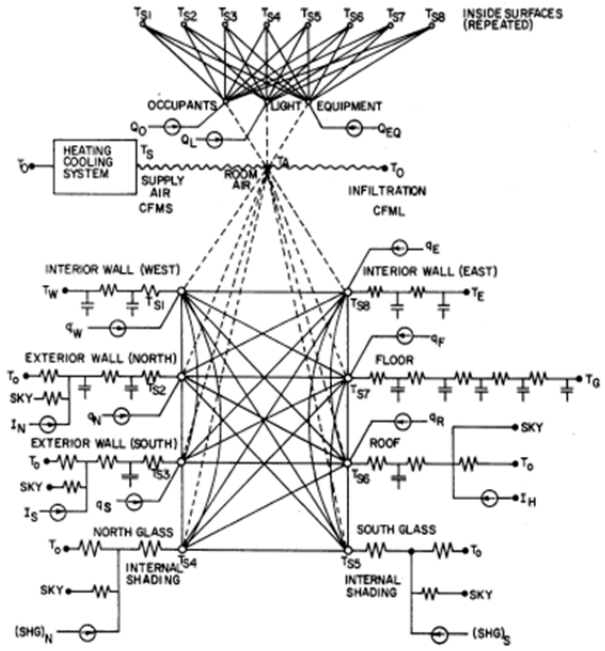

Figure 4.1. Thermal network for a zone[2]

4.3.1 State space representation of a single zone thermal building model

Conduction Through Wall

A finite volume formulation is used to describe the heat conduction through walls and is depicted in Figure 4.2. Node number "j" is assigned from outside to inside of a wall so that the first node and last node represent the temperature of the outside and inside surface, respectively.

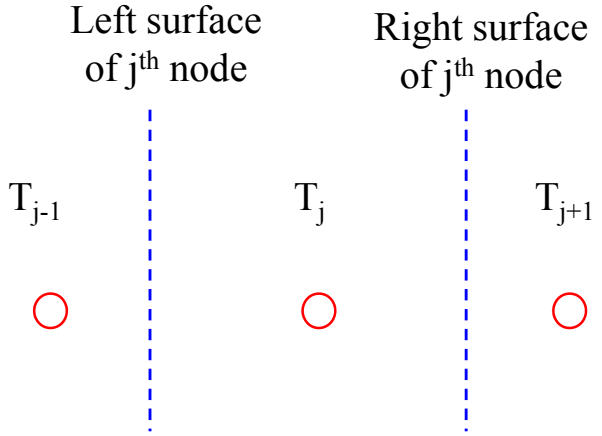

Figure 4.2. Notation for conduction through walls

For any j^{th} node in a wall except the first and last nodes, an energy balance leads to

$$\rho_j^i C_j^i w_j^i \frac{dT_j^i}{dt} = h_{cd}^L|_j^i \, T_{j-1}^i - (h_{cd}^L|_j^i + h_{cd}^R|_j^i) T_j^i + h_{cd}^R|_j^i \, T_{j+1}^i + q_{gen\,j}^{\;\;i} \tag{4.1}$$

where $h_{cd}^{\;\;L}|_j^i = \frac{k^L|_j^i}{w^L|_j^i}$ and $q_{gen\,j}^{\;\;i} = \frac{Q_{gen\,j}^{\;\;i}}{Area^i}$ is an energy source [W/m^2] inside the jth finite control volume that belongs to the ith wall.

By using the following matrix notation,

$$\vec{q}_j \equiv \begin{bmatrix} q_{gen}^1 \\ q_{gen}^2 \\ .. \\ q_{gen}^{Nw} \end{bmatrix} \tilde{H}_j^L \equiv \begin{bmatrix} h_{cd}^L|_j^1 & & & 0 \\ & h_{cd}^L|_j^2 & & \\ & & .. & \\ 0 & & & h_{cd}^L|_j^{Nw} \end{bmatrix}, \quad \vec{T}_j \equiv \begin{bmatrix} T_j^1 \\ T_j^2 \\ .. \\ T_j^{Nw} \end{bmatrix}$$

$$\tilde{C}_j \equiv \begin{bmatrix} \rho Cw|_j^1 & & & 0 \\ & \rho Cw|_j^2 & & \\ & & .. & \\ 0 & & & \rho Cw|_j^{Nw} \end{bmatrix}$$

Equation 4.1 can be expressed in the following matrix form.

$$\tilde{C}_j \frac{d\vec{T}_j}{dt} = \tilde{H}_{cd,j}^L \vec{T}_{j-1} - (\tilde{H}_{cd,j}^L + \tilde{H}_{cd,j}^R)\vec{T}_j + \tilde{H}_{cd,j}^R \vec{T}_{j+1} + \vec{q}_j \tag{4.2}$$

Note that $\vec{T}_j$ is a group of all of wall temperature nodes belonging to an individual zone.

Heat Balance at Outside Surface

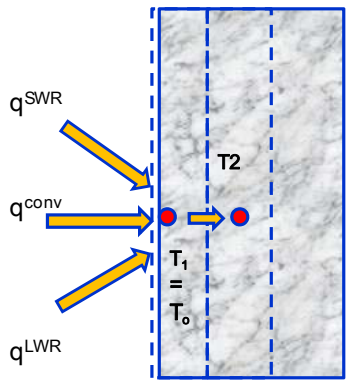

Figure 4.3. Heat balance at outside walls

For any i[th] outside wall (connected to the external ambient) belonging to an individual zone, the heat balance equation at the surface is

$$\rho_1^i C_1^i w_1^i \frac{dT_1^i}{dt} = h_{cv,ex}^i (T_a - T_1^i) + h_{cd}^R \mid_1^i (T_2^i - T_1^i) + \alpha_1^i q_{SWR}^i + q_{LWR}^i \tag{4.3}$$

where T_1^i represents the wall temperature of the first node which is set to be an outside surface of the wall.

With the assumptions that the outside surface is gray and diffuse and the air is a non-participating radiation media, net long wavelength interactions with the environment can be expressed as

$$q_{LWR}^i = \sigma \epsilon_1^i F_{sky}^i (T_{sky}^4 - T_1^{i4}) + \sigma \epsilon_1^i F_{grd}^i (T_{grd}^4 - T_1^{i4})$$

Using a linear approximation of the long-wave heat exchange term gives

$$\rho_1^i C_1^i w_1^i \frac{dT_1^i}{dt} = -(h_{cv,ex}^i + h_{cd}^R \mid_1^i + h_{rad,ex}^i) T_1^i + h_{cd}^R \mid_1^i T_2^i + q_1^i$$

where

$$h_{rad,ex}^i = 4\sigma \epsilon_1^i (F_{sky}^i \overline{T}_{sky}^3 + F_{grd}^i \overline{T}_{grd}^3),$$

$$q_1^i = h_{cv,ex}^i T_a + 4\sigma \epsilon_1^i (F_{sky}^i \overline{T_{sky}^3 T_{sky}} + F_{grd}^i \overline{T_{grd}^3 T_{grd}}) + \alpha_1^i q_{SWR}^i$$

$$\overline{T}_{sky} = \frac{T_{sky} + T_1}{2}, \quad \overline{T}_{gnd} = \frac{T_{gnd} + T_1}{2}$$

The mean temperatures for long-wave exchanger between the surface and sky and surface and ground are assumed to be the same for all outside surfaces

Equation 4.3 can be generalized and written compact matrix form as

$$\tilde{C}_1 \frac{d\vec{T}_1}{dt} = -(\tilde{H}_{cd,1}^R + \tilde{H}_{rad,ex} + \tilde{H}_{cv,ex}) \vec{T}_1 + \tilde{H}_{cd,1}^R \vec{T}_2 + \vec{q}_1 \tag{4.4}$$

where

$$(\vec{q}_1)_i = q_1^i = h_{cv,ex}^i T_a + 4\sigma \epsilon_1^i (F_{sky}^i \overline{T}_{sky}^3 T_{sky} + F_{grd}^i \overline{T}_{grd}^3 T_{grd}) + \alpha_1^i q_{SWR}^i \tag{4.5}$$

Heat Balance at Inside Surface

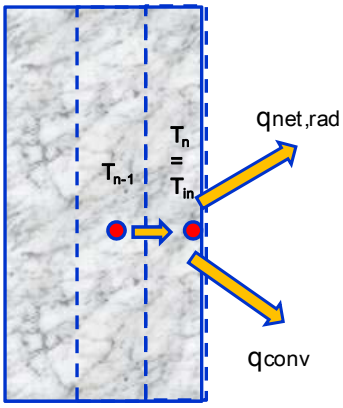

Figure 4.4. Heat balance at inside walls

For the I[th] zone and i[th] wall, the energy balance equation for the inside surface is

$$\rho_n^i C_n^i w_n^i \frac{dT_n^i}{dt} = h^i{}_{cv,in}(T_z - T_n^i) + h_{cd}^L|_n^i\,(T_{n-1}^i - T_n^i) + q_{net,rad}^i$$

where $q_{net,rad}$ is the net radiative flux out of the inside wall.

The radiosity method is utilized to express the net flux under the assumption that the walls are opaque. A detailed derivation is given in appendix 4.A.1. The main result is

$$\vec{q}_{net,rad} = \tilde{A}^{-1}[\tilde{B}'\vec{T}_n - \vec{h}_o]$$

where,

$$\tilde{B}'_{ij} = 4\sigma(\delta_{ij} - F_{ij})\bar{T}^3$$

Radiosity does not appear explicitly in the above expression, which is convenient for building simulation. Since h_o^i represents an external radiative source acting on the i[th] surface, the effect of internal sources or transmitted solar energy though windows are treated in a consistent manner. For any shaped room, the net radiative flux can be explicitly calculated as a function of surface temperatures if the view factors and the external radiative sources are known.

By letting $\tilde{H}_{rad,in} \equiv \tilde{A}^{-1}\tilde{B}'$ and $\vec{q}_n \equiv \tilde{A}^{-1}\vec{h}_o$

$$\tilde{C}_n \frac{d\vec{T}_n}{dt} = \tilde{H}_{cd,n}^L \vec{T}_{n-1} - (\tilde{H}_{cd,n}^L + \tilde{H}_{rad,in} + \tilde{H}_{cv,in})\vec{T}_n + \vec{h}_{cv,in}T_z + \vec{q}_n \qquad (4.6)$$

State-Space Representation of Thermal Network Module

Gathering the systems of heat balance equations from external to internal wall (Equations 4.2, 4.4, and 4.6) gives

$$\begin{bmatrix} \tilde{C}_1 & & & \\ & \tilde{C}_2 & & \\ & & .. & \\ & & & \tilde{C}_n \end{bmatrix} \frac{d}{dt} \begin{bmatrix} \vec{T}_1 \\ \vec{T}_2 \\ .. \\ \vec{T}_n \end{bmatrix} =$$

$$\begin{bmatrix} -(\tilde{H}^R_{cd,1} + \tilde{H}_{cv,ex} + \tilde{H}_{rad,ex}) & \tilde{H}^R_{cd,1} & & & \\ \tilde{H}^L_{cd,2} & -(\tilde{H}^L_{cd,2} + \tilde{H}^R_{cd,2}) & \tilde{H}^R_{cd,2} & & \\ & .. & .. & .. & \\ & & \tilde{H}^L_{cd,n} & -(\tilde{H}^L_{cd,n} + \tilde{H}_{cv,in} + \tilde{H}_{rad,in}) \end{bmatrix} \begin{bmatrix} \vec{T}_1 \\ \vec{T}_2 \\ .. \\ \vec{T}_n \end{bmatrix} \quad (4.7)$$

$$+ \begin{bmatrix} 0 \\ 0 \\ .. \\ \vec{h}_{cv,in} \end{bmatrix} T_z + \begin{bmatrix} \vec{q}_1 \\ \vec{q}_2 \\ .. \\ \vec{q}_n \end{bmatrix}$$

This expresses the complex thermal network of a zone with relatively simple physical terms. As expected, a tri-diagonal block matrix is formed with parameters that characterize heat transfer due to conduction in the walls (from node number 2 to node number n-1) and radiative/convective heat transfer at the boundaries (first and last nodes only). The terms $\vec{q}_2$ and $\vec{q}_{n-1}$ vanish if there are no heat flux sources inside the wall such as embedded radiant heating or cooling systems. The linearized state-space equations for the thermal network of an individual zone are basically time variant if the temperature dependence of radiative and convective heat transfer coefficients is neglected.

Equation (4.7) can be expressed in simpler form as

$$\tilde{C}_w \dot{\vec{T}}_w = \tilde{H}_w \vec{T}_w + \hat{h}_{cv,in} T_z + \vec{q}_w \quad (4.8)$$

where $\vec{T}_w = \left[\vec{T}_1^T, \vec{T}_2^T, \ . \ . \ \vec{T}_n^T \right]^T$ are all of the states for wall temperatures in an individual zone with $\vec{T}_j = \left[T_j^1 \quad T_j^2 \quad .. \quad T_j^{Nw} \right]^T$ and $\hat{h}^I_{cv,in} = \left[0 \quad 0 \quad .. \quad (\vec{h}^I_{cv,in})^T \right]^T \in R^{Nw(I)}$

Since the thermal capacitance matrix, $\tilde{C}_w$, is diagonal, its inverse is the reciprocal of the diagonal components. The model assumes one-dimensional heat flow and uniform surface temperatures.

However, a wall can be discretized into several segments with multiple surfaces in this formulation. This feature allows coupling with a more detailed indoor air model, such as CFD, when there are significant surface temperature variations due to solar or other effects. A slightly modified form of Equation 4.8 is used for CFD coupling where the convective heat flux from a local control volume to its surrounding walls is treated as input.

4.3.2 State-Space Representation of a Multi- Zone Thermal Building Model

As mentioned previously, the terminology multi-zone is meant to represent a group of thermal networks. Only the conductive heat exchange among zones through adjacent walls is considered in the building envelope formulation. However, convective coupling could be considered through a reduced-order CFD model that is coupled to the multi-zone building envelope model.

The strategy for constructing a multi-zone model involves constructing a global matrix, which describes all heat balance equations for all zones and their "connectivity" (e.g., I^{th} zone, i^{th} outside wall connected to J^{th} zone, j^{th} outside wall) and is based on the individual zone module matrices. The nomenclature of a connecting temperature node, T_C, is introduced for the connection of the each network unit. The advantage of utilizing the connecting node is that each zone matrix is independent of the assembly of the global matrix. The strategy for constructing the global matrix is depicted in Figure 4.5. The first node (outside surface) of the i^{th} wall of the I^{th} zone (Iz,iw,1) is connected to the first node (outside surface) of the j^{th} wall of the J^{th} zone (Jz,jw,1).

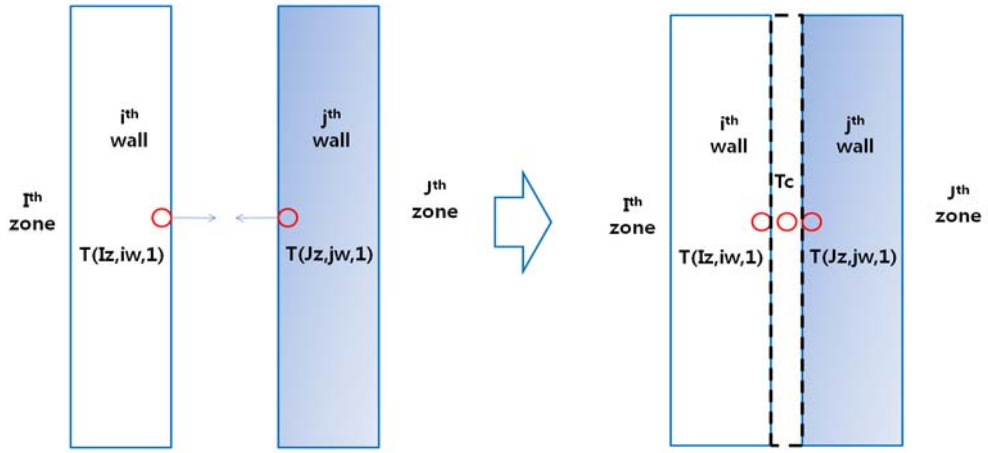

Figure 4.5. Connecting thermal network modules

$$\begin{bmatrix} \tilde{C}_1 & & & & & & \\ & .. & & & & & \\ & & \tilde{C}_I & & & & \\ & & & .. & & & \\ & & & & \tilde{C}_J & & \\ & & & & & .. & \\ & & & & & & C_c \end{bmatrix} \frac{d}{dt} \begin{bmatrix} \vec{T}_w^1 \\ .. \\ \vec{T}_w^I \\ .. \\ \vec{T}_w^J \\ .. \\ T_C \end{bmatrix} =$$

$$\begin{bmatrix} \tilde{H}_w^1 & & & & & 0 & 0 \\ & .. & & & & & .. \\ & & \tilde{H}_w^I & & & & (Iz,iw)\ \&\ C \\ & & & .. & & & 0 \\ & & & & \tilde{H}_w^J & & (Jz,\ jw)\ \&\ C \\ 0 & & & & & .. & 0 \\ 0 & .. & (Iz,iw)\ \&\ C & 0 & (Jz,\ jw)\ \&\ C & 0 & (Iz,iw)\ \&\ C + (Jz,\ jw)\ \&\ C \end{bmatrix} \begin{bmatrix} \vec{T}_w^1 \\ .. \\ \vec{T}_w^I \\ .. \\ \vec{T}_w^J \\ .. \\ T_C \end{bmatrix} \quad (4.9)$$

$$+ \begin{bmatrix} \hat{h}_{cv,in}^1 & & & & & 0 \\ & .. & & & & .. \\ & & \hat{h}_{cv,in}^I & & & . \\ & & & .. & & . \\ & & & & \hat{h}_{cv,in}^J & . \\ & & & & & .. \\ 0 & & . & . & . & 0 \end{bmatrix} \begin{bmatrix} T_z^1 \\ .. \\ T_z^I \\ .. \\ T_z^J \\ .. \\ T_z^{Nz} \end{bmatrix} + \begin{bmatrix} \vec{q}_w^1 \\ .. \\ \vec{q}_w^I \\ .. \\ \vec{q}_w^J \\ .. \\ 0 \end{bmatrix}$$

The notation (Iz,iw) & C represents the conductive HTC between the connecting node and the i^{th} node of the outside wall which belongs to I^{th} zone. The formulation is derived from conduction equations. The thermal capacitance of the connecting node, C_c, must approach zero since the control volume of the connecting node must vanish. Also, the HTC between the connecting node and its neighboring nodes must approach infinity. However, for numerical reasons, relatively small and high values are assigned to the capacity and HTC, respectively.

This simple approach has been found to work well for several test cases. However, for better numerical stability, alternative approaches for constructing the global multi-zone matrix will be investigated.

Based on Equation (4.9), the dynamics of all wall temperatures are expressed as

$$\tilde{C}_W \dot{\vec{T}}_W = \tilde{H}_{WW} \vec{T}_W + \tilde{H}_{WZ} \vec{T}_Z + \vec{q}_W \tag{4.10}$$

where $\vec{T}_W = \left[(\vec{T}_w^1)^T \ (\vec{T}_w^2)^T, \ ...(\vec{T}_w^{Nz})^T, \vec{T}_C \right]^T$ is the set of all wall temperatures and connections belonging to the multi-zone building.

State-Space Representation of Zone Air Balance

To complete the state-space representation of a multi-zone building, the dynamics of zone air temperatures need to be included. Heat fluxes to an air control volume within a zone can be categorized as follows.

- Ventilation
- Infiltration
- Air mixing among rooms
- Convective internal source due to computers, occupants, lights, etc.
- Convective heat exchange between a zone air and its surrounding walls

The balance equation for the Ith zone is

$$\rho^I C_V^I V^I \frac{\partial T_z^I}{\partial t} = \dot{Q}_{cv} + \dot{Q}_{cpl}^I + \dot{Q}_{inf}^I + \dot{Q}_S^I + \dot{Q}_{vent}^I \tag{4.11}$$

where

$\dot{Q}_{cv} = \sum_{i=1}^{Nw(I)} h_{cv,in}^i A_i (T_n^i - T_z^I) =$ convective heat transfer from the surfaces to the Ith zone air [W]

$\dot{Q}_{cpl}^I = \sum_{J=1}^{Nz} \dot{m}_{IJ} C_p (T_z^J - T_z^I)$ = heat transfer due to inter-zone air mixing (coupling of zone air) [W]

$\dot{Q}_{inf}^I = \dot{m}_{inf}^I C_p (T_a - T_z^I)$ = heat transfer due to infiltration [W]

$\dot{Q}_S^I$ = convective internal sources inside the Ith zone [W]

$\dot{Q}_{vent}^I$ = ventilation to Ith zone [W]

The final state-space representation for the multi-zone thermal network considering all walls and zone temperatures is shown below with the derivation presented in appendix 4.A.2.

$$\begin{bmatrix} \tilde{C}_W & 0 \\ 0 & \tilde{C}_Z \end{bmatrix} \begin{bmatrix} \dot{\vec{T}}_W \\ \dot{\vec{T}}_Z \end{bmatrix} = \begin{bmatrix} \tilde{H}_{WW} & \tilde{H}_{WZ} \\ \tilde{H}_{ZW} & \tilde{H}_{ZZ} \end{bmatrix} \begin{bmatrix} \vec{T}_W \\ \vec{T}_Z \end{bmatrix} + \begin{bmatrix} \vec{q}_W \\ \vec{Q}_Z \end{bmatrix} \tag{4.12}$$

The physical meaning of different terms is summarized as follows.

$\tilde{C}_W \in R^{(Nz \cdot Nw \cdot nnod + Nc) \times (Nz \cdot Nw \cdot nnod + Nc)}$ = thermal capacitance matrix for wall nodes per unit area [J/K-m^2]

$\tilde{C}_Z \in R^{Nz \times Nz}$ = thermal capacitance matrix of zone air [J/K]

$\tilde{H}_{WW} \in R^{(Nz \cdot Nw \cdot nnod + Nc) \times (Nz \cdot Nw \cdot nnod + Nc)}$ = HTC matrix describing heat transfer between wall nodes and other walls, zone air, sky and ground via convection, radiation and conduction [W/m^2-K]

$\tilde{H}_{WZ} \in R^{(Nz \cdot Nw \cdot nnod + Nc) \times Nz}$ = HTC matrix describing how zone air temperatures affect the wall temperatures [W/m^2-K]

$\tilde{H}_{ZW} = \tilde{H}_{cv,z} + \tilde{H}_{cpl} + \tilde{H}_{\inf} \in R^{Nz \times (Nz \cdot Nw \cdot nnod + Nc)}$ HTC matrix describing how wall temperatures affect on zone air temperatures via convection [W/K]

$\tilde{H}_{ZZ} \in R^{Nz \times Nz}$ = HTC matrix describing inter-zone air mixing, heat transfer from a zone to walls and infiltration [W/K]

$\vec{q}_W \in R^{(Nz \cdot Nw \cdot nnod + Nc)}$ = heat flux input assigned to all wall nodes [W/m^2]

The set of all heat fluxes into all wall nodes in the Ith zone is

$$\vec{q}_W = \begin{bmatrix} (\vec{q}_w^{\,1})^T & .. & (\vec{q}_w^{\,Nz})^T & \mathbf{0}^T \end{bmatrix}^T \text{ and } \vec{q}_w^{\,I} = \begin{bmatrix} (\vec{q}_1^{\,I})^T & .. & (\vec{q}_n^{\,I})^T \end{bmatrix}^T$$

where each term is defined by

$$q_1^i = h_{cv,ex}^i T_a + 4\sigma \epsilon_1^i (F_{sky}^i \overline{T_{sky}^3} T_{sky} + F_{grd}^i \overline{T_{grd}^3} T_{grd}) + \alpha_1^i q_{SWR}^i$$

$$\vec{q}_j \equiv \begin{bmatrix} q_{\dot{g}en}^1 \\ q_{\dot{g}en}^2 \\ .. \\ q_{\dot{g}en}^{Nw} \end{bmatrix}$$

$$\vec{q}_n \equiv \tilde{A}^{-1} \vec{h}_o$$

The inputs assigned to the wall nodes consist of heat fluxes due to the outdoor air temperature, sky and ground temperatures, short-wave solar radiation, and internal radiative sources.

For the zone air,

$\vec{Q}_Z \in R^{Nz}$ = heat flow rate input assigned on the zone airs [W].

This term includes ventilation, convective internal sources and infiltration.

$$(\vec{Q}_Z)_I = \dot{Q}_S^I + \dot{m}_{inf}^I C_p T_a + \dot{Q}_{vent}^I$$

Input Vector Formulation with Radiant Sources

When constructing the thermal network in the form of $\dot{x} = Ax + Bu$ from Equation (4.11), the size of the B matrix will be same as the size of $A \in R^{(Nz \cdot Nw \cdot nnod + Nc + Nz) \times (Nz \cdot Nw \cdot nnod + Nc + Nz)}$.

$$\begin{bmatrix} \dot{\vec{T}}_W \\ \dot{\vec{T}}_Z \end{bmatrix} = \begin{bmatrix} \tilde{C}_W & 0 \\ 0 & \tilde{C}_Z \end{bmatrix}^{-1} \begin{bmatrix} \tilde{H}_{WW} & \tilde{H}_{WZ} \\ \tilde{H}_{ZW} & \tilde{H}_{ZZ} \end{bmatrix} \begin{bmatrix} \vec{T}_W \\ \vec{T}_Z \end{bmatrix} + \begin{bmatrix} \tilde{C}_W & 0 \\ 0 & \tilde{C}_Z \end{bmatrix}^{-1} \begin{bmatrix} \vec{q}_W \\ \vec{Q}_Z \end{bmatrix}$$

Since the heat sources inside the wall are zero except for the case of radiant floor heating and cooling, the matrix size B can be dramatically reduced by introducing the following simple transformation.

$$\begin{bmatrix} \vec{q}_W \\ \vec{Q}_Z \end{bmatrix} = \tilde{T} \begin{bmatrix} \vec{q}_{EI} \\ \vec{Q}_Z \end{bmatrix}$$

where

$$\vec{q}_{EI} \equiv \begin{bmatrix} \vec{q}_{ei}^{\,1} \\ .. \\ \vec{q}_{ei}^{\,Nz} \end{bmatrix} \in R^{2 \cdot Nw \cdot Nz} \text{ and } \vec{q}_{ei}^{\,I} = \begin{bmatrix} \vec{q}_1^{\,I} \\ \vec{q}_n^{\,I} \end{bmatrix} \in R^{2 \cdot Nw}$$

which represents the group of heat fluxes assigned at the external and interior walls of the Ith zone and $\tilde{T} \in R^{(Nz \cdot Nw \cdot nnod + Nc + Nz) \times (2 \cdot Nw \cdot Nz + Nz)}$ is the corresponding transformation.

Electronic or hydraulic radiant floor heating and cooling systems can be treated as uniform surface heat (current) sources under the assumption that the heat flux from the system over the wall surface is uniform. For the case of a wall source, the source term is added at the end of the input as

$$\begin{bmatrix} \vec{q}_{ei}^{\,1} & .. & \vec{q}_{ei}^{\,Nz} & \vec{Q}_Z & q_{gen} \end{bmatrix}^T$$

For example if a radiant floor is installed at middle of the ith wall in the Ith zone, a term is added as follows.

$$\vec{u}^T = \begin{bmatrix} \vec{q}_{ei}^{\,1} & .. & \vec{q}_{ei}^{\,Nz} & \vec{Q}_Z & q_{gen}^{(Iz,iw,nnod/2)} \end{bmatrix}^T$$

where $q_{gen}^{(Iz,iw,nnod/2)}$ is a heat flux source [W/m^2] at the middle of the ith wall in the Ith zone.

In this case, the corresponding transformation can be changed to

$$\tilde{T}' = \left[\begin{array}{c|c} & 0 \\ & .. \\ \tilde{T} & 1 \\ & .. \\ & 0 \end{array}\right] \in R^{(Nz\cdot Nw\cdot nnod+Nc+Nz)\times(2\cdot Nw\cdot Nz+Nz+1)} \quad \text{in order to make} \quad \begin{bmatrix} \vec{q}_W \\ \vec{Q}_Z \end{bmatrix} = \tilde{T}'\vec{u}\,.$$

Output Matrix Formulation including Mean Radiant Temperature

Various output matrices, $\tilde{C}$, which map states ($x(t) \in R^n$) to outputs ($y(t) \in R^{n_o}$), are possible depending on the quantities of interests. For example, when the zone air temperatures are of interest, the corresponding output matrix is

$$\vec{T}_Z = [\ \mathbf{0} \quad .. \quad \mathbf{0} \quad \mathbf{0} \quad I_{Nz}] \begin{bmatrix} \vec{T}_W \\ \vec{T}_Z \end{bmatrix}$$

The mean radiant temperature (MRT) is a necessary input to evaluate occupant thermal comfort. Various approaches are possible to calculate MRT but a simple area-weighted mean radiant temperatures is employed here for simplicity.

$$T_{MRT} \approx \sum_{i=1}^{Nw(Iz)} \frac{A_i T_n^i}{A_{tot}}\,.$$

In this case, the output matrix is formulated as

$$T_{MRT}(Iz) \approx \begin{bmatrix} \mathbf{0} & .. & \begin{bmatrix} \mathbf{0} & .. & \begin{bmatrix} \frac{A_1}{A_{tot}(Iz)} & \frac{A_2}{A_{tot}(Iz)} & .. & \frac{A_{Nw(Iz)}}{A_{tot}(Iz)} \end{bmatrix} \end{bmatrix} & . \ . \ . & \mathbf{0} \end{bmatrix} \begin{bmatrix} \vec{T}_W \\ \vec{T}_Z \end{bmatrix}$$

The final state-space formulation for a multi-zone thermal network is

$$\begin{bmatrix} \dot{\vec{T}}_w \\ \dot{\vec{T}}_z \end{bmatrix} = \begin{bmatrix} \tilde{C}_w & 0 \\ 0 & \tilde{C}_z \end{bmatrix}^{-1} \begin{bmatrix} \tilde{H}_{ww} & \tilde{H}_{wz} \\ \tilde{H}_{zw} & \tilde{H}_{zz} \end{bmatrix} \begin{bmatrix} \vec{T}_w \\ \vec{T}_z \end{bmatrix} + \begin{bmatrix} \tilde{C}_w & 0 \\ 0 & \tilde{C}_z \end{bmatrix}^{-1} \tilde{T}'\vec{u}$$
$$\vec{y} = \tilde{C} \begin{bmatrix} \vec{T}_w \\ \vec{T}_z \end{bmatrix} + \tilde{D}\vec{u} \tag{4.13}$$

Some advantages of this modeling representation are:

- Based on the compact state-space representation of equation 4.13, various model reduction techniques can be readily utilized to construct a reduced-order building model. In order to reduce the number of states while keeping the input-output behavior, techniques based on balanced realization[11] are applied. The reduced form is a linear state-space representation that can be readily utilized in an optimal control formulation. The next section provides some case studies for this approach that demonstrate the ability to significantly reduce the number of states and computational requirements to achieve accurate predictions.

- Compared to a system identification method, this approach starts from a detailed physical description and can provide a more reliable and robust model.

- The physics based multi-zone building model lends itself to application of control theory to investigate system properties and to evaluate control performance with the help of control toolkits such as Matlab/Simulink. For example, the system time constant, DC gain under various control inputs, frequency response, stability, controllability and observability can easily be investigated.

- Parameter studies involving physical parameters are possible since it is not a black box model identification method. As a result, the modeling approach could be used as part of a retrofit analysis that involves both physical and control changes.

- The modeling approach is general for any shaped building (i.,e., not restricted to rectangular shapes of walls) because it is developed using the radiosity method that incorporates view factors that can be determined for any geometry.

- Individual wall elements can be divided into separate smaller elements to facilitate coupling to a CFD model for the indoor environment. This is appropriate when surface temperatures along a wall vary significantly due to solar or other non-uniform inputs.

- The system of equations is continuous in time and not restricted to a fixed time step. Variable time-step algorithms can be employed, which is helpful in handling different time scale problems that are inherent for building systems.

- Various source terms such as radiant heating and cooling can be treated easily.

4.4 Model Order Reduction (MOR) of Thermal Building Network

4.4.1 Categories of MOR techniques

MOR techniques can be grouped into three categories:

- Polynomial reduction methods.
- State-space transformation-based techniques
- System identification method

Polynomial reduction methods are applied to transfer functions in the frequency domain and have low computational requirement.

State-space transformation relies on a balanced model reduction technique proposed by Moore[12]. The approach is based on the evaluation of the stability of different state coordinate selections in the full order model and on the selection of a reduced-order model maintaining, as much as possible, the original model properties (time response, observability, controllability, closed-loop performance[4]. The first step is to find a transformation that balances the observability/controllability gramians to determine which states have the greatest contribution to the input–output behavior. The second step is to construct and to perform a Galerkin projection based on the largest singular values of the balanced gramians for the region of interest in the space of states[7].

System identification aims at generating a model of a physical system from observations (measurements or simulation predictions). Contrary to the first two methods, this approach belongs to the category of black box models since it does not rely on "first principles".

4.4.2 Model Order Reduction Method and Test Case Results

The state-space transformation method has been chosen for this study because of its advantages and since the building envelope model lends itself to a linearized state-space representation of the following form.

$$\dot{\vec{T}} = \tilde{A}\vec{T} + \tilde{B}\vec{u}$$
$$\vec{y} = \tilde{C}\vec{T}$$

The main additional assumption in constructing a reduced-order building model is constant heat transfer coefficients. Various algorithms for building a lower-order model have been developed and the "Square -root method for Balanced Truncation Model Reduction"[13] was chosen for this problem. However, the investigation of other reduced-order algorithms is ongoing.

Various cases including multi-layer, multi-zone cases with windows have been investigated. For validation of the original and the reduced-order models, TRNSYS Version 16.01.0003 was utilized. Two example case studies are presented in this section.

Case Study 1

The main purpose of this case study was initial code validation. The building description is summarized in Figure 4.6.

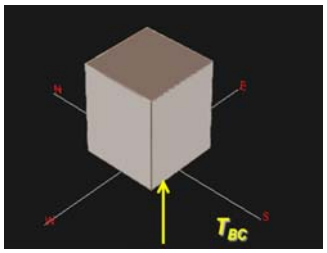

- Indiana TMY2 weather data (1st of Jan to 31st of Jan)
- 10 by 10 by 10 [m] building
- Single zone
- Wall construction is concrete.
- Ground temperature fixed at -1 ºC
- No windows, no internal sources, no ventilation

Figure 4.6. Input data for simple reduced-order modeling case study

In order to construct a linear time invariant system, average values of T_{sky}, T_{grd} and T_w are needed for linearization of the radiation heat transfer coefficient and are determined prior to simulation. The average sky and air temperature were determined from the TMY2 weather file, whereas the mean external wall temperature was set to 5 ºC. To generate an accurate model, 17 nodes per wall were assigned or 103 (17×6+1) total nodes for the zone. A reduced-order model was found having 8 states. Model output comparisons between TRNSYS, the full-order and the reduced- order model are shown in Figure 4.7.

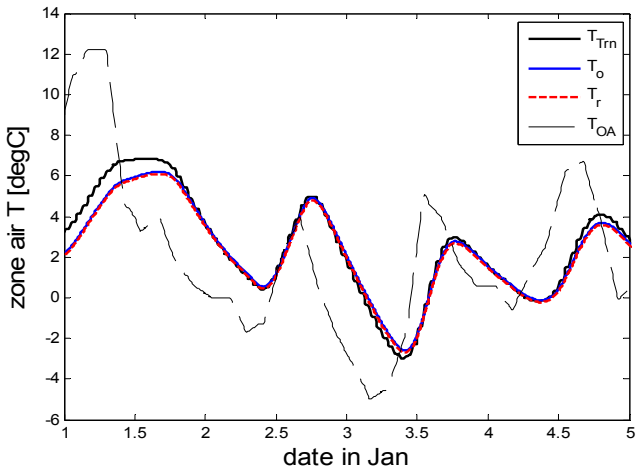

T_{Trn} (Black solid line): zone air temperature profile generated by TRNSYS.

T_o (Blue solid line) : zone air temperature profile generated by full-order linearized model

T_r (Red dashed line): zone air temperature profile generated by reduced-order model

T_{OA} (Black dashed line): outdoor air temperature

Figure 4.7. Comparisons of TRNSYS, full-order, and reduced-order state-space models

The original and reduced-order model produce nearly identical results and agree very closely with the TRNSYS output for this simple case study. Furthermore, the computing time for this month simulation was approximately half for the reduced-order model compared to the original model.

To further test the validity of the reduced-order model, the responses under PID controller were compared in SIMULINK environment. The SIMULINK implementation is shown in Figure 4.8

with results presented in Figure 4.9. A zone air temperature setpoint of 22ºC was used and appropriate controller gains were chosen. The closed-loop response is nearly identical for the two models, but the reduced-order model requires about half the computation. Greater computational savings would be expected for more complicated case studies. More detailed analyses to understand limitations of the reduced-order modeling is underway using step responses, impulse responses, and Bode or singular value plots.

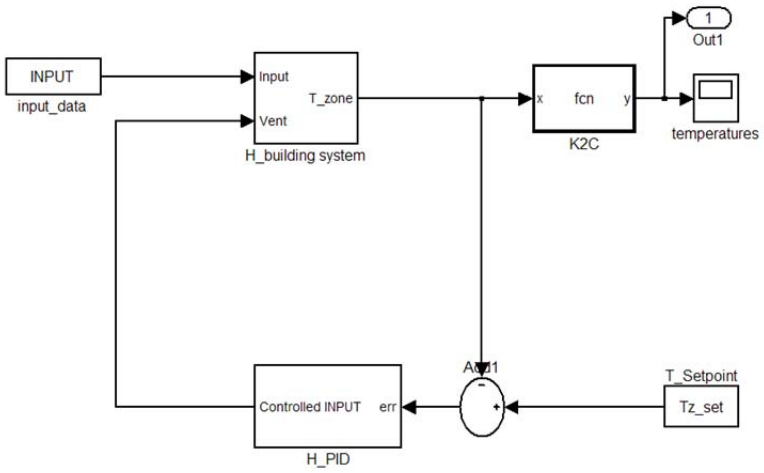

Figure 4.8 SIMULINK model

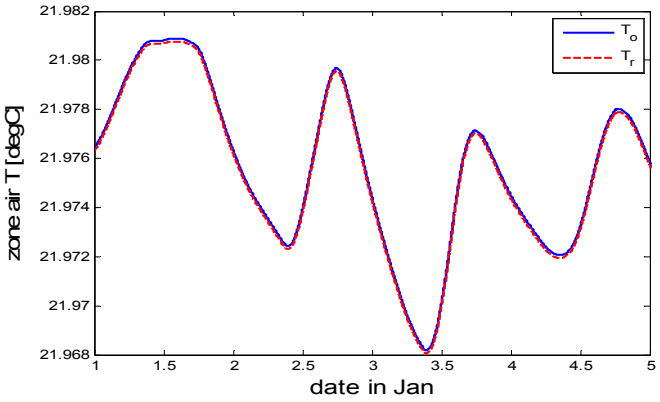

Figure 4.9, Closed-loop response comparisons for PID control example

Case Study 2

In order to test the performance of the reduced-order model for the case of a multi-zone building with walls having multiple layers, the simple two-zone building described in Figure 4.9 was considered. The zone colored in gray has 6 walls and each wall consists of three layers. The brown zone has also 6 walls but each wall consists of only one layer, which is concrete. Different boundary conditions were applied to the zones. It was located in Indianapolis and TMY2 weather

data was used. For testing the reduced-order model, both free-floating temperature and closed-loop response with a PID controller were simulated in SIMULINK.

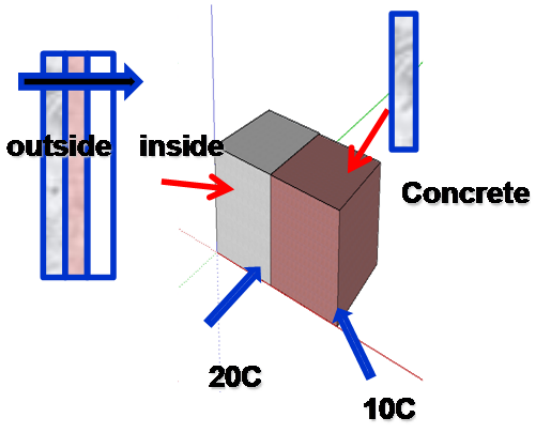

Material properties of layers

	Concrete Layter	Insulation Layer	Gypsum Layer
ρ[kg/m3]	2400	288.33	800.92
k[W/mK]	2.1	0.055	0.16
Cv[J/kgK]	800	1297.9	837
t[m]	0.025	0.029	0.013

Figure 4.9. Multi-zone test case for reduced-order model

Results are shown in Figures 4.10 and 4.11. The solid line and the dotted line represent the original and reduced-order models, respectively. The X axis is "day" from January 1st to 5th and the Y axis is "zone air temperature" in degree C. The blue and green lines are the time histories of zone air temperatures of the gray and brown zones depicted in Figure 4.9. The original model had 303 states, whereas the reduced-order model had 14 states that were selected based on the Hankel singular values. The computation time for a one-month simulation was reduced by a factor of about 10 for the reduced-order model compared to the full-order model for this case study. Furthermore, as demonstrated in Figures 4.10 and 4.11, the reduced-order model provides dynamic response that is quite similar to the full-order model for both zones.

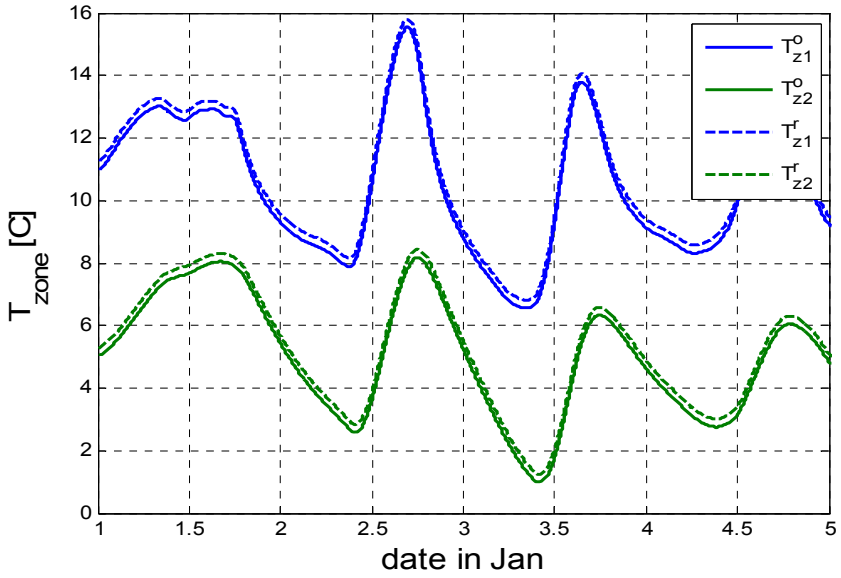

Figure 4.10. Free-floating temperature history without any controller

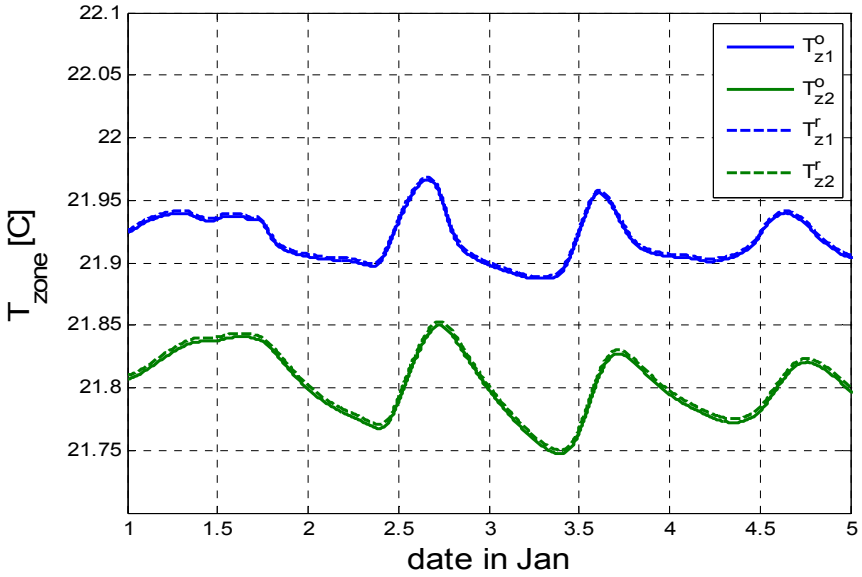

Figure 4.11. Temperature history with PID controller, 10 degree C setpoints

Another case study for the Purdue Living Lab #1 was performed and results are presented in Section 6.

4.5 References

1. J. Casillas, O. Cordón, F. Herrera, L. Magdalena, "Interpretability issues in fuzzy modeling",Vol. 128 of Studies in Fuzziness and Soft Computing, Springer, 2003

2. T. Kusuda, "Computer program for heating and cooling loads in buildings", NBSIR 74-574 National

Bureau of Standards, 1974

3. ASHRAE Fundamentals, 29.22, 1997
4. M. Wetter, "Multizone building model for thermal building simulation in modelica", *5th International Modelica Conference*, 2006
5. M.M. Goudaa, S. Danahera, C.P. Underwoodb , "Building thermal model reduction using nonlinear constrainedoptimization", *Building and Environment*, 37 , 2002
6. C. Menezo, J.J. Roux, J. Virgone, "Modelling heat transfers in building by couplingreduced-order models", *Building and Environment*,37 , 133–144, 2002
7. S. Lall, J.E. Marsden, S. Glavaski, "A subspace approach to balanced truncation for model reduction of nonlinear control system", *International Journal of Robust and Nonlinear control*, 2000
8. J. Hahn, T.F. Edgar, "An improved method for nonlinear model reduction usingbalancing of empirical gramians", *Computers and Chemical Engineering*, 26, 1379–1397, 2002
9. J.R. Phillips, "Projection-based approaches for model reduction of weakly nonlinear, time-varying systems", *IEEE Transactions On Computer-Aided Design Of Integrated Circuits And Systems*, vol. 22, no. 2, 2003
10. C. Menezo, J.J. Roux, J. Virgone, "modelling heat transfers in building by coupling reduced-order models", *Building and Environment*, 37, 133–144, 2002
11. M. Green, D.J. Limebeer, "Linear robust control", Prentice hall information and system science series
12. B.C. Moore, "Principal component analysis in linear systems: controllability, observability, and model reduction", *IEEE Transactions on Automatic Control*, vol. AC-26, NO. 1, 1981
13. M.G. Safonov, R.Y. Chiang, "A schur method for balanced model reduction", *IEEE Transactions on Automatic Control*, Vol. 34, No. 7, 1989

4.A Appendix

4.A.1 Linear Approximation of Radiative Interaction between Inside Surfaces

Assumptions

- Gray, diffuse and opaque surface.
- Idealized enclosure.

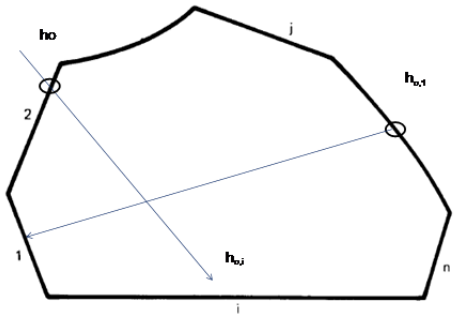

Definitions

q_i = net radiative heat flux leaving from ith surface
J_i = radiocity from ith surface
G_i = irradiation onto ith surface
$E_{b,i}$ = black body emission from ith surface
$H_{o,i}$ = external radiation arriving at ith surface
F_{ij} = view factor from i to j surface.

From the definition of radiosity

$$q_i = J_i - G_i \tag{4.A.1}$$

From the mechanisms of radiosity and the assumption of an opaque surface,

$$J_i = \rho_i G_i + \epsilon_i E_{b,i} \tag{4.A.2}$$

From the definition of view factor and the equality of $F_{ij}A_j = F_{ji}A_i$,

$$G_i = \sum_{j=1}^{N} F_{ij} J_j + H_{o,i} \tag{4.A.3}$$

Equations (4.A.1) and (4.A.2) result in

$$\frac{\rho_i q_i}{\epsilon_i} = -J_i + E_{b,i} \tag{4.A.4}$$

Here, the relationship of $1-\rho=\alpha$ for opaque surfaces has been used.

Equations (4.A.2) and (4.A.3) result in

$$J_i - \rho_i \sum_{j=1}^{N} F_{ij} J_j = \rho_i H_{o,i} + \epsilon_i E_{b,i}$$

Using the Kronecker delta, the above equation becomes

$$\sum_{j=1}^{N} (\delta_{ij} - \rho_i F_{ij}) J_j = \rho_i H_{o,i} + \epsilon_i E_{b,i}$$

For simplicity, let $A_{ij} \equiv \delta_{ij} - \rho_i F_{ij}$. Then,

$$\sum_{j=1}^{N} A_{ij} J_j = \rho_i H_{o,i} + \epsilon_i E_{b,i} \tag{4.A.5}$$

By multiplying Equation (4.A.4) with A_{ij} and summing over all surfaces, the radiosity in Equation (4.A.4) is eliminated using Equation (4.A.5). The detailed formulation is as follows.

$$\begin{aligned}\sum_{j=1}^{N} A_{ij}\frac{\rho_j q_j}{\epsilon_j} &= -\sum_{j=1}^{N} A_{ij}J_j + \sum_{j=1}^{N} A_{ij}E_{b,j} \\ &= -\rho_i H_{o,i} - \epsilon_i E_{b,i} + \sum_{j=1}^{N} A_{ij}E_{b,j} \\ &= -\rho_i H_{o,i} + \sum_{j=1}^{N} (A_{ij} - \epsilon_i\delta_{ij})E_{b,j} \\ &= -\rho_i H_{o,i} + \sum_{j=1}^{N} (\rho_i\delta_{ij} - \rho_i F_{ij})E_{b,j} \quad (\because \epsilon = \alpha)\end{aligned}$$

or

$$\sum_{j=1}^{N} A_{ij}\frac{\rho_j q_j}{\epsilon_j \rho_i} = -H_{o,i} + \sum_{j=1}^{N} (\delta_{ij} - F_{ij})E_{b,j}\,.$$

The right-hand-side can be further simplified as

$$\begin{aligned}\sum_{j=1}^{N} (\delta_{ij} - \rho_i F_{ij})\frac{\rho_j q_j}{\epsilon_j \rho_i} &= \sum_{j=1}^{N} (\delta_{ij}\frac{\rho_j q_j}{\epsilon_j \rho_i} - \rho_i F_{ij}\frac{\rho_j q_j}{\epsilon_j \rho_i}) \\ &= \sum_{j=1}^{N} (\frac{\delta_{ij} q_j}{\epsilon_j} - F_{ij}\frac{\rho_j q_j}{\epsilon_j}) \\ &= \sum_{j=1}^{N} (\frac{\delta_{ij}}{\epsilon_j} - F_{ij}\frac{\rho_j}{\epsilon_j})q_j\end{aligned}$$

Finally we obtain the net radiative flux as a function of surface temperatures and external sources.

$$\sum_{j=1}^{N} (\frac{\delta_{ij}}{\epsilon_j} - F_{ij}\frac{\rho_j}{\epsilon_j})q_j = \sum_{j=1}^{N} (\delta_{ij} - F_{ij})E_{b,j} - H_{o,i} \tag{4.A.6}$$

However the black body emission term is nonlinear and a linear approximation is preferred leading to

$$\sum_{j=1}^{N}(\delta_{ij}-F_{ij})E_{b,j}=\sigma\sum_{j=1}^{N}(\delta_{ij}-F_{ij})T_j^4=\sigma(T_i^4-\sum_{j=1}^{N}F_{ij}T_j^4)=\sigma(\sum_{j=1}^{N}F_{ij}T_i^4-\sum_{j=1}^{N}F_{ij}T_j^4)=\sigma\sum_{j=1}^{N}F_{ij}(T_i^4-T_j^4)$$

$$\approx 4\sigma\bar{T}^3\sum_{j=1}^{N}F_{ij}(T_i-T_j)=4\sigma\bar{T}^3(T_i-\sum_{j=1}^{N}F_{ij}T_j)$$

$$=4\sigma\bar{T}^3\sum_{j=1}^{N}(\delta_{ij}-F_{ij})T_j$$

Equation (4.A.6) with the linear approximation of black body emission gives

$$\sum_{j=1}^{N}(\frac{\delta_{ij}}{\epsilon_j}-F_{ij}\frac{\rho_j}{\epsilon_j})q_j=4\sigma\bar{T}^3\sum_{j=1}^{N}(\delta_{ij}-F_{ij})T_j-H_{o,i}$$

By letting $\tilde{A}_{ij}\equiv\frac{\delta_{ij}}{\epsilon_j}-\frac{\rho_j}{\epsilon_j}F_{ij}$, $\tilde{B}'_{ij}\equiv 4\sigma\bar{T}^3\sum_{j=1}^{N}(\delta_{ij}-F_{ij})$, $(\vec{h}_o)_i\equiv H_{o,i}$ we can get

$$\vec{q}=\tilde{A}^{-1}[\tilde{B}'\vec{T}-\vec{h}_o]$$

4.A.2 State-Space Representation of Zone Air Balance

For any I[th] zone, the energy balance equation is

$$\rho^I C_V^I V^I\frac{\partial T_z^I}{\partial t}=\dot{Q}_{cv}+\dot{Q}_{cpl}^I+\dot{Q}_{inf}^I+\dot{Q}_S^I+\dot{Q}_{vent}^I$$

where,

$\dot{Q}_{cv}=\sum_{i=1}^{Nw(I)}h_{cv,in}^i A_i(T_n^i-T_z^I)$ = convective heat transfer from the surfaces to I[th] zone air [W]

$\dot{Q}_{cpl}^I=\sum_{J=1}^{Nz}\dot{m}_{IJ}C_p(T_z^J-T_z^I)$ = heat transfer due to inter-zone air mixing (zone air coupling) [W]

$\dot{Q}_{inf}^I=\dot{m}_{inf}^I C_p(T_a-T_z^I)$ = heat transfer due to infiltration [W]

$\dot{Q}_S^I$ = convective internal source inside the I[th] zone [W]

$\dot{Q}_{vent}^I$ = ventilation to I[th] zone [W]

Let

$$\tilde{C}_Z \equiv \begin{bmatrix} \rho^1 C_V^1 V^1 & & & 0 \\ & \rho^2 C_V^2 V^2 & & \\ & & .. & \\ 0 & & & \rho^{Nz} C_V^{Nz} V^{Nz} \end{bmatrix} \text{ and } \vec{T}_Z \equiv \begin{bmatrix} T_z^1 \\ T_z^2 \\ .. \\ T_z^{Nz} \end{bmatrix}$$

The convective heat exchange between a zone air and its surrounding walls is

$$\dot{Q}_{cv}^I = \sum_{i=1}^{Nw(I)} h_{cv,in}^i A_i (T_n^i - T_z^I) = [\mathbf{0}^T \ \mathbf{0}^T \ .. \ (\vec{H}_{cv,in}^I)^T] \vec{T}_w^I - (\sum_{i=1}^{Nw(I)} h_{cv,in}^i A_i) T_z^I \equiv (\hat{H}_{cv,in}^I)^T \vec{T}_w^I - (\sum_{i=1}^{Nw(I)} h_{cv,in}^i A_i) T_z^I$$

where $\vec{H}_{cv,in}^I \in R^{Nw(I)}$ and $(\vec{H}_{cv,in}^I)^T = [h_{cv,in}^{1(I)} A_{1(I)}, h_{cv,in}^{2(I)} A_{2(I)}, ..., h_{cv,in}^{Nw(I)} A_{Nw(I)}]$.

By letting

$$\tilde{H}_{cv,z} \equiv \begin{bmatrix} \sum_{i=1}^{Nw(1)} h_{cv,in}^i A_i & & & 0 \\ & \sum_{i=1}^{Nw(2)} h_{cv,in}^i A_i & & \\ & & .. & \\ 0 & & & \sum_{i=1}^{Nw(Nz)} h_{cv,in}^i A_i \end{bmatrix} \in R^{Nz \times Nz}$$

and

$$\tilde{H}_{ZW} \equiv \begin{bmatrix} [0\ 0\ (\vec{H}_{cv,in}^1)^T] & & \mathbf{0} & \mathbf{0} \\ & .. & & \\ \mathbf{0} & & [0\ 0\ (\vec{H}_{cv,in}^{Nz})^T] & \mathbf{0} \end{bmatrix} = \begin{bmatrix} (\hat{H}_{cv,in}^1)^T & & \mathbf{0} & \mathbf{0} \\ & .. & & \\ \mathbf{0} & & (\hat{H}_{cv,in}^{Nz})^T & \mathbf{0} \end{bmatrix} \in R^{Nz \times (Nz \cdot Nw \cdot nnod + Nc)}$$

then

$$\vec{Q}_{cv} = \tilde{H}_{ZW} \vec{T}_W - \tilde{H}_{cv,z} \vec{T}_Z = \begin{bmatrix} \tilde{H}_{ZW} & -\tilde{H}_{cv,z} \end{bmatrix} \begin{bmatrix} \vec{T}_W \\ \vec{T}_Z \end{bmatrix} \tag{4.A.7}$$

The air coupling between rooms can be expressed as

$$\dot{Q}_{cpl}^{I} = (\tilde{H}_{cpl}\vec{T}_z)_I \tag{4.A.8}$$

where $(\tilde{H}_{cpl})_{IJ} \equiv \dot{m}_{IJ}C_p(\delta_{IJ} - 1)$.

The infiltration is

$$\vec{Q}_{inf} = \vec{m}_{inf}C_pT_a - \tilde{H}_{inf}T_z^I \tag{4.A.9}$$

where

$$\tilde{H}_{\inf} \equiv \begin{bmatrix} \dot{m}_{inf}^1 C_p & & & \\ & \dot{m}_{inf}^2 C_p & & \\ & & .. & \\ & & & \dot{m}_{inf}^{Nz} C_p \end{bmatrix}$$

Gathering Equations (4.A.7), (4.A.8), and (4.A.9) results in the following matrix from.

$$\tilde{C}_Z\frac{d\vec{T}_Z}{dt} = \tilde{H}_{ZW}\vec{T}_W - (\tilde{H}_{cv,z} + \tilde{H}_{cpl} + \tilde{H}_{\inf})\vec{T}_Z + \vec{Q} \tag{4.A.10}$$

where $(\vec{Q})_I = \dot{Q}_S^I + \dot{m}_{inf}^I C_p T_a + \dot{Q}_{vent}^I$ and $\tilde{H}_{ZW} \in R^{Nz\times(Nz\cdot Nw\cdot nnod+Nc)}$, $\tilde{C}_Z, \tilde{H}_{xxZ}, \tilde{H}_{cpl}, \tilde{H}_{\inf} \in R^{Nz\times Nz}$.

From Equations (4.10) and (4.A.10),

$$\tilde{C}_W\dot{\vec{T}}_W = \tilde{H}_{WW}\vec{T}_W + \tilde{H}_{WZ}\vec{T}_Z + \vec{q}_W$$
$$\tilde{C}_Z\dot{\vec{T}}_Z = \tilde{H}_{ZW}\vec{T}_W - (\tilde{H}_{cv,z} + \tilde{H}_{cpl} + \tilde{H}_{\inf})\vec{T}_Z + \vec{Q}$$

The final form can be constructed by letting $\tilde{H}_{ZZ} = -(\tilde{H}_{cv,z} + \tilde{H}_{cpl} + \tilde{H}_{\inf})$

$$\begin{bmatrix} \tilde{C}_W & 0 \\ 0 & \tilde{C}_Z \end{bmatrix}\begin{bmatrix} \dot{\vec{T}}_W \\ \dot{\vec{T}}_Z \end{bmatrix} = \begin{bmatrix} \tilde{H}_{WW} & \tilde{H}_{WZ} \\ \tilde{H}_{ZW} & \tilde{H}_{ZZ} \end{bmatrix}\begin{bmatrix} \vec{T}_W \\ \vec{T}_Z \end{bmatrix} + \begin{bmatrix} \vec{q}_W \\ \vec{Q} \end{bmatrix}$$

5. Indoor-Air Environment Modeling

This is a summary of year 1 activities at Virginia Tech related to CFD modeling of the indoor environment for control purposes.

5.1 Overview

In Section 3 we introduced the notion of decomposing the building-energy model into building-envelope and indoor-air sub-systems. There we developed a transfer-function representation of the *Standard Model* wherein there is a single zone and m interior surfaces that are convectively coupled to the well-mixed indoor-air. In this section we develop an alternative indoor-air model based on Computational Fluid Dynamics (CFD) and model-order reduction. In particular, we stress a data-driven approach wherein time-accurate simulations of step-like changes to wall-surface temperatures are used to produce heat-load time-histories. The heat-load data are used to construct the *Markov parameters* of the wall-temperature to heat-load system. The resulting high-order transfer function is *optimally* approximated by a low-order system of specified order.

5.2 The Purdue Living Laboratory Radiant Room

The initial application for our work is the proposed *Purdue Living Laboratory Radiant Room*. A sketch of the facility, which is expected to be available in the Spring 2013, is shown in Figure 5.1. The room is $9.75 \times 9.75 \times 4.42\,\mathrm{m}$. For orientation, the $\min y$-wall faces South and contains a window. There are two half-round inlets on the East (West) walls, one quarter-round inlet in the North-East corner, and a flat, rectangular inlet on the (lower) North wall. There is a single return-vent on the upper North wall. The small square regions on the East, North and West wall are potential locations for temperature sensors. Other features, such as chilled-beams and radiant heating panels, are not shown in this figure. The horizontal lines on the walls, as well as the lines on the floor serve to partition the surfaces for purposes of specifying boundary temperatures. This is further clarified in Figure 5.2 where the various surface segments are assigned numeric labels $\{1,2,\ldots,19\}$.

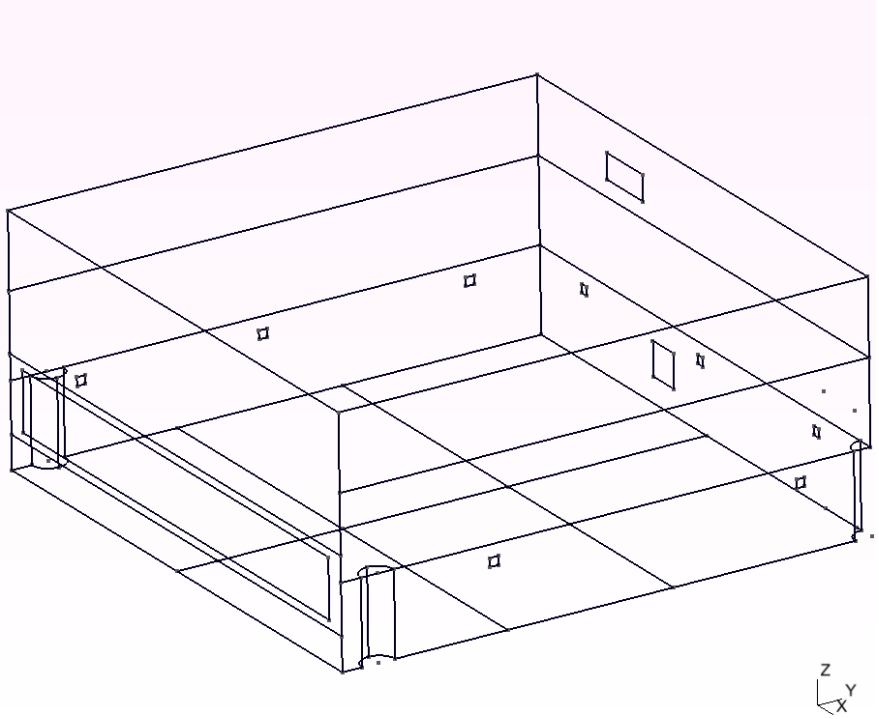

Figure 5.1. Sketch of Purdue Living Lab

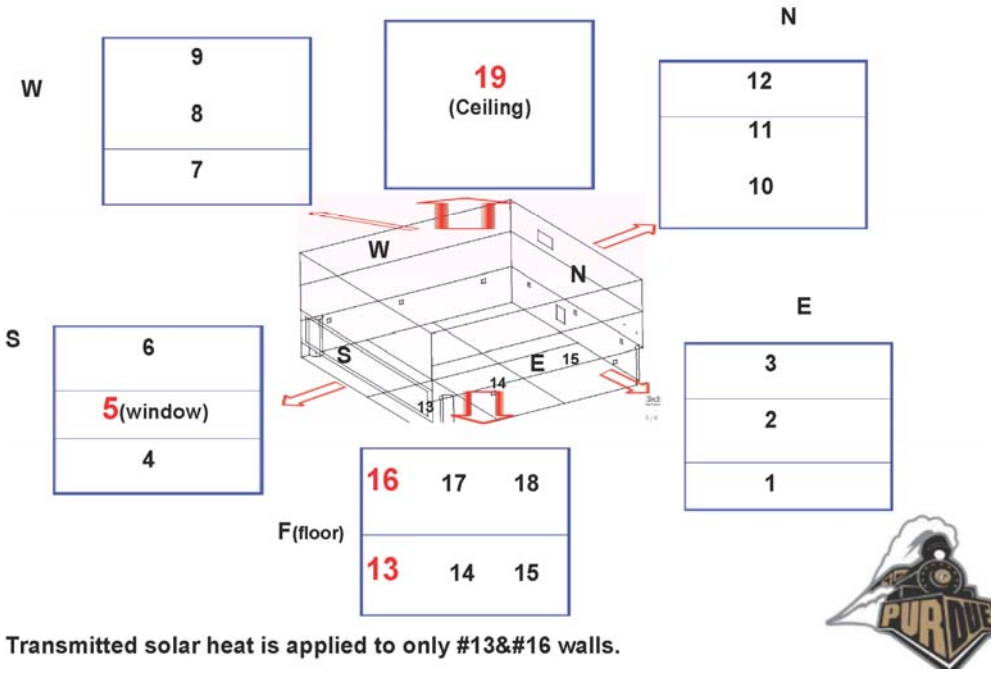

Figure 5.2. Purdue LL with wall zones

5.2.1 Continuum Model

The CFD model accounts for conservation of mass (dry-air & water-vapor), momentum, and energy. Viscous forces in the fluid are approximated using a $K-\epsilon$ turbulence model, and density change is treated in the Boussinesq approximation. A no-slip boundary condition is imposed on all solid surfaces, except the interior surfaces of the chilled-beam cooling zones wherein a body-force drag is imposed (see next section). Air is supplied, at a net-rate of 0.678 kg/s (≈ 20 cfm), through the four vents enumerated previously. The supply air is at $12.7^{o}C$, contains water vapor at 0.008 gm/gm.; the supply is apportioned among the inlets according to their surface area.

5.2.2 FLUENT

A finite-element tetrahedral grid (see Figure 5.3) was generated using the GMSH software (`http://geuz.org/gmsh`). The (24) yellow regions are *occupied zones* wherein one might be interested in human comfort metrics (temperature/humidity). These regions have no special effect on the dynamics. The horizontal (black) elements are (9) cloud-like structures that hold (29) chilled beams (green/brown).

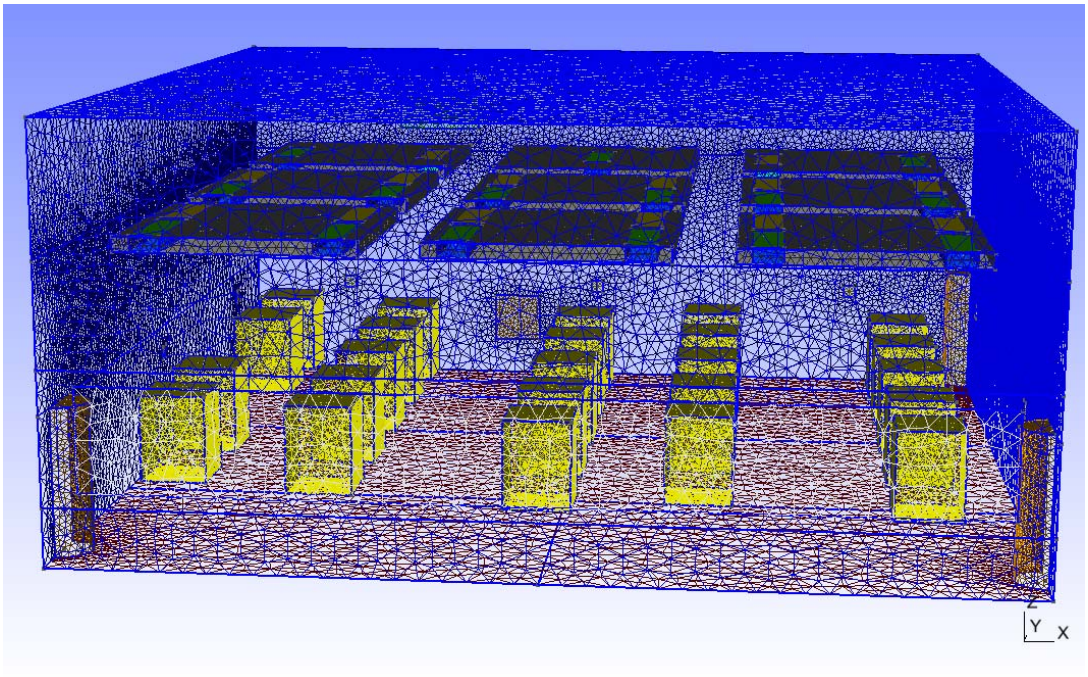

Figure 5.3. Purdue LL Grid

In FLUENT these are characterized as source zones for energy and w-momentum. Based on data from HALTON the active cooling zone of each chilled beam has a volume $0.04955\,\mathrm{m}^3$ and thermal energy is removed (cooling) at the rate

$$Q_{\text{vol}} = R \ \frac{\text{w}^3}{\text{m}} \ ,$$

where R is a specified cooling rate for a given chilled beam (here $200\,\text{w/m}^3 \approx 10\,\text{w/beam}$). The drag induced by the cross-flow tubes and associated fins is modeled as a z-force/unit volume as

$$Z(w) = \ C\,w^2 \ , \qquad \text{where } C = \begin{cases} \dfrac{-60\ \frac{N}{m^3}}{\left(\frac{m}{s}\right)^2} & : \ w \geq 0 \\ \\ \dfrac{6\ \frac{N}{m^3}}{\left(\frac{m}{s}\right)^2} & : \ w < 0 \ . \end{cases}$$

The numerical value for C with $w < 0$ is based on data from HALTON; the value for $w \geq 0$ implements a *trap-door feature* to inhibit upward flow through the chilled beam.

Pseudo Steady State

Surface temperatures for the 19[2] surfaces were fixed at average values from a building-envelope model coupled to a *Standard Model* for the indoor-air. These temperatures are shown in Table 5.1. A FLUENT run was re-started from an earlier case and run for an additional 60 minutes. Time histories for the volume-averaged and averaged-outflow temperatures are shown in Figure 5.4. Clearly, these temperatures approach and maintain steady values. The (19) surface heat loads were recorded; these serve as the nominal steady-state values. Note in Table 5.1 that the temperatures along any vertical surfaces are within a few tenths of a degree, whereas the fluxes vary by a factor of three or more. This variation suggests strong vertical gradients in the indoor-air. The increased fluxes on Floor_1 and Floor_2 arise from increased surface temperatures due to imposed solar heating.

[2]In the FLUENT model the South_2 and Window surfaces are distinct; South_2 (3.75 m^2) is an opaque surface that surrounds the Window (9.63 m^2).

	FLUENT *Name*	*Temp.* (^oC)	*Load* (w)	*Flux* w/m^2		FLUENT *Name*	*Temp.* (^oC)	*Load* (w)	*Flux* w/m^2
1	East_1	21.42	373.1	27.80	10	North_1	21.27	307.9	22.06
2	East_2	21.45	215.5	14.50	11	North_2	21.36	177.6	11.95
3	East_3	21.47	94.2	7.04	12	North_3	21.42	92.4	7.16
4	South_1	22.13	208.0	34.97	13	Floor_2	22.18	515.3	35.00
5	South_2	22.48	117.4	31.29	14	Floor_4	20.74	170.5	11.47
6	South_3	21.95	174.4	7.33	15	Floor_6	21.71	350.5	19.73
7	West_1	21.92	285.5	20.59	16	Floor_1	22.21	529.1	35.95
8	West_2	21.95	212.0	14.26	17	Floor_3	20.76	166.9	11.23
9	West_3	21.98	113.8	8.51	18	Floor_5	20.73	278.3	15.60
	Window	22.48	205.5	21.34	19	Ceiling	22.01	531.9	5.59

Table 5.1. Pseudo Steady-State Temperatures and Heat Loads

Step Response

For each of the 19 surfaces, we ran a FLUENT case wherein that temperature was subjected to a step-like change. The wall temperature was varied with time as shown in Figure 5.5 (for $t > 60$ s the temperature is maintained at $\approx 32^o$ C). This continuous change was used because FLUENT uses an iterative linear update and with such continuity in the boundary data only a few iterations were required for convergence.

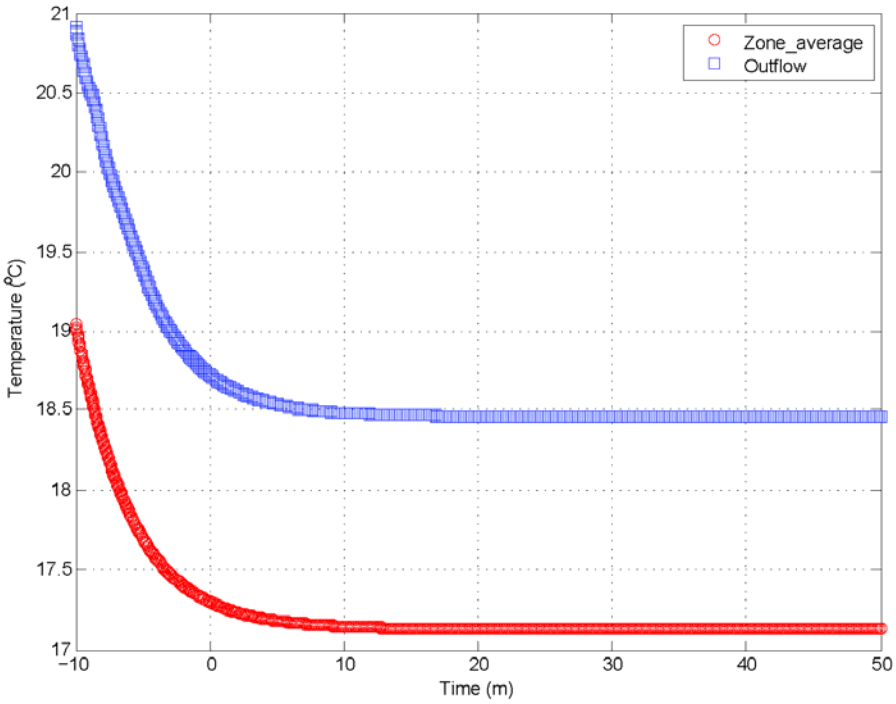

Figure 5.4. Time history of nominal case

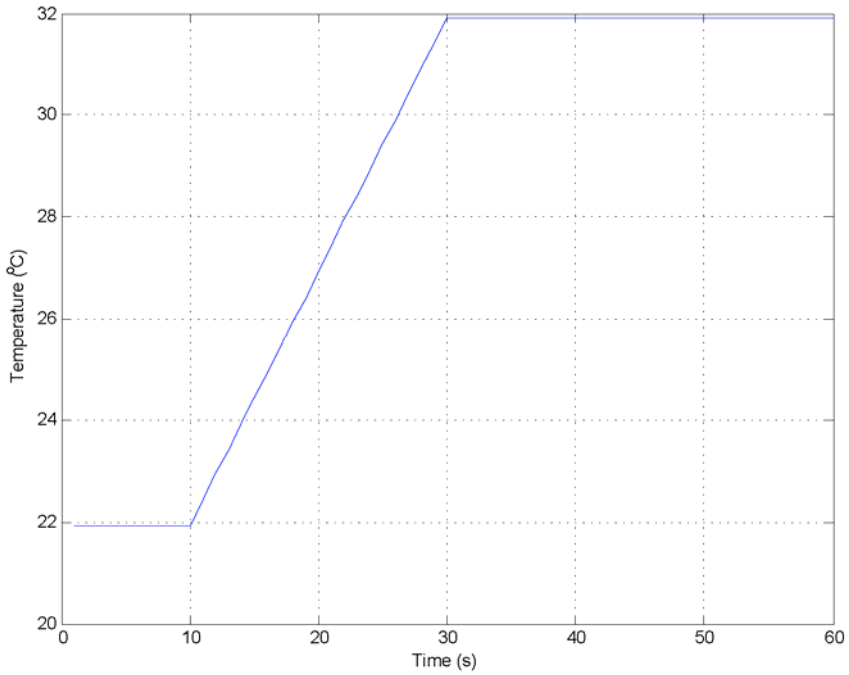

Figure 5.5. Applied change in West_1 temperature

Figure 5.6 displays time-histories of the heat load responses from the East, and West walls. As expected the response from the West_1 surface is most pronounced. The *Standard Model* prediction (see Section 3) for the steady-state change in the heat load on *West_1* due to a unit-change in its temperature is given by the appropriate diagonal element in $H^{\mathrm{std}}(0)$. Accordingly, the expected increase in heat load on *West_1* due to the 10^o C step in temperatures (see Section 3)

$$\Delta Q = (h\,A)_\iota \left[\frac{\sum_{k\neq i}(h\,A)_k}{\sum(h\,A)_k}\right] 10^o\ \mathrm{C} \approx 301\ \mathrm{w}\ ,$$

where we have used the steady-state $(h\,A)$ parameter-values from FLUENT. The actual increase is ≈ 517.6 w (see Table 5.1, Figure 5.6 - right).

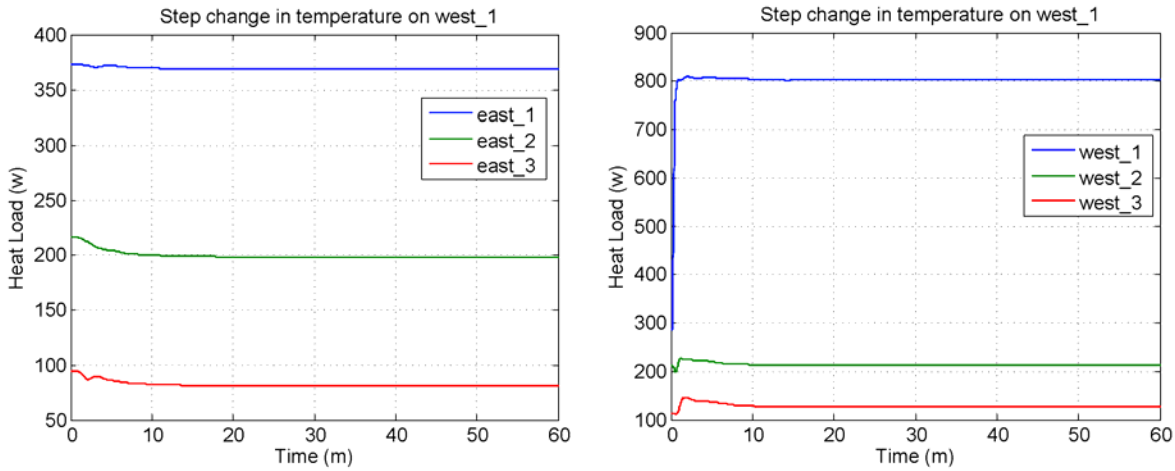

Figure 5.6. Heat loads from East & West surfaces: step change in $\boldsymbol{T}$-West_1

In Figure 5.7 (left) we compare the FLUENT prediction for the response in heat load from the *South_3* surface to a transient based on the single-zone time constant ($\tau = M/\sum_k (h\,A)_k \approx$ 11 minutes, see Section 3). Here we used the initial and final values for the heat-load from the FLUENT transient response, and the thermal capacitance (M) and heat transfer parameters ($h\,A$) from the steady-state FLUENT results. Whereas the results are qualitatively similar, the FLUENT transient is seen to respond somewhat faster, and has additional ripples, suggesting added dynamic modes.

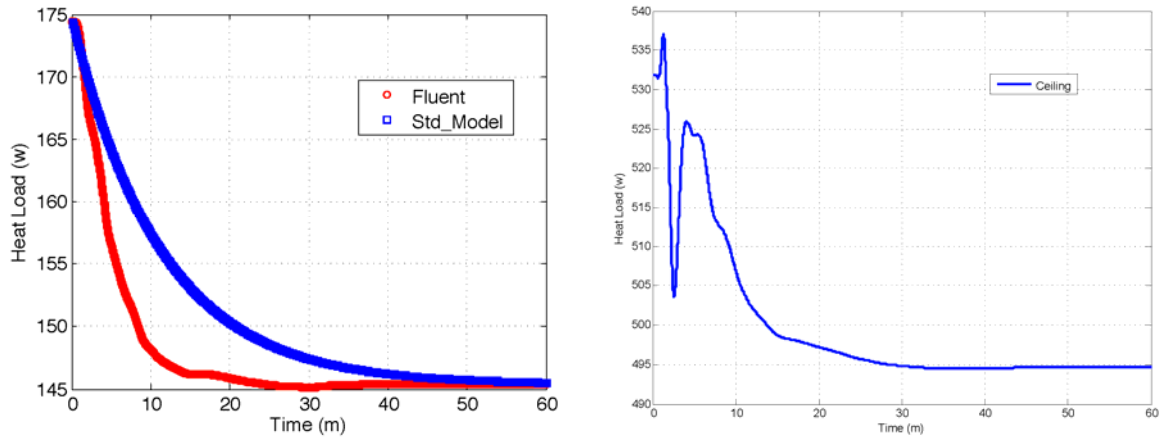

Figure 5.7. Heat loads from South_3 & Ceiling surfaces: step change $\boldsymbol{T}$-West_1

The richer dynamic response is more clearly seen in Figure 5.7 (right), which displays the response of the *Ceiling* heat-load. Clearly, this response is not well-modeled by a single time-constant.

In summary we see that the *Fluent* transient responses are not predicted well by the *Standard Model*. It remains to demonstrate how control design is affected by such model inaccuracy.

5.3 Reduced-Order Modeling

In some applications, one does not have access to the system dynamics, i.e. the state-space representation, so that the usual projection methods (such as balanced truncation) are not applicable. In these cases, instead of state-matrices, one usually has access to an abundant amount of input-output measurements. The goal in this case is to construct a reduced-order model directly from data without any knowledge of the state-space quantities. Whereas our theoretical discussion below will assume that the measured data correspond to sampling of the transfer function at arbitrary frequencies, in our numerical setting this frequency was at infinity. This indeed corresponds to sampling the impulse response of the underlying model. Thus the data in our numerical study was obtained by time-domain simulations. This issue has been discussed in § 5.2.2 and is clarified further in § 5.3.3.

We will treat the data-driven model reduction using an interpolation framework, so that the problem is formulated as follows: Given are the transfer function, $\boldsymbol{G}(s)$, measurements at the interpolation points $s_1, s_2, \dots, s_N$; in other words, the available measured data is $\boldsymbol{G}(s_i)$ for $i = 1,2, \dots, N$. We will assume that the underlying system has m-inputs and p-outputs; thus $\boldsymbol{G}(s_i) \in R^{p\times m}$. Given this measured data, the goal is to construct a reduced-model $\boldsymbol{G}_r(s) = \boldsymbol{C}_r(s\boldsymbol{E}_r - \boldsymbol{A}_r)^{-1}\boldsymbol{B}_r$ so that $\boldsymbol{G}_r(s)$ interpolates the measured data, i.e.

$$\boldsymbol{G}_r(s_i) = \boldsymbol{G}(s_i) \text{ for } i = 1,2, \dots, N.$$

The problem can be easily generalized to higher-order interpolation. Solution to this problem in the general case including repeated interpolation points with higher-order interpolation has recently been provided by Mayo and Antolas [9] using the concept of Loewner and shifted Loewner matrices. As explained below in §5.3.3, in our application, all the measured data will be at $s = \infty$, leading to the classical problem of partial realization [8] where Loewner matrices are replaced by the classical Hankel matrices. Here, we present the solution using the framework of [9] as this framework does not force $\boldsymbol{E}_r = \boldsymbol{I}_r$. Therefore, in the case that the interpolation data leads to a (near) rank deficient Loewner matrix, a lower-order (approximate) interpolant is directly obtained by singular value decomposition (SVD).

Let

$$\boldsymbol{G}(s) = \sum_{k=1}^{\infty} \boldsymbol{g}_k\, s^{-k} \tag{5.1}$$

be the expansion of $\boldsymbol{G}(s)$ around $s = \infty$. In (5.1), $\boldsymbol{g}_k \in R^{p\times m}$ is called the k^{th} Markov parameter of $\boldsymbol{G}(s)$. Assume that the first $2N + 1$ Markov parameters of $\boldsymbol{G}(s)$ are measured. Construct

$$\boldsymbol{L} = \begin{bmatrix} \boldsymbol{g}_1 & \boldsymbol{g}_2 & \cdots & \boldsymbol{g}_N \\ \boldsymbol{g}_2 & \boldsymbol{g}_3 & \cdots & \boldsymbol{g}_{N+1} \\ \vdots & \vdots & \cdots & \vdots \\ \boldsymbol{g}_N & \boldsymbol{g}_{N+1} & \cdots & \boldsymbol{g}_{2N-1} \end{bmatrix}, \tag{5.2}$$

$$\boldsymbol{M} = \begin{bmatrix} \boldsymbol{g}_2 & \boldsymbol{g}_3 & \cdots & \boldsymbol{g}_{N+1} \\ \boldsymbol{g}_3 & \boldsymbol{g}_4 & \cdots & \boldsymbol{g}_{N+2} \\ \vdots & \vdots & \cdots & \vdots \\ \boldsymbol{g}_{N+1} & \boldsymbol{g}_{N+2} & \cdots & \boldsymbol{g}_{2N} \end{bmatrix}, \tag{5.3}$$

$$\boldsymbol{Z} = [\boldsymbol{g}_1^T \quad \boldsymbol{g}_2^T \quad \cdots \quad \boldsymbol{g}_N^T]^T, \tag{5.4}$$

and

$$\boldsymbol{T} = [\boldsymbol{g}_1 \quad \boldsymbol{g}_2 \quad \cdots \quad \boldsymbol{g}_N]. \tag{5.5}$$

If $\boldsymbol{L}$, and consequently, $\boldsymbol{M}$ are not square (*i.e.* when $m \neq p$), one can simply use the leading square submatrices. Then, the matrices $\boldsymbol{Z}$ and $\boldsymbol{T}$ will be modified accordingly. For details, we refer the reader to [1]. Here, to simplify the discussion and the notation, we will assume that this process has already been performed and $\boldsymbol{L}$ and $\boldsymbol{M}$ are square matrices with $\boldsymbol{Z}$ and $\boldsymbol{T}$ having the corresponding size as well. Let $\boldsymbol{L} = \boldsymbol{Y}\Theta\boldsymbol{X}^T$, be the SVD of $\boldsymbol{L}$ with $\text{rank}(\boldsymbol{L}) = k$. Let $\boldsymbol{Y}_k$ and $\boldsymbol{X}_k$ be the leading k columns of $\boldsymbol{Y}$ and $\boldsymbol{X}$, respectively. Define the reduced-order model, $\boldsymbol{G}_k(s) = \boldsymbol{C}_k(s\boldsymbol{E}_k - \boldsymbol{A}_k)^{-1}\boldsymbol{B}_k$, where

$$\boldsymbol{E}_k = \boldsymbol{Y}_k^T\boldsymbol{L}\boldsymbol{X}_k,\ \boldsymbol{A}_k = \boldsymbol{Y}_k^T\boldsymbol{M}\boldsymbol{X}_k,\ \boldsymbol{B}_k = \boldsymbol{Y}_k^T\boldsymbol{Z},\ \ \boldsymbol{C}_k = \boldsymbol{T}\boldsymbol{X}_k. \tag{5.6}$$

Then, $\boldsymbol{G}_k(s)$ is the solution to partial realization problem matching the first $2N$ Markov parameters.

5.3.1. Reducing $\boldsymbol{G}_k(s)$ Further

The model $\boldsymbol{G}_k(s)$ above is not our final reduced-order model. The reason is as follows: Assume, for example, that $2N + 1 = 2001$ Markov parameters are measured. Further assume that the system has 3 inputs and 3 outputs. Assuming no rank deficiency,this would lead to a partial realization $\boldsymbol{G}_k(s)$ of order k=3000. By no means, is this a reduced order model. Of course one can choose to match only leading 10 Markov parameters to obtain a reduced-order model of order k=30 but this approach would waste the measured data in the remaining Markov parameters. Instead, we propose to use as much of the information as possible from the Markov parameters. This is where we deviate from other approaches. We use the measured data to its fullest extent, and then optimally reduce this intermediate model. In other words, we will construct an *intermediate* model $\boldsymbol{G}_k(s)$ of order k; for the numbers mentioned above, this will correspond to k = 3000. This would be the best model one can construct using the measured data. The power of modern computer hardware, algorithms and software are such that reducing a model of order 3000 is trivial. Additionally, now that $\boldsymbol{G}_k(s)$ has a state-space realization we can apply optimal projections based methods to search for an effective reduced model. We will use

the Iterative Rational Krylov Method (*IRKA*), the optimal- model reduction technique of Gugercin *et al.* [7] to optimally reduce . In other words, using the measured Markov parameter data to their fullest extent, we construct an intermediate model with an explicit state-space representation. Then, we use our optimal projection-based method to construct our final reduced-order model . Before the numerical examples, we briefly explain the *IRKA*.

5.3.2. Optimal Model Reduction by IRKA

Given the full-order model B of order *n*, the goal of the optimal- model reduction is to find a reduced-order model . of order *r* that solves

$$\|\mathbf{G} - \mathbf{G}_r\|_{\mathcal{H}_2} = \min_{\dim(\widetilde{\mathbf{G}}_r) = r} \left\|\mathbf{G} - \widetilde{\mathbf{G}}_r\right\|_{\mathcal{H}_2} \tag{5.7}$$

where

$$\|\mathbf{G}\|_{\mathcal{H}_2} := \left(\frac{1}{2\pi}\int_{-\infty}^{\infty} \|\mathbf{G}(\imath\omega)\|_{\mathrm{F}}^2 \, d\omega\right)^{1/2}.$$

One can easily show that

$$\max_{t>0} \|\mathbf{y}(t) - \mathbf{y}_r(t)\|_\infty \leq \|\mathbf{G} - \mathbf{G}_r\|_{\mathcal{H}_2} \|\mathbf{u}\|_2. \tag{5.8}$$

Indeed, for the multi-input single-output and single-input multi-output cases, (5.8) holds with equality as the norm is equal to the induced norm of the underlying convolution operator (see [1] for details). Hence, when one wants to minimize the difference in each component of the output error for all , the norm of the error system is the obvious error measure to minimize.

Several methods have been developed to solve the optimal model reduction problem (5.7); see, for example, [10,13,7,11,5,12,6,2,3,14] and references therein. Since (7) is a nonconvex optimization problem, the typical approach is to find reduced-order models that satisfy the first-order necessary conditions. These conditions can be given either in terms of solutions to Lyapunov equations (e.g., [11, 13, 14]) or in terms of rational interpolation (e.g., [3, 7, 12, 13]): As shown in [7], these two frameworks are theoretically equivalent. However interpolation-based optimal methods are computationally more advantageous as they only require solving sparse linear systems. Here we focus on interpolation-based approaches.

Meier and Luenberger [10] have initially introduced the interpolation-based -optimality conditions for SISO systems. Recently [4, 7, 12] generalized these conditions to MIMO systems as shown in the next result.

Theorem 5.1 *Let* $\mathbf{G}_r(s) = \sum_{i=1}^{r} \frac{1}{s-\hat{\lambda}_i} \mathsf{c}_i \mathsf{b}_i^T$ *be an* r^{th} *order optimal* $\mathcal{H}_2$ *approximation to* $\mathbf{G}(s)$*, i.e. it solves (5.7). Then*

$$(a)\ \mathbf{G}(-\hat{\lambda}_k)\mathsf{b}_k = \mathbf{G}_r(-\hat{\lambda}_k)\mathsf{b}_k, \tag{5.9}$$

$$(b)\ \mathsf{c}_k^T\mathbf{G}(-\hat{\lambda}_k) = \mathsf{c}_k^T\mathbf{G}_r(-\hat{\lambda}_k),\ \textit{and} \tag{5.10}$$

$$(c)\ \mathsf{c}_k^T\mathbf{G}'(-\hat{\lambda}_k)\mathsf{b}_k = \mathsf{c}_k^T\mathbf{G}_r'(-\hat{\lambda}_k)\mathsf{b}_k \tag{5.11}$$

for $k = 1, 2, \ldots, r$.

Theorem 5.1 states that the optimal- approximant to is a rational bitangential Hermite interpolant to at the mirror images of the reduced system poles. Hence, the optimal interpolation points and corresponding tangent directions clearly depend on the knowledge of , the model we want to compute, and will not be available *a priori*. This requires an iterative process as developed in [7]. *IRKA* iteratively corrects the interpolation points and tangent directions until (5.9)-(5.11) holds. During *IRKA*, interpolation points are updated as reflection of the poles of the current reduced-system. Similarly, the tangent directions are updated as residue directions from the current reduced model. Upon convergence, the optimality conditions (5.9)-(5.11) are met. Below, we give a brief sketch of *IRKA*. For details, we refer the reader to the original source [7].

Algorithm 5.1 Iterative Rational Krylov Algorithm (IRKA)

1. $\mathbf{G}(s) = \mathbf{C}(s\mathbf{E} - \mathbf{A})^{-1}\mathbf{B}$.
2. *Choose initial interpolation points* $\{s_1, \ldots, s_r\}$*; and tangential directions* $\{\mathsf{b}_1, \ldots, \mathsf{b}_r\}$ *and* $\{\mathsf{c}_1, \ldots, \mathsf{c}_r\}$*; all three sets chosen are closed under conjugation.*
3. *Construct*
   $\mathbf{V}_r = [(s_1\mathbf{E} - \mathbf{A})^{-1}\mathbf{B}\mathsf{b}_1, \ldots, (s_r\mathbf{E} - \mathbf{A})^{-1}\mathbf{B}\mathsf{b}_r]$.
   $\mathbf{W}_r = [(s_1\mathbf{E} - \mathbf{A})^{-T}\mathbf{C}^T\mathsf{c}_1, \ldots, (s_r\mathbf{E} - \mathbf{A})^{-T}\mathbf{C}^T\mathsf{c}_r]$.
4. *until convergence*
   (a) $\mathbf{A}_r = \mathbf{W}_r^T\mathbf{A}\mathbf{V}_r$, $\mathbf{E}_r = \mathbf{W}_r^T\mathbf{E}\mathbf{V}_r$, $\mathbf{B}_r = \mathbf{W}_r^T\mathbf{B}$, *and* $\mathbf{C}_r = \mathbf{C}\mathbf{V}_r$.
   (b) *Compute* $\mathbf{A}_r\mathbf{x}_i = \hat{\lambda}_i\mathbf{E}_r\mathbf{x}_i$ *and* $\mathbf{y}_i^*\mathbf{A}_r = \hat{\lambda}_i\mathbf{y}_i^*\mathbf{E}_r$ *with* $\mathbf{y}_i^*\mathbf{E}_r\mathbf{x}_j = \delta_{ij}$ *where* $\mathbf{y}_i^*$ *and* $\mathbf{x}_i$ *are left and right eigenvectors associated with* $\tilde{\lambda}_i$.
   (c) $s_i \leftarrow -\hat{\lambda}_i$, $\mathsf{b}_i^T \leftarrow \mathbf{y}_i^*\mathbf{B}_r$ *and* $\mathsf{c}_i \leftarrow \mathbf{C}_r\mathbf{x}_i$, *for* $i = 1, \ldots, r$.
   (d) *Construct*
   $\mathbf{V}_r = [(s_1\mathbf{E} - \mathbf{A})^{-1}\mathbf{B}\mathsf{b}_1, \ldots, (s_r\mathbf{E} - \mathbf{A})^{-1}\mathbf{B}\mathsf{b}_r]$.
   $\mathbf{W}_r = [(s_1\mathbf{E} - \mathbf{A})^{-T}\mathbf{C}^T\mathsf{c}_1, \ldots, (s_r\mathbf{E} - \mathbf{A})^{-T}\mathbf{C}^T\mathsf{c}_r]$.
5. $\mathbf{A}_r = \mathbf{W}_r^T\mathbf{A}\mathbf{V}_r$, $\mathbf{E}_r = \mathbf{W}_r^T\mathbf{E}\mathbf{V}_r$, $\mathbf{B}_r = \mathbf{W}_r^T\mathbf{B}$, $\mathbf{C}_r = \mathbf{C}\mathbf{V}_r$.

5.3.3. Numerical Results

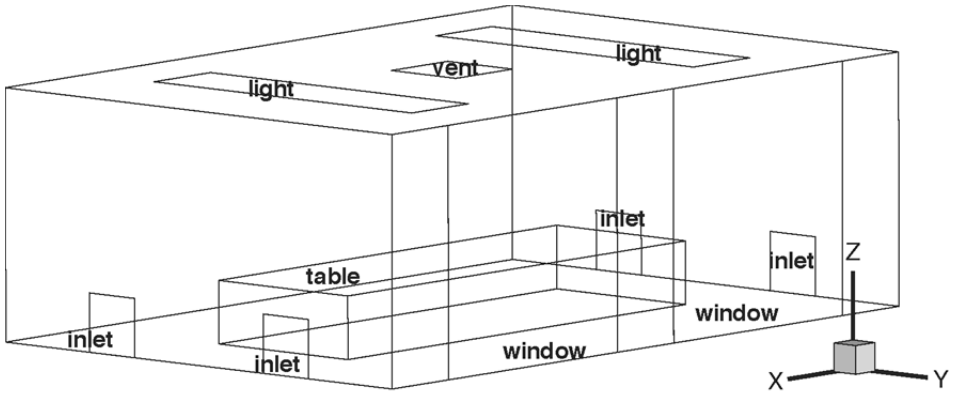

Figure 5.8. Geometry for indoor-air simulation

Since data for the *Purdue Living Laboratory* is not yet available, we consider the indoor-air environment in a simple conference room with four inlets, one return vent and thermal loads provided by two windows, two overhead lights and occupants (see Figure. 5.8). We use the FLUENT CFD software package to perform simulations of the indoor-air velocity, temperature and moisture. These quantities are modeled using the Boussinesq equations and the transport equation given below:

$$\frac{\partial \mathbf{v}}{\partial t} + \mathbf{v} \cdot \nabla \mathbf{v} = -\nabla P + \frac{1}{\mathrm{Re}} \Delta \mathbf{v} + \frac{\mathrm{Gr}}{\mathrm{Re}^2} T \hat{k} \tag{5.12}$$

$$\nabla \cdot \mathbf{v} = 0 \tag{5.13}$$

$$\frac{\partial T}{\partial t} + \mathbf{v} \cdot \nabla T = \frac{1}{\mathrm{RePr}} \Delta T + Bu, \tag{5.14}$$

$$\frac{\partial S}{\partial t} + \mathbf{v} \cdot \nabla S = \frac{1}{Pe} \Delta S, \tag{5.15}$$

where v is the velocity vector, P is the pressure, T is the temperature and S is the moisture concentration. Nondimensionalization has been carried out such that Re is the Reynolds number, Pr is the Prandtl number, Gr is the Grashof number and Pe is the Peclet number. All of these have been set using according to FLUENT's default air properties. We assume adiabatic boundary conditions on all surfaces except the inlets, windows and lights.

We obtain a reduced-model for the coupled velocity-temperature-moisture dynamics directly from simulations (measurements). The simulation data for this problem were produced by a FLUENT simulation with the geometry of Figure 5.8. The coupled velocity-temperature-humidity dynamics were simulated on a grid with nodes. The inputs to the FLUENT simulation included:

1. the flow-rate on the inlets (all the same),

2. the temperature of the inlet air,
3. the water-vapor mass fraction of the inlet air, and
4. energy and water-vapor source disturbances in an occupied region around the table.

The monitored outputs were

1. the water-vapor mass fraction in the *occupied* region,
2. the temperature at a sensor location on the *max x* wall, and
3. the temperature in the *occupied* region.

Each input was subjected to a step-like change from an initial *steady* value. The outputs were sampled at 2 second intervals over a period of 3600 seconds. Impulse response data was simulated by differentiating (finite-difference) the step-response data, consequently leading to the sampling of 1801 Markov parameters $\boldsymbol{g_j} \in R^{3\times4}$ for j = 1, 2, …, 1801. This corresponds to N = 900 in (5.2). As we have 4 inputs and 3 outputs, then using (5.2)-(5.6), we first produce an intermediate reduced-order model $\boldsymbol{G_k}(s)$ of order k = 2700. Then, by using *IRKA* we further reduce this model to obtain our final reduced-order model $\boldsymbol{G_r}(s)$ of order r = 50. Since we don't have the full state-space matrices for this model, we cannot compare Bode plots. However, we have the time domain FLUENT simulations. We run our reduced-order model using the same step-like change input used for the FLUENT simulation and compare the reduced-order outputs with the original data. The results for some representative input/output combinations are shown in Figures 5.9 and 5.10 below. As both figures clearly illustrate, the reduced-model obtained directly from measurements does a very good job of matching the full-order simulation.

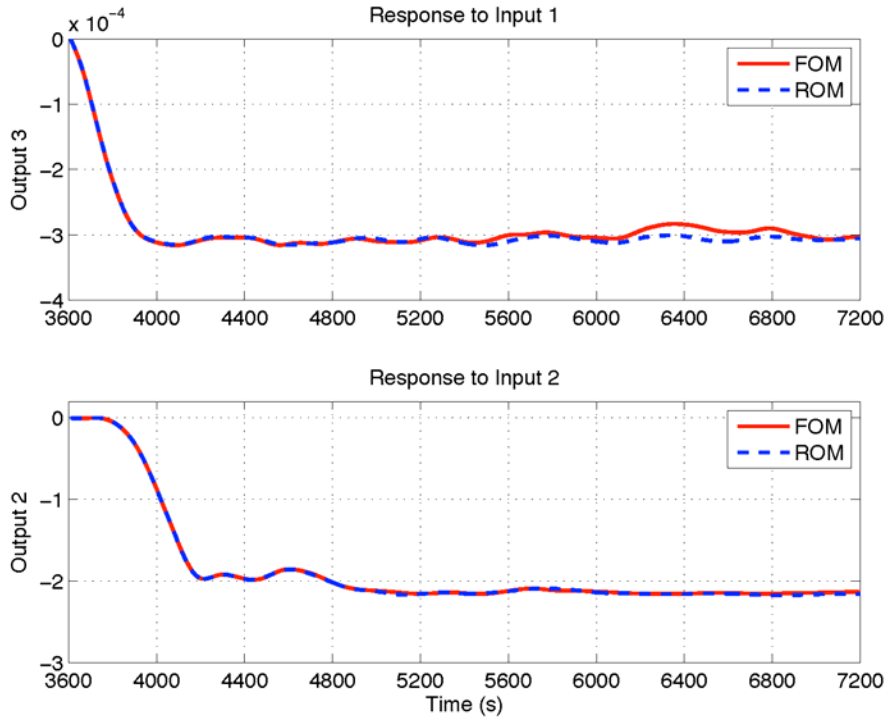

Figure 5.9. Time Domain Responses of $\boldsymbol{G}(\boldsymbol{z})$ and $\boldsymbol{G_r}(\boldsymbol{z})$

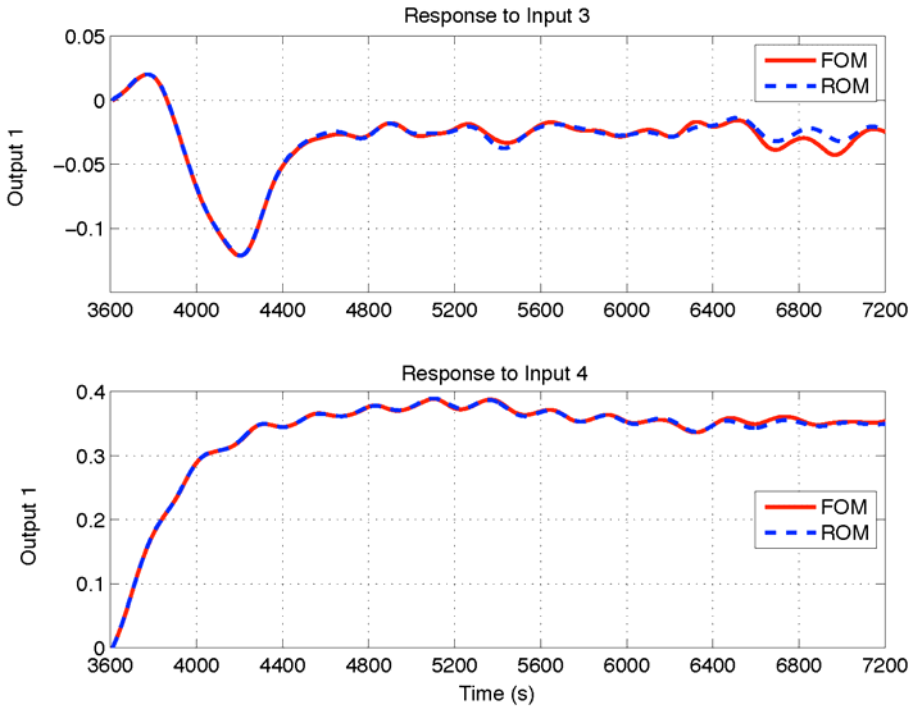

Figure 5.10. Time Domain Responses of $\boldsymbol{G(z)}$ and $\boldsymbol{G_r(z)}$

5.4. References

[1] A. C. Antoulas. *Approximation of large-scale dynamical systems*. SIAM, 2005.

[2] C. A. Beattie and S. Gugercin. Krylov-based minimization for optimal H2 model reduction. *th IEEE Conference on Decision and Control*, pages 4385–4390, Dec. 2007.

[3] C. A. Beattie and S. Gugercin. A trust region method for optimal H_2 model reduction. *In Proceedings of the 48th IEEE Conference on Decision and Control*, Dec. 2009.

[4] A. Bunse-Gerstner, D. Kubalinska, G. Vossen, and D. Wilczek. h2-norm optimal model reduction for large scale discrete dynamical MIMO systems. *Journal of computational and applied mathematics*, 233(5):1202–1216, 2010.

[5] P. Fulcheri and M. Olivi. Matrix rational H_2 approximation: a gradient algorithm based on Schur analysis. *SIAM Journal on Control and Optimization*, 36(6):2103–2127, 1998.

[6] S. Gugercin. An iterative rational Krylov algorithm (IRKA) for optimal H_2 model reduction. In *Householder Symposium XVI*, Seven Springs Mountain Resort, PA, USA, May 2005.

[7] S. Gugercin, A. C. Antoulas, and C. A. Beattie. H_2 model reduction for large-scale linear dynamical systems. *SIAM J. Matrix Anal. Appl.*, 30(2):609–638, 2008.

[8] R. E Kalman. On partial realizations, transfer functions, and canonical forms. *Acta Polyt.*

Scand. Ma., 31:9–32, 1979.

[9] A. J. Mayo and A. C. Antoulas. A framework for the solution of the generalized realization problem. *Linear Algebra and Its Applications*, 425(2-3):634–662, 2007.

[10] L. Meier III and D. Luenberger. Approximation of linear constant systems. *IEEE Trans. Automatic Control*, 12(5):585–588, 1967.

[11] J. T. Spanos, M. H. Milman, and D. L. Mingori. A new algorithm for H_2 optimal model reduction. *Automatica (Journal of IFAC)*, 28(5):897–909, 1992.

[12] P. Van Dooren, K. A. Gallivan, and P. A. Absil. H2-optimal model reduction of MIMO systems. *Applied Mathematics Letters*, 21(12):1267–1273, 2008.

[13] D. A. Wilson. Optimum solution of model-reduction problem. *Proc. Inst. Elec. Eng.*, 117(6):1161–1165, 1970.

[14] D. Zigic, L. T. Watson, and C. Beattie. Contragredient transformations applied to the optimal projection equations. *Linear Algebra Appl.*, 188:665–676, 1993.

6. Data-driven Approach to Modeling & Supervisory Control

An alternative to using reduced-order models derived from first principles, as outlined in section 4, is to identify a model using system identification with data from measurements or simulation. This section presents a case study for application of MPC to a multi-zone building using a data-driven model obtained from simulation results. In contrast, section 7 provides some initial case study results for MPC that utilizes the reduced-order modeling approach presented in section 4.

6.1 Introduction

Constrained optimal control for building HVAC systems has received significant attention recently. The most attractive features of such control approaches include the possibility to explicitly specify the desired cost of energy as a performance measure and to incorporate constraints on control and state variables in a systematic way. The most popular and practical of optimization–based control strategies is certainly *model–predictive control* (MPC). MPC utilizes a dynamical model to predict a plant's future behavior and make decisions on control inputs that minimize a certain cost function. In order to implement MPC one clearly needs a dynamical model of a plant of sufficient accuracy that is also amenable to efficient implementation necessary for real-time operation. One possibility is to derive a detailed physical model of the controlled building and simplify the model though a model reduction procedure as outlined in section 4. The main difficulty with such a modeling approach is the large number of parameters that need to be estimated from measurement data and the lack of tools for systematic model reduction for nonlinear models. In this report we document a simple simulation study of MPC application to supervisory control of a building in the Philadelphia Navy Yard. The approach we are taking is based on standard system identification of local *linear models* for each thermal zone in the building. The rationale for basing our control design on linear dynamical models is the following:

- In HVAC control, such as temperature control of a thermal zone, the optimal operation tends to be in a tight interval around the bounds of controlled variables. This suggests that for control design purposes dynamic behavior of the plant can be locally described by linear models with sufficient accuracy.

- System identification of parametric linear input-output models is a mature field with a number of numerically robust and highly efficient tools such as the System Identification Toolbox for Matlab [1], which allows model parameter estimation to be performed either off-line or recursively during the plant operation.

- Local linear models allow highly efficient real-time implementation of optimization-based algorithms and thus facilitate scalability of the optimal control approaches for HVAC systems.

Naturally, if the dynamics of the plant are highly nonlinear, as for instance in the case of dynamic switching, the modeling approach based on linear models may not be applicable.

Another potential drawback of the proposed approach is the effort required to prepare and perform identification experiments under controlled conditions.

We start in Section 6.2 with a short description of the Philadelphia Navy Yard Building 14 whose detailed TRNSYS model is used as a plant in our simulation experiments. Development of models needed for control synthesis is described in Section 6.3. Details on synthesis and implementation of a model-predictive controller based on the chiller and thermal zone models are provided in Section 6.4. Analysis of the controller performance and potential improvements are given in Section 6.5, followed by concluding remarks and recommendations for further improvements in Section 6.6.

6.2 Case Study: Building 14 (Philadelphia Navy Yard)

For our simulation studies we used a detailed energy model of Building 14 located in the Philadelphia Navy Yard. Fidelity of the model is limited due to the lack of detailed design information and measurement data for calibration. However, parameters of the detailed model and model components are realistic and correspond to the actual parameters of the specific HVAC components.

The TRNSYS model consists of two parts - building envelope and the HVAC system with control logic [2]. For the building envelope part, the building is divided into a number zones based on geometry and function. The internal heat gains from lighting, equipment and occupancy, as well as thermal performance data of the envelope, are introduced from PSU's EnergyPlus model. In all simulations recorded weather data for Philadelphia area for the year 2011 is used.

The building is functionally divided into five office spaces, which are referenced according to their orientation in the building: North-South (NS), North-North (NN), South-West (NN) and South-East (SE) office area with an additional South-East Office (SEO). The location of each area within the building is shown in Figure 6.1.

Thermal comfort in these areas is maintained by five air-handling units (AHUs) with variable-speed fans. Each AHU comes with a heating and a cooling coil that are controlled to supply enough capacity to cover heating or cooling loads of a served zone. An AHU capacity is also adjusted by varying supply-air flow rate to accommodate variations in heating or cooling loads over time. Zones NS, NN, SW and SE are each served by a single AHU, with a single temperature controller per zone. The office space SEO is served by an AHU connected to three variable air volume (VAV) boxes. A water-cooled chiller with a cooling tower provides chilled water to AHUs, and gas boilers supply AHUs with hot water for heating. In addition to heating from AHUs, the perimeter zones are also installed with hydronic baseboard heaters to cover heating loads.

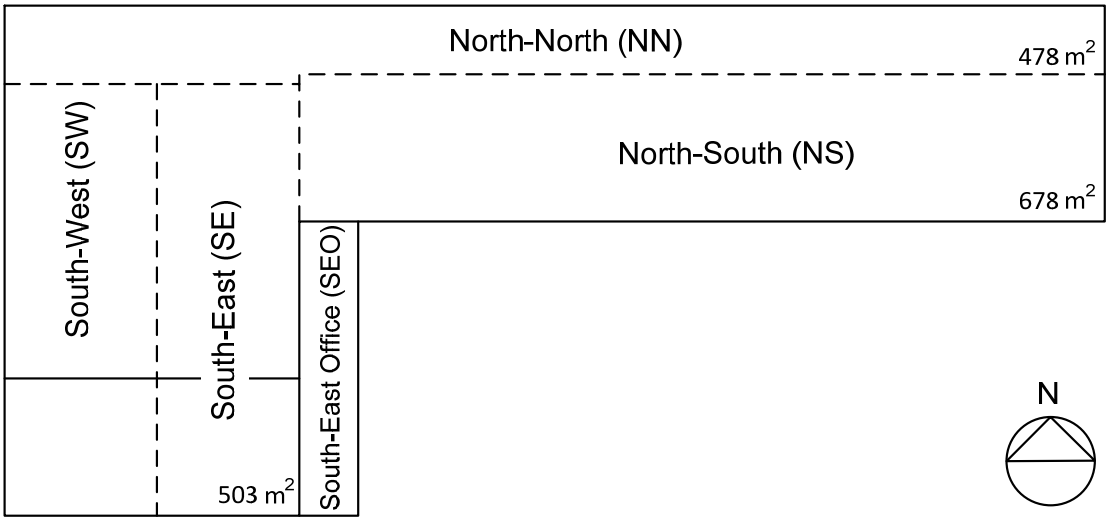

Figure 6.1. Functional subdivision of Building 14

In our study we focus on the largest four zones: NS, NN, SW and SE, whose average energy demand amounts to 90-95% of the whole building energy consumption. Current baseline control architecture for the considered zones is shown in Figure 6.2.

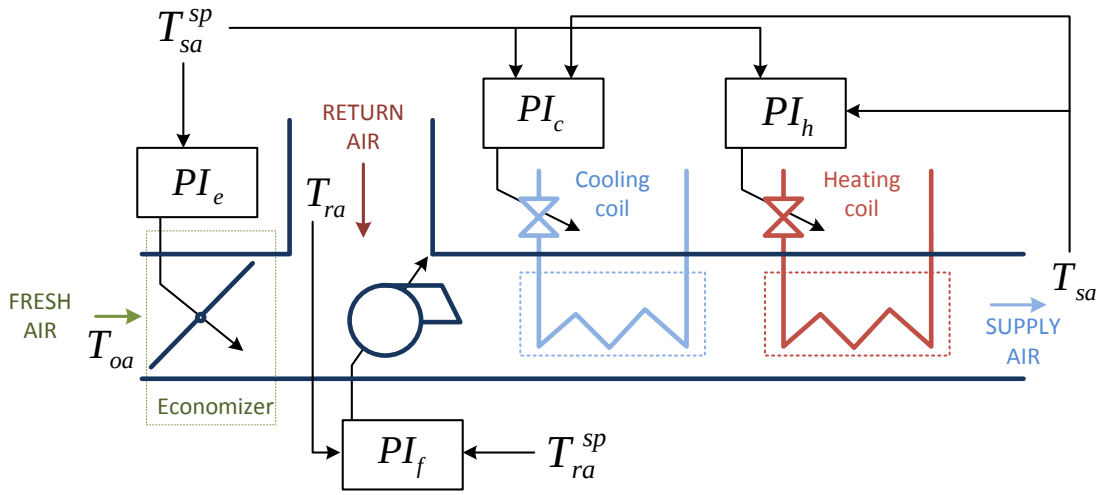

Figure 6.2. Baseline AHU control structure for Building 14 zones NS, NN, SW and SE

The temperature of each zone is controlled by the controller PI_f, which modifies the inflow of the supply air in order to maintain zone temperature at the desired setpoint. The temperature of the supply air is regulated by the controllers PI_c and PI_h, which control the opening of the cooling and heating coil valve, i.e. the flow rate of the chilled and heated water. Supply air temperature is additionally regulated by the controller PI_e, which adjusts the economizer valve opening to increase or decrease inflow of the fresh air and maintain the supply air temperature at

the desired level. All control components of AHUs are enabled and disabled according to a heating (cooling) schedule depending on hour of the day and actual weather conditions.

In our study we consider supervisory control at the level of each AHU as well as coordinated supervisory control of the chiller plant. On the AHU level the controller decides on the temperature and inflow of the supply air in order to maintain the zone temperatures in a prescribed comfort interval. Simultaneously, a controller computes the optimal values for the chilled and cooling water temperature that maximize the coefficient of performance of the chiller plant while satisfying the current load. We make the following simplifying modifications to the original control architecture:

1. The original component scheduling is disabled and continuous controller operation is introduced, with different constraints for "occupied" and "unoccupied" hours.

2. Only cooling mode is considered; controller commands for supply air temperature setpoints which would require reheating of the incoming air cannot be executed.

3. Economizer control is not taken into account; economizer is set to provide *fixed* minimal inflow of the fresh air.

4. Interaction between the zones is not considered in the control design.

The modified control architecture for a single zone and chiller plant of the Building 14 is shown in Figure 6.3.

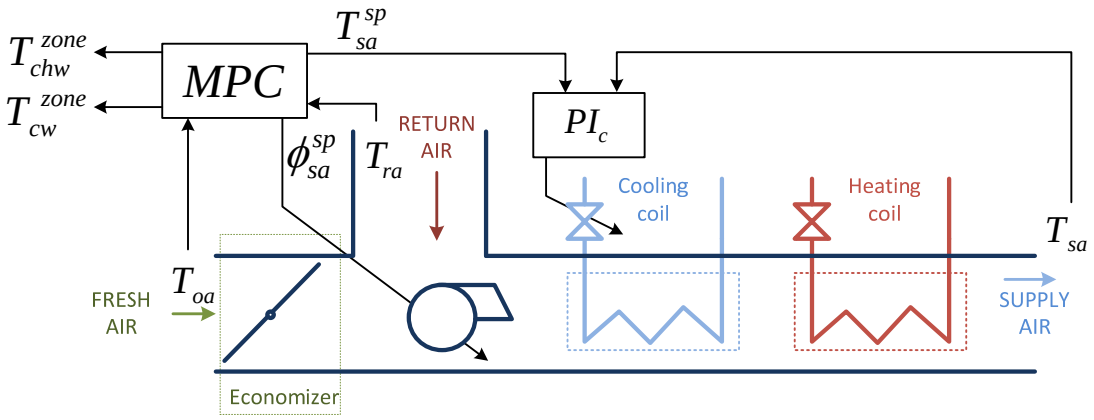

Figure 6.3. Control architecture used for optimization-based supervisory control of zones NS, NN, SW and SE in cooling regime

6.2 Plant Model

In order to design a controller that would reduce the energy required to maintain thermal comfort in each zone, we need models for the zones and chiller plant. For each thermal zone a dynamical model is used. As we show next, a simple linear ARX model identified from the designed input–

output response of the thermal zones provides sufficient accuracy for predictive control design. We neglect dynamics of the chiller and cooling tower and perform static optimization of their efficiency utilizing a simple empirical model for chiller efficiency in static operating conditions [3].

6.2.1 System Identification of Models of Thermal Zones

System identification is a procedure for building a mathematical model of a dynamical system from input-output data. In this section we discuss identification of parametric linear models for thermal zones of Building 14. The procedure can be represented as a sequence of three steps:

1. Selection of appropriate excitation signals and data collection.
2. Data pre-processing, selection of the model structure and estimation of model parameters using an identification data set.
3. Validation of the model performance on a different data set.

System identification is typically an iterative procedure; the above three steps are often repeated until a satisfactory result is achieved. For detailed discussion of both theoretical and practical aspects of system identification the reader is referred to [4].

The considered input-output model of building thermal zones is shown in Figure 6.4.

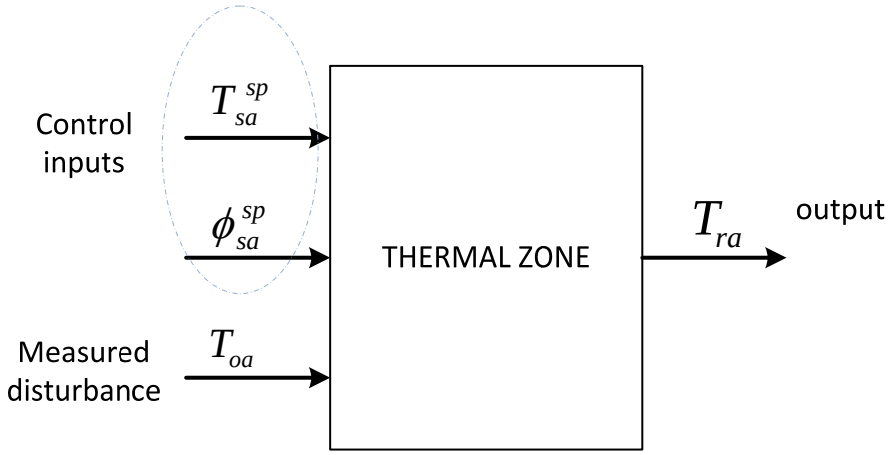

Figure 6.4. Input–output representation of Building 14 thermal zones

In this study we limit our attention to control of the zone temperature and take the temperature of the return air (T_{ra}) as the only output of our zone model. The temperature and mass flow rate of the supply air, T_{sa}^{sp} and ϕ_{sa} are *controlled* inputs. The values of these inputs, within certain bounds, are decided by a control algorithm. The behavior of the system is affected by a number of disturbances (uncontrolled inputs) such as heat transfer caused by solar heat gain, varying thermal load due to occupancy, varying temperature of the ambient air, etc. Preliminary simulation experiments showed that disturbances, such as solar heat gain, are strongly correlated with the ambient temperature. We also observed that the thermal load caused by occupancy,

equipment and lighting is not dominant. Therefore, the only uncontrolled input we consider in our model is varying ambient temperature T_{oa}.

In cases when the thermal load due to occupancy represents a significant portion of the overall load, it must be included in the dynamical model of a thermal zone as an uncontrolled input. In that case an accurate estimation or certain measurement of the occupancy is needed for the system identification. The first step in the identification procedure is design of the identification experiment. From the perspective of system identification, excitation must be performed under controlled conditions in order to reduce the influence of disturbances that are not accounted for in the model. The ramification of this requirement in case of commercial buildings is that an identification experiment should be performed under stationary conditions, with low or no occupancy.

Additionally, in order to capture the influence of the varying ambient temperature and its correlation with the solar radiation, experiments must be performed during the daytime and over several days in order to collect sufficient data samples. Performing preliminary small step excitations and using standard first order approximations we estimated that the dominant time constants for the zones vary from 30 min (for SE) to 60 min (for NS). In that respect, we select the sampling time for the identification experiment and subsequent controller to be $T_s = 3[\text{min}]$ *for all zones*.

Alternatively, one can select a larger sampling period for zones with "slower" dynamics. In this case, for the sake of simplicity, we opted for a uniform sampling period. When it comes to the choice of the excitation signals, there are several standard types of signals which produce "sufficiently informative" or *persistent* excitation (cf. [4] [Chapter 13]). We use standard *band–limited "white noise"* with the cut-off frequency for individual zones selected according to estimates of their time constants. Identification experiments are performed in the period from 9AM till 7PM on a simulation day of July 11, 2011, with the corresponding recorded ambient temperature. An additional set of validation data with different excitation signals is collected for July 13, 2011. Excitation signals for controlled inputs (T_{sa}^{sp} and ϕ_{sa}) and the measured disturbance (ambient temperature T_{oa}) are shown in Figures 6.5(a) to 6.5(c). Figure 6.5 (d) shows the responses of the return air temperature under excitation.

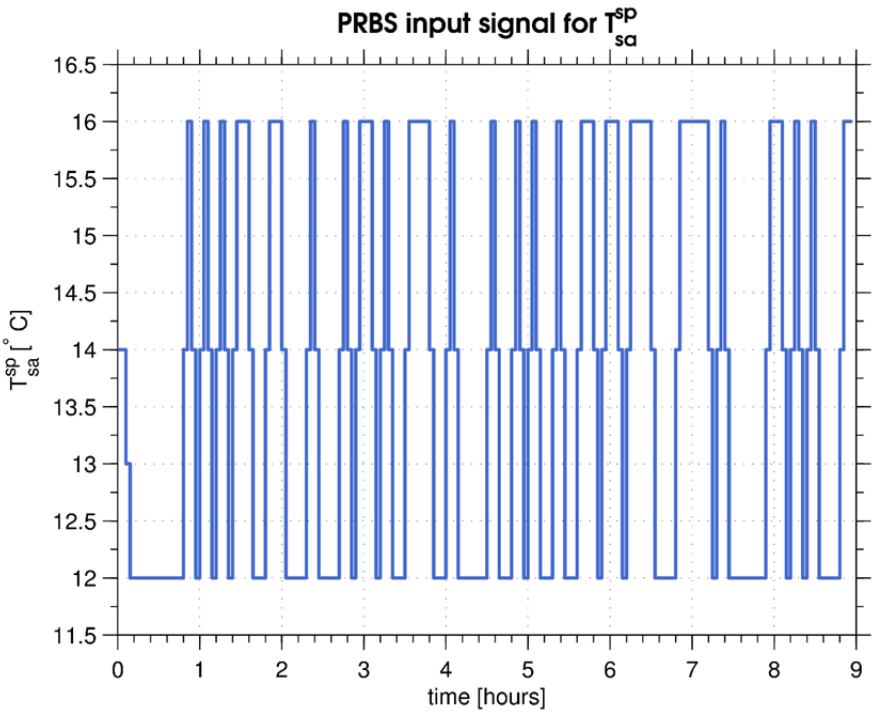

(a) Excitation signal for

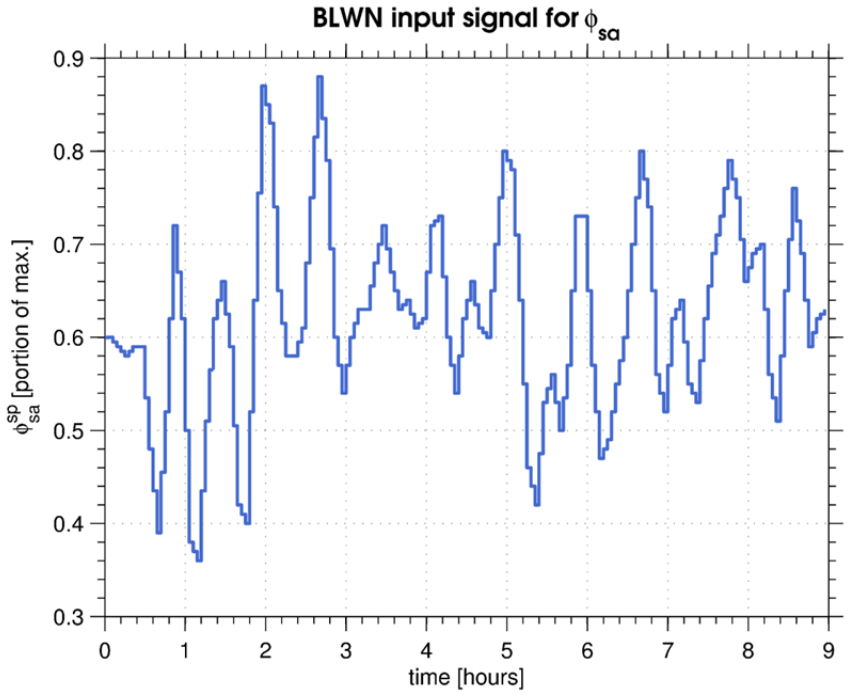

5.

(b) Excitation signal for

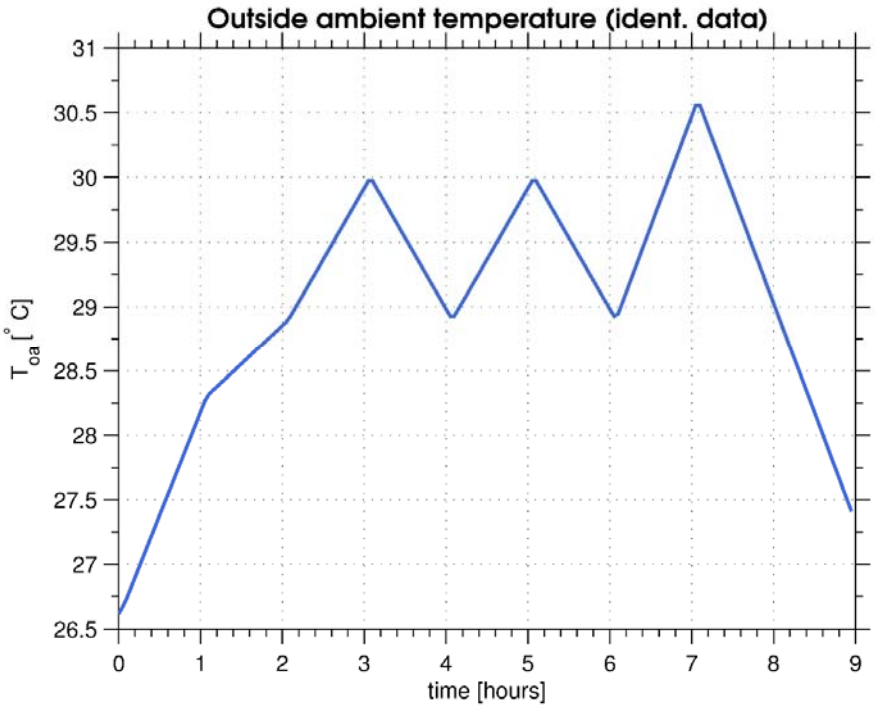

(c) Outside ambient temperature

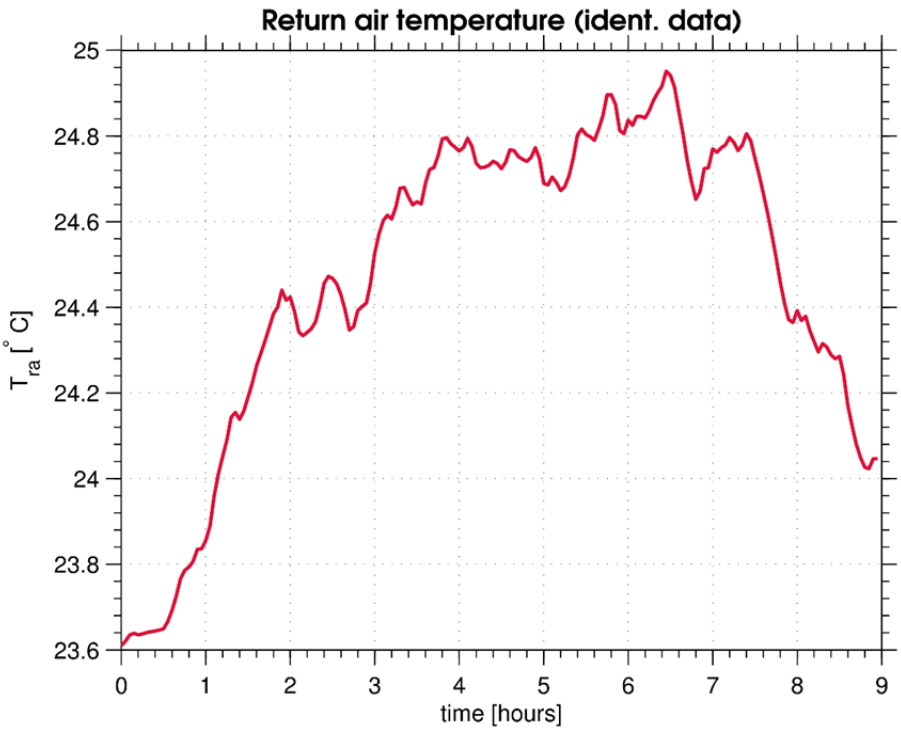

(d) Return air temperature response

Figure 6.5. Identification experiment for the NS zone

As a starting point we tested the ability of linear models to represent dynamics of the Building 14 thermal zones. We considered a standard ARX (Auto-Regressive with exogenous input) model structure, described by the equation:

(6.1)

where denotes model outputs and , are model inputs. Structure of the model, i.e. the set of values , , and for individual zones, is selected with the help of the System Identification Toolbox for Matlab [1]. An initial guess for the model order is obtained using information criterion (Akaike's information criterion) and further modified using several iterations to improve data fitting and transient (step input) response of the model. Simulated response of the identified ARX model for the zone NS and the response of the plant (TRNSYS model) for the validation input data is given in Figure 6.6.

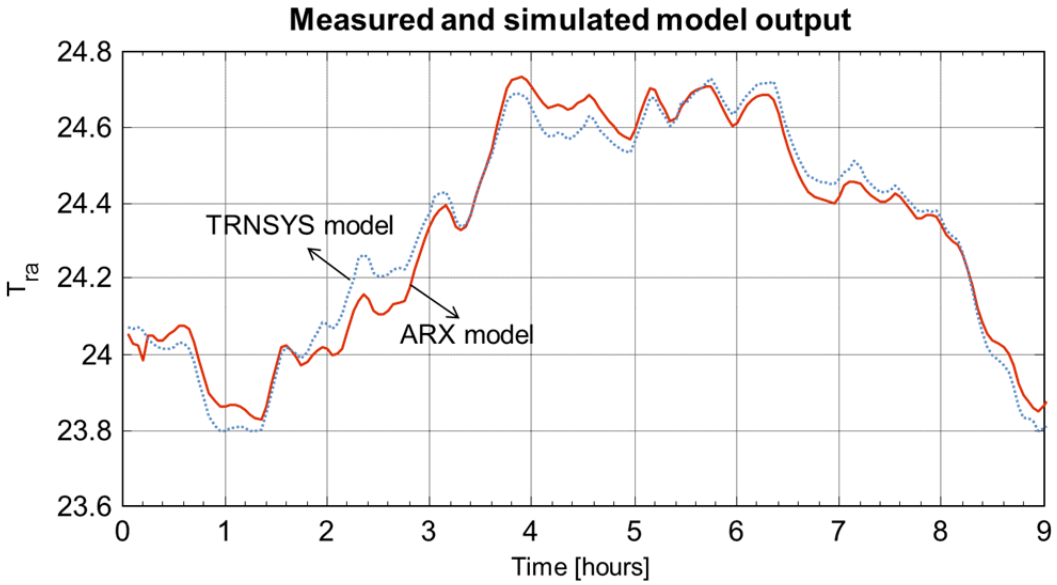

Figure 6.6. Simulated response of the ARX model of the Building 14 NS wing and the actual return air temperature for the validation data set

6.2.2 Chiller Plant Model

A static model for electric chillers introduced in [3] is commonly used in HVAC control and optimization. In this model the chiller power is defined as a function of the chilled water temperature , condenser (cooling) water temperature , and the actual chiller capacity :

(6.2)

where P_{ref} is a constant referent power for the specific chiller, and $c_{av}(\cdot)$, $E_{fl}(\cdot)$, $E(\cdot)$ stand for, respectively, the available capacity, the full-load efficiency and the efficiency as a function of the percentage unloading:

$$c_{av}(T_{chw}, T_{cw}) = \begin{bmatrix} T_{chw} \\ T_{cw} \end{bmatrix}^T \begin{bmatrix} a_{11} & a_{12} \\ a_{21} & a_{22} \end{bmatrix} \begin{bmatrix} T_{chw} \\ T_{cw} \end{bmatrix} + \begin{bmatrix} a_1 & a_2 \end{bmatrix} \begin{bmatrix} T_{chw} \\ T_{cw} \end{bmatrix} + a_0 \tag{6.3a}$$

$$E_{fl}(T_{chw}, T_{cw}) = \begin{bmatrix} T_{chw} \\ T_{cw} \end{bmatrix}^T \begin{bmatrix} b_{11} & b_{12} \\ b_{21} & b_{22} \end{bmatrix} \begin{bmatrix} T_{chw} \\ T_{cw} \end{bmatrix} + \begin{bmatrix} b_1 & b_2 \end{bmatrix} \begin{bmatrix} T_{chw} \\ T_{cw} \end{bmatrix} + b_0 \tag{6.3b}$$

$$P_{lr}(Q, T_{chw}, T_{cw}) = \frac{Q}{Q_{ref} c_{av}(T_{chw}, T_{cw})}, \tag{6.3c}$$

$$E(Q, T_{chw}, T_{cw}) = d_0 + d_1 P_{lr} + d_2 P_{lr}^2, \tag{6.3d}$$

where Q is the actual chiller capacity and Q_{ref} is the chiller capacity at reference conditions. In the TRNSYS model of the Building 14, coefficients for the chiller *Multistack MS70X* are used, with the simplifying assumption:

$$E(Q, T_{chw}, T_{cw}) \approx P_{lr}(Q, T_{chw}, T_{cw}). \tag{6.4}$$

From equations (6.2) through (6.4) we derive expression for the chiller's *coefficient of performance* (COP):

$$COP(T_{chw}, T_{cw}) = \frac{Q}{P_{ch}} = \frac{Q_{ref}}{P_{ref} E_{fl}(T_{chw}, T_{cw})}. \tag{6.5}$$

6.3 Control Architecture, Design and Implementation

We consider a standard model–predictive control algorithm for each thermal zone, as illustrated in Figure 6.3. At each time instance the local zone controller obtains measurements of the return air temperature T_{ra} and outside ambient temperature T_{oa}, and computes optimal values for the supply air temperature reference (T_{sa}^{sp}) and the reference for the supply air mass flow rate ϕ_{sa}^{sp}. In addition, optimal values for the chilled water temperature T_{chw}^{zone} and T_{cw}^{zone} are computed. Those values are preferred values for the particular zone; other zones may need lower chilled water temperature in order to maintain the zone air temperature within comfort bounds. Actual values for T_{chw} and T_{cw} that are set as references for the chiller plant controller are the *lowest* of all requested temperatures T_{chw}^{zone} among the zones and the corresponding condenser water temperature that maximizes chiller COP. The whole control architecture for multiple zones is shown in Figure 6.7.

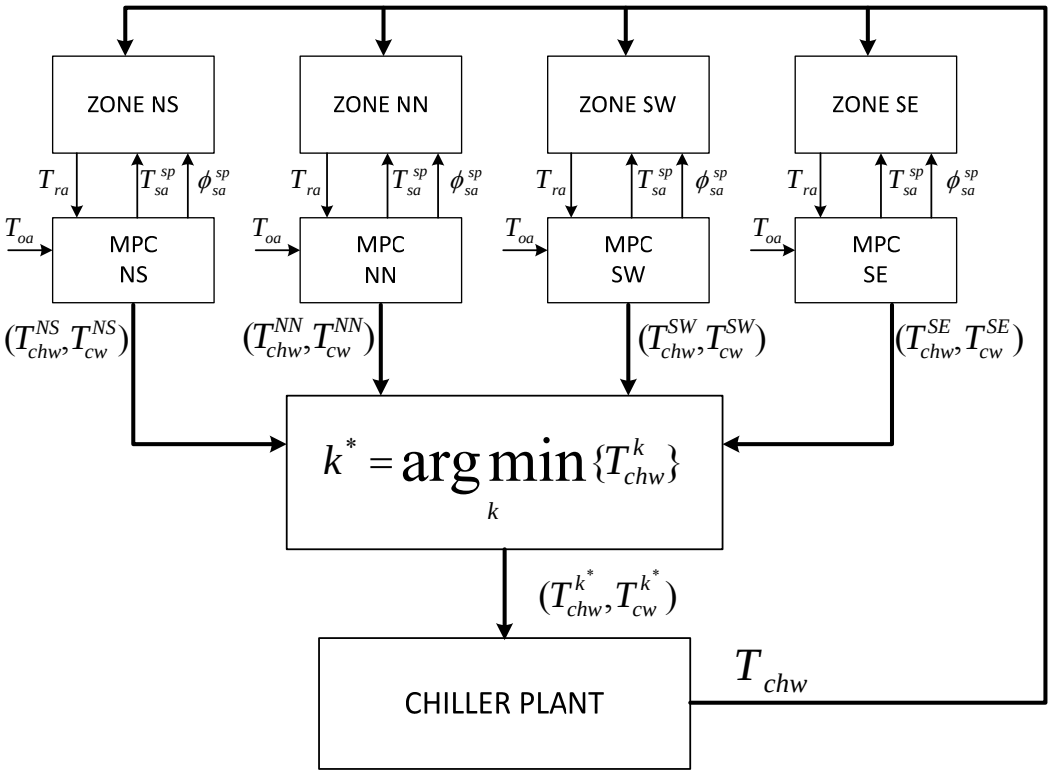

Figure 6.7. Multi–zone control architecture

In this section we discuss details of the design of MPC algorithms used for control of each of the four AHUs. In particular, we give details of the constraints on decision variables and the optimality criterion (the cost). We also give some details related to computational aspects of the implemented controller.

6.4.1 Supervisory MPC Design

In the generic formulation of the considered MPC algorithm, at each discrete time step t and for each thermal zone the following constrained finite-time optimal control problem is solved:

$$\boldsymbol{z}^* = \text{argmin}_{\mathbf{z}} \sum_{k=0}^{N-1} \ell_k\,(y_{t+k}, z_{t+k}, w_{t+k}), \tag{6.6a}$$

$$\text{subj. to} \quad y_{t+j} = f_{ARX}(Y_{t+j}^-, U_{t+j}^-, W_{t+j}^-), \quad j = 1, \dots, N \tag{6.6b}$$

$$(y_{t+k}, z_{t+k}) \in \mathcal{C}_{t+k}, \quad k = 0,2, \dots, N, \tag{6.6c}$$

where the output y_{t+k} is the zone return air temperature (T_{ra}), The decision vector z_{t+k} comprises the supply air temperature reference (T_{sa}^{sp}), supply air flow rate ϕ_{sa}, chilled water temperature T_{chw} and condenser (cooling) water temperature T_{cw} at time $t + k$. The variable w_{t+k} represents the ambient temperature T_{oa} at stage k, as a measured disturbance. Equations (6.6b) are dynamic constraints, where $f_{ARX}(\cdot)$ stands for the linear ARX equation (6.1) and Y_{t+k}^-, U_{t+k}^- and W_{t+k}^- represent *past values* of the ARX model output (T_{ra}) and controlled and

uncontrolled inputs (T_{sa}^{sp}, ϕ_{sa} and T_{oa}), respectively. In the same equation, the values of y_t and w_t correspond to measurements of output T_{ra} and the disturbance T_{oa} at the time instant t. Constraints on ARX model outputs and decision variables are defined by Equation (6.6c). A solution to the problem (6.6) gives a sequence of decision variables $\boldsymbol{z}^*$, of which only the first one, $\boldsymbol{z}_t^\star$, is applied to the plant.

All decision variables are restricted between their minimal and maximal value. Supply air temperature for each zone is bounded to the interval $[55,68]°F$, supply air mass flow rate ϕ_{sa} ranges between 5 and 100 percent of the maximal supply air flow rate for the corresponding zone and minimal and maximal values for the chilled and condenser water temperature are: $T_{chw} \in [40,50]°F$, $T_{cw} \in [75,95]°F$. The temperature of the chilled water T_{chw}^{zone}, required by the AHU of the particular zone, is additionally restricted by following inequality in order to track the reference for the supply air temperature T_{sa}^{sp}:

$$T_{chw}^{zone} \leq T_{ma} - \frac{1}{\varepsilon}\left(T_{ma} - T_{sa}^{sp}\right), \tag{6.7}$$

where ε is the coil efficiency coefficient and T_{ma} is the temperature of the air streaming over the cooling coil, estimated as the temperature of the return and fresh air mixture corrected with the maximal temperature increase over the AHU fan:

$$T_{ma} = \frac{\phi_{ra}T_{ra} + \phi_{fa}T_{oa}}{\phi_{fa} + \phi_{ra}} + \Delta T_{fan}. \tag{6.8}$$

In the TRNSYS model of Building 14 it is assumed that the inflow of fresh air ϕ_{fa} is set to the minimal value corresponding to 5 percent of the *maximal* zone supply air flow. The model can be easily adapted for a more realistic scenario in which the ϕ_{fa} corresponds to a specific portion of the ϕ_{sa}. The temperature increase over the fan, ΔT_{fan} in general depends on the fan speed; for simplicity we used the "worst case" fixed value of $0.85°C$. Constraints on the zone chilled water temperature T_{chw}^{zone} are derived from the *dry cooling coil model* (cf. [5][Sec. 4.1.2]). Coil efficiency ε in Equation (6.7) is set to the fixed minimal value, determined through simulation experiments, in order to compensate for the latent heat component omitted in the cooling coil model.

The return air temperature T_{ra} should remain inside the "comfort zone" corresponding to the interval $[71,75]°F$ for the “occupied hours” (weekdays from 5AM until 7PM) and $[62,84]°F$ for the unoccupied time (after 7PM and before 5AM and during the weekends and holidays). In the actual implementation of the optimization problem (6.6) constraints on return air temperature are implemented as “soft” constraints; instead of enforcing the constraints strictly, their violation is penalized by introducing an additional term in the cost.

The stage cost $\ell_k(\cdot)$ in problem (6.6) consists of three components:

$$\ell_k(y_{t+k}, z_{t+k}, w_{t+k}) = \ell_k^{pow}(y_{t+k}, z_{t+k}, w_{t+k}) + \ell_k^{constr}(y_{t+k}) + \ell_k^{\Delta}(u_{t+k}, U_{t+k}^{-}). \quad (6.9)$$

The first term $\ell_k^{pow}(\cdot)$ reflects the primary objective of the control algorithm to minimize the over–all energy consumption needed for cooling the air in the thermal zone and contains the current fan power (as implemented in the TRNSYS model) and the required *sensible* heat transfer from the air at the inlet of the cooling coil:

$$\ell_k^{pow}(y_{t+k}, z_{t+k}, w_{t+k}) = k_1\phi_{sa} + \frac{k_2}{COP(T_{chw}^{zone}, T_{cw})}\phi_{sa}(T_{ma} - T_{sa}^{sp}), \quad (6.10)$$

where k_1 and k_2 are normalizing constants, $COP(\cdot)$ is the chiller coefficient of performance given by Equation (6.5) and the air temperature at the cooling coil inlet, T_{ma} is approximated by Equation (6.8). The first term $k_1\phi_{sa}$ represents the actual power of the fan. We are using the simple linear model which is implemented in TRNSYS; implementation of the more common (and more realistic) non–linear model based on a cubic polynomial approximation would be a straightforward extension. As already hinted previously, the component of the cost (Equation (6.10)) amounts only to the sensible cooling load. The latent cooling load due to the air humidity is not directly considered in the optimization part. It is however practically accounted for through constraints on the zone chilled water temperature (Equation (6.7)), where the chiller efficiency coefficient ε is set to the lowest observed value for the considered simulation period.

The second term of the stage cost $\ell_k^{constr}(\cdot)$ is a penalty term for the violation of bounds on the return air temperature T_{ra}. Instead of strictly enforcing the constraint $T_{ra} \in [T_{ra}^{\min}, T_{ra}^{\max}]$, we introduce an additional "slack" variable s_k and the constraints:

$$\begin{aligned} T_{ra} - T_{ra}^{\max} &\leq s_k, \\ T_{ra}^{\min} - T_{ra} &\leq s_k, \\ s_k &\geq 0. \end{aligned}$$

Violations of constraints on the return air temperature, T_{ra}, are penalized by augmenting the stage cost with the quadratic term:

$$\ell_k^{constr} = g_k s_k^2,$$

where g_k is the tuning coefficient.

The last term in the stage cost (6.9), $\ell_k(u_{t+k}, U_{t+k}^{-})$, is a quadratic penalty term for variation of the AHU control inputs u_{t+k} (the supply air flow rate ϕ_{sa} and supply air temperature reference T_{sa}^{sp}):

$$\ell_k^{\Delta}(u_{t+k}, U_{t+k}^{-}) = h_k \parallel u_{t+k} - u_{t+k-1} \parallel^2,$$

with the tuning parameter h_k.

Remark 1 Based on our simulation tests, the dominant time constants of the zone temperature vary from 30 to 60 [min] in different zones. Thus, in the current implementation the measured disturbance at time instance t, the ambient temperature T_{oa}, is assumed to remain constant over the prediction horizon of $N = 40$, corresponding to $2[h]$. Future studies can be carried out to investigate the potential benefits or issues by adopting a longer prediction horizon. Also, the control performance may be improved by taking into account temperature predictions from meteorological data.

Remark 2 We must stress the importance of well–tuned low level controllers for successful operation of the presented supervisory MPC approach. In all our discussions we implicitly assume that the reference points passed from the MPC to low level PI controllers are actually attained with negligible transient period and tracking error. We also emphasize the fact that the dynamic models of the zones are obtained for a fixed, nominal value of the chilled water temperature ($44°F$). By changing the chilled water temperature, dynamic behavior of the thermal zone with AHU effectively change. If the local controller that manipulates the valve opening of the cooling coil in order to track the supply air temperature setpoint is tuned to accommodate variations of the chilled water temperature, this change of the zone dynamic behavior will be minor and will not influence the over-all control performance, as is the case in our simulation study.

Remark 3 In our model as well as in the cost we omit the latent part of the thermal load, caused by the incoming air humidity; in a humid climate, where the load due to latent heat is significant, this must be addressed in order to achieve optimal performance of the MPC.

Remark 4 As will be shown in the next section, the MPC algorithm is quite robust and maintains the zone temperatures very close to comfort bounds even in the presence of disturbances not explicitly taken into account in the control design (occupancy, lighting and equipment thermal load). The dominant load part comes from solar radiation, which is well correlated with the ambient temperature most of the day. In smaller spaces, like the SEO office of the Building 14, the occupancy load is most likely going to play a more significant role, and as such must be considered in the control algorithm.

6.4.2 Computational Aspects

In each sampling time step a nonlinear optimization problem (6.6) needs to be solved. With the chosen prediction horizon of $N = 40$, the resulting nonlinear optimization problem has 240 decision variables (160 control variable + 80 variables for predicted outputs and “soft constraint"

slack variables) and 200 inequality constraints. The size of the optimization problem can be significantly reduced if a *move blocking* is applied.

A move blocking is a standard approach in MPC (cf. [6]) to reduce computational complexity of an MPC optimization problem by limiting degrees of freedom. In particular, certain control variables can be restricted to change a limited number of times over the prediction horizon. In our case, move blocking is applied to chiller optimization variables; the number of "moves" for chilled and condenser water temperature for each zone is restricted to 3 with the pattern 6,6,6 and 22 prediction samples over which the values for T_{chw} and T_{cw} are kept constant. This reduces the number of decision variables to 166 and the number of constraints to 123. In the actual implementation, variables of the chiller plant are computed and modified every 6 samples and for the intermediate 5 samples only the values for supply air flow rate and temperature setpoint are computed, while the chiller COP value is kept constant.

The resulting optimization problem is implemented in Matlab and solved using the IPOPT optimization tool [7] with the HSL MA27 sparse linear solver [8]. The IPOPT interface for Matlab is used for this purpose [9]. Computation times required to solve te MPC optimization problem for all 4 zones over the simulation period of 4 days are shown in Figure 6.8.

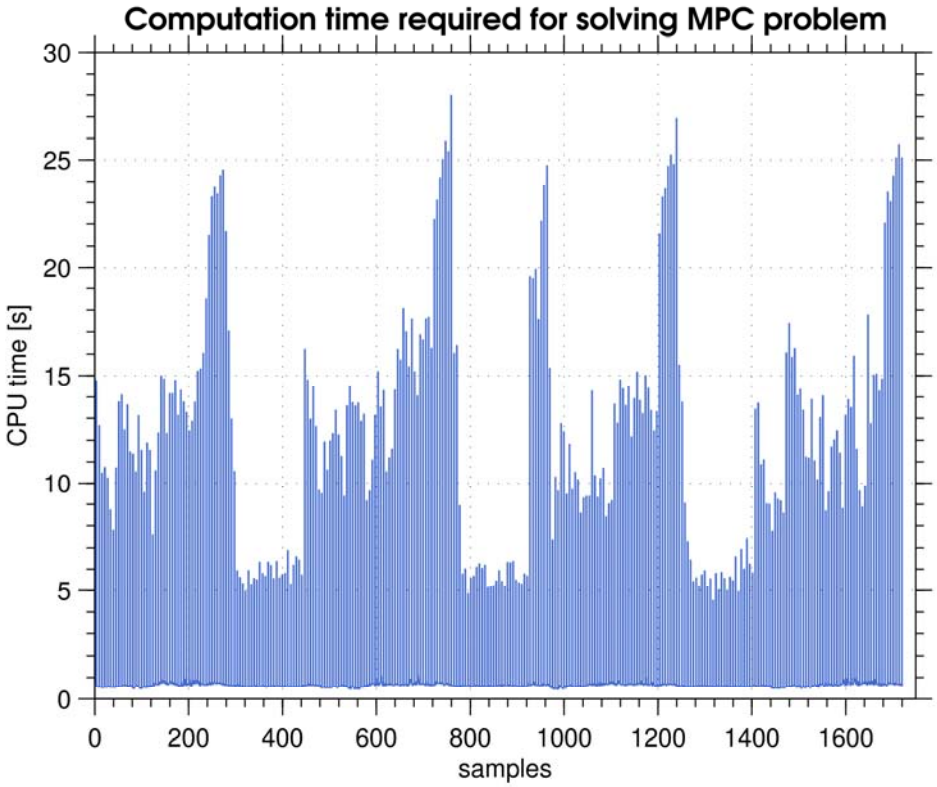

Figure 6.8. Computation times required for solving MPC optimization problem for all 4 zones. Sampling period is $\boldsymbol{T_s = 3[min]}$

Considering that the sampling period is $T_s = 3[\text{min}]$, computation times of max. $30[\text{sec}]$ may be neglected in the prediction of the controlled system behavior. Computational delay can be straightforwardly accounted for by adding the actuation time delays in the model used for prediction.

The current implementation uses only gradient and constraint Jacobian information. Significant performance improvements could be achieved if the Hessian matrix of the Lagrangian was efficiently computed and made available for the IPOPT solver. Exact analytic computation of the Hessian is usually very tedious and time consuming and efficient implementation of Hessian evaluation may be a challenging problem on its own. As an alternative, one should consider, in combination with efficient nonlinear optimization solvers such as IPOPT, an application of *automatic differentiation tools*. More information on the topic and overview of available automatic differentiation methods and software implementations can be found on: http://www.autodiff.org/ .

6.4 Simulation Results

A simulation study was performed on the Building 14 model developed in TRNSYS to evaluate the performance of the MPC controller and investigate the energy savings and causes of performance brought by the MPC controller compared to the baseline control strategy.

6.5.1 Simulation Scenario

As already indicated in Section 6.3, in this study we consider only a cooling scenario during a summer period. In our simulation experiment we consider five days in July (from July 10 to July 15, 2011) in Philadelphia, PA. Weather data used in simulation are actual data recorded by meteorological stations for the selected location and the aforementioned time period are shown in Figure 6.9.

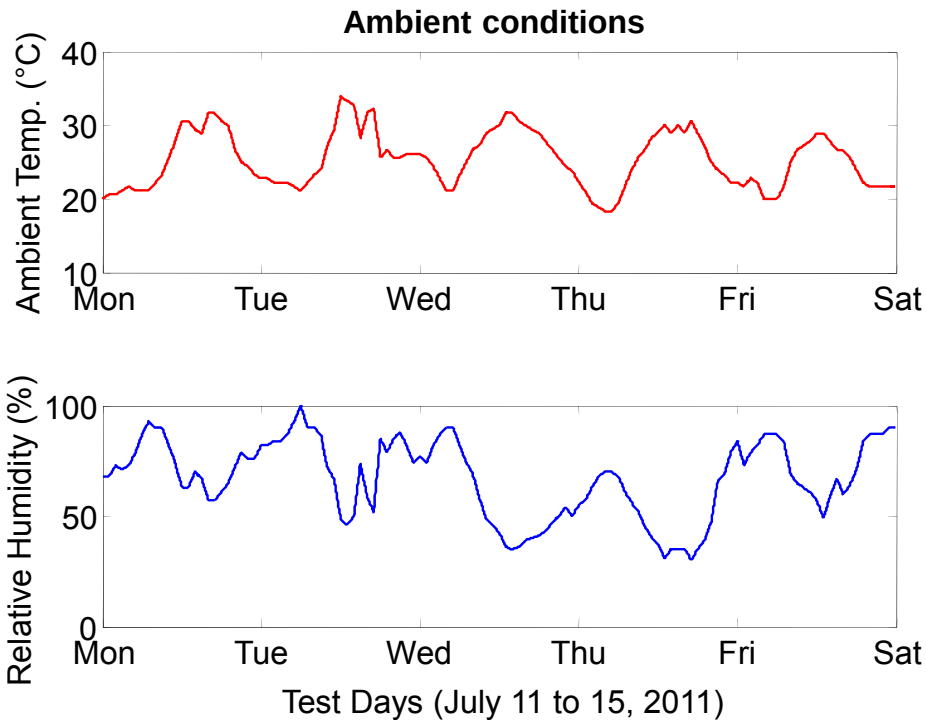

Figure 6.9. Ambient temperature recorded in Philadelphia, PA from July 10-15 2011

Additional thermal load in each zone comes from the zone occupancy, lighting and office equipment. The occupancy schedule and office equipment load for the largest thermal zone (NS wing) are given in Figure 6.10.

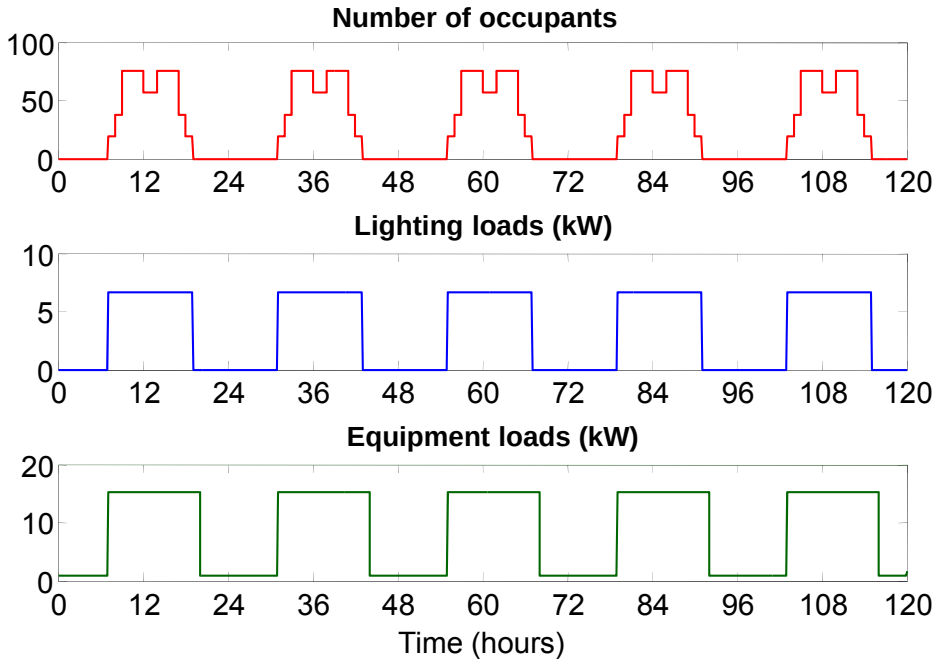

Figure 6.10. Internal load profiles for Building 14 NS wing

The baseline control strategy described in Section 6.3 adjusts the flow of the supply air (ϕ_{sa}^{sp}) in order to maintain the return air temperature of each zone (T_{ra}) during the öccupied hours" (9AM-7PM) at the fixed value of $23.89°C$ $(75°F)$. At the same time, reference values for supply air temperature (T_{sa}^{sp}) and chilled and condenser water temperatures (T_{ch} and T_{cw}) are kept at $12.78°C$, $6.67°C$ and $29.4°C$, respectively.

The goal of the model–predictive control strategy introduced in Section 6.4 is to maintain the return air temperature of each zone in a "comfort interval" by adjusting the inflow and temperature of the supply air for each zone. At the same time, the setpoints for chilled and condenser water temperatures are modified in order to increase the chiller's coefficient of performance (COP). Bounds on the aforementioned temperatures used in MPC are given in Table 6.1.

Table 6.1. Bounds on control variables for MPC

	Min. [°C]	Max. [°C]
T_{ra}	21.00	23.89
T_{sa}^{sp}	12.78	20.00
T_{chw}^{sp}	6.67	10.00
T_{cw}^{sp}	23.89	35.00

6.5.2 Performance Assessment of MPC

Figures 6.11 and 6.12 present the temperature profile of each zone controlled by MPC and also the corresponding control setpoints on the AHU side. As can be observed, the MPC is trying to regulate the temperature in each zone around the upper bound of the thermal comfort region and meanwhile exploiting the trade-offs of supply air temperature and fan flow rate to minimize the energy-based cost function, which is a combination of the fan power and the sensible energy consumption of the cooling coil divided by chiller COP.

Figure 6.13 shows an enlarged view for the comparison of NS zone temperature control for the occupied and unoccupied hours on a particular day (July 12, 2011). Compared to the baseline PI controller, the MPC controller introduced less oscillation and maintained itself very well around the upper bound of the comfort region during most of the time. Such a good tracking performance gives us confidence of further relieving the thermal comfort bound once new energy-saving based thermal comfort metrics (not just zone temperature setpoints) are available.

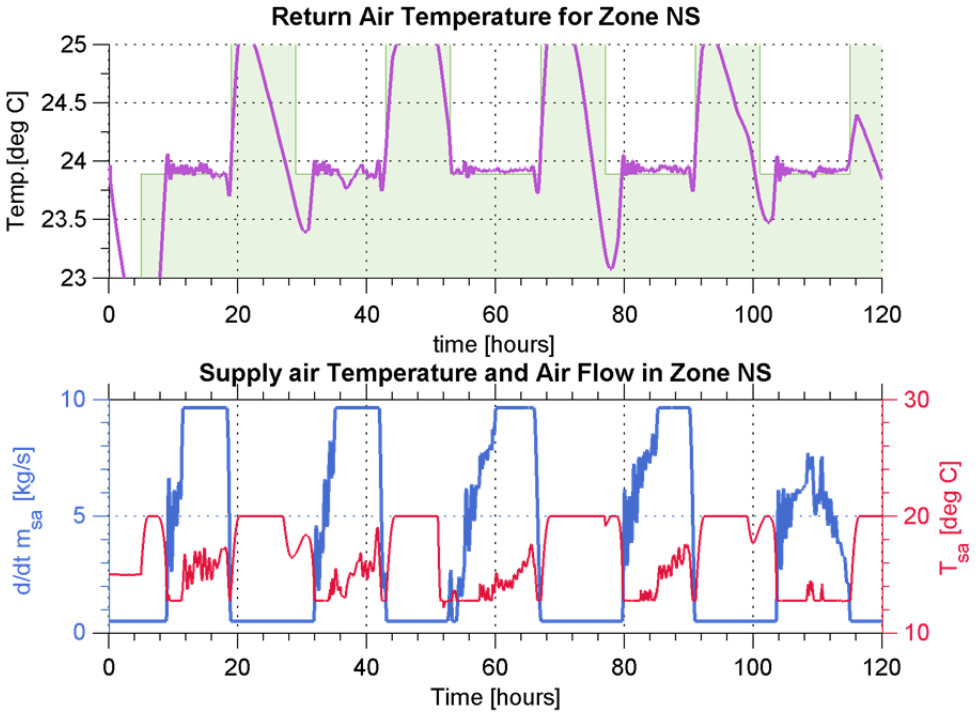

(a) Return air temperature and control inputs for Zone NS

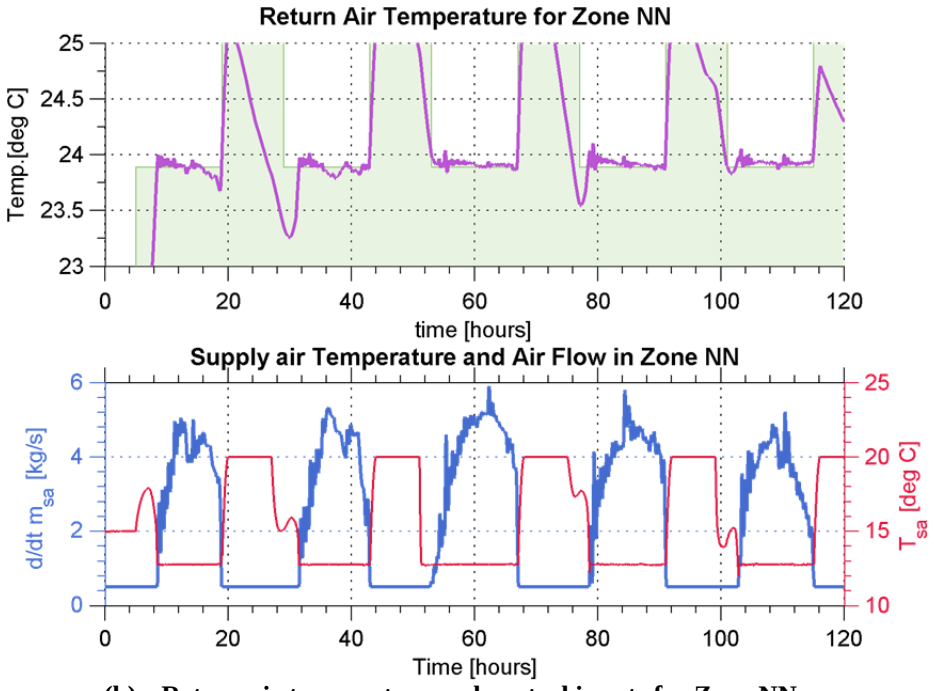

(b) Return air temperature and control inputs for Zone NN

Figure 6.11. Return air temperatures and control inputs for zones NS and NN. Green area on the return air plot marks the desired temperature range

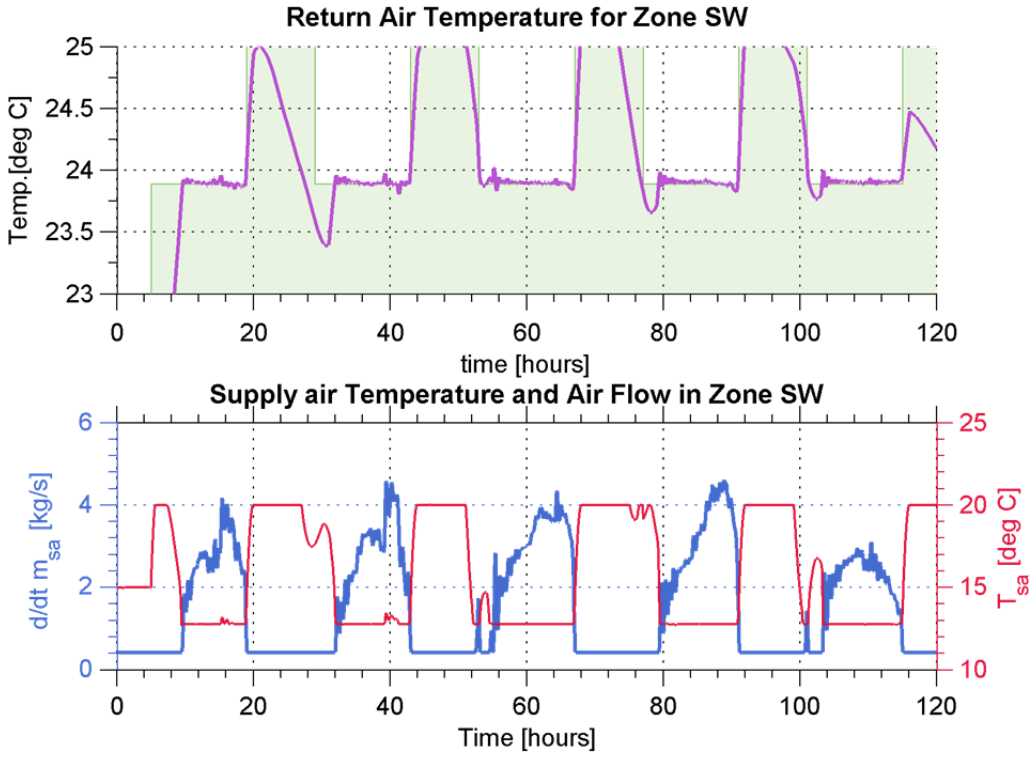

(a) Return air temperature and control inputs for Zone SW

(b)

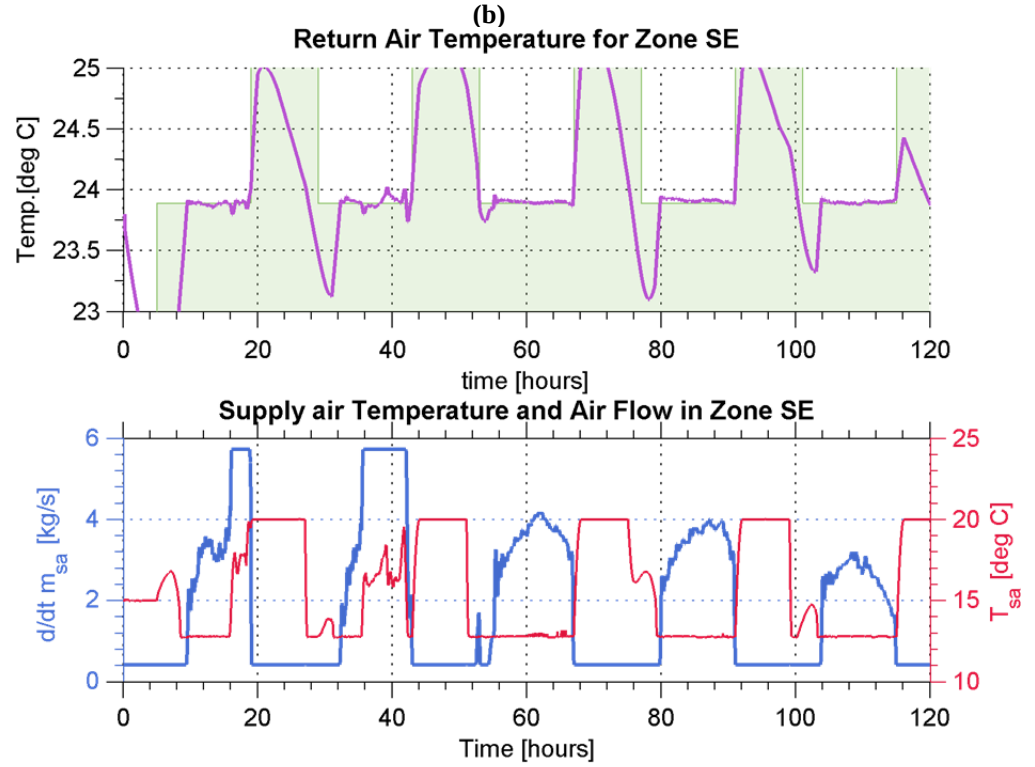

(c) Return air temperature and control inputs for Zone SE

Figure 6.12. Return air temperatures and control inputs for zones SW and SE. Green area on the return air plot marks the desired temperature range

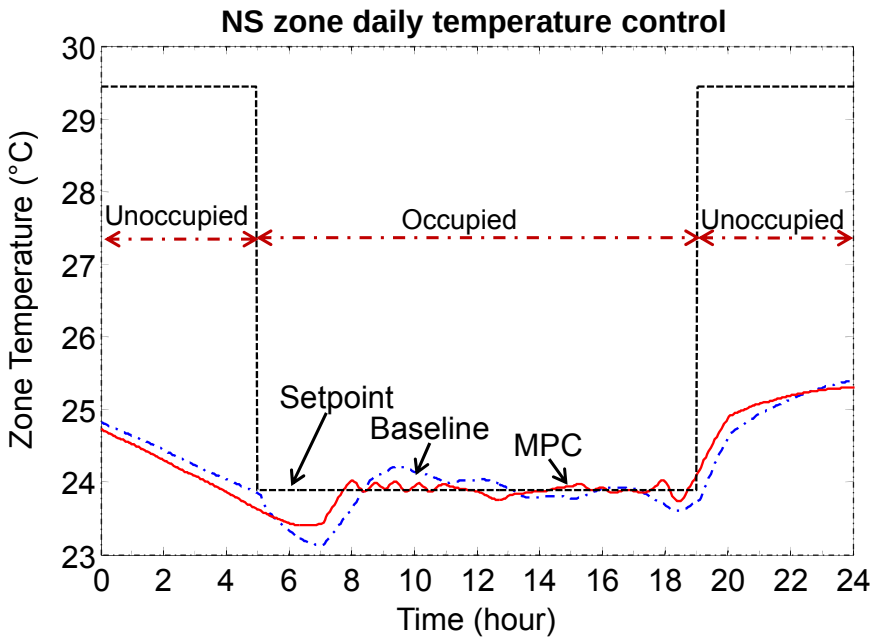

Figure 6.13. NS Zone temperature control and performance of controlled variables from MPC

Figure 6.14 shows results of including chiller plant optimization in the MPC. In the TRNSYS model, the chiller COP is a function of the chilled-water leaving temperature and condenser water entering temperature. In general, higher leaving chilled-water temperature would produce a higher COP at a fixed condenser water entering temperature. Also, from the chiller COP expression (Equation (6.5)), it is obvious that at a given chilled-water temperature, maximum COP is always achieved at the boundary point of the condenser water temperature, i.e., the lower temperature bound. Figure 6.14(a) shows the chiller COP for the test week. The upper bound of the chilled water temperature shown in Figure 6.14(b) is determined by the thermal load from the AHU level. Compared to the baseline temperature of $6.67°C$, the MPC typically maintains the chilled water around half degree higher during the occupied hours. Note that the chiller COP in the first and second day are lower than on other days although the two water temperature setpoints in Figures 6.14(b) and 6.14(c) look very similar. This is due to the high web-bulb temperature in the first and second day so that the actual condenser water entering temperature cannot be lowered further to track its setpoints. This observation motivates us to incorporate the wet-bulb temperature into the chiller COP expression in future work to set a realistic lower bound for the condenser entering water temperature. In addition, for the particular HVAC system of Building 14, the energy consumption of the cooling tower fans and pumps are nearly negligible compared to the chiller energy consumption. Thus the penalty of lowering the condenser water temperature in order to increase the chiller efficiency is not accounted for. In general, due to the lower condenser water temperature, increasing the tower relative airflow (ratio of the airflow to the maximum possible airflow) could help reduce the chiller power. However, this would in turn cause an increase in the tower fan power. Thus, one should consider optimizing the combined chiller and tower power consumption by adjusting the relative tower airflow [10]. In particular, one should check the sensitivity of the chiller power and the tower fan

power to the relative tower airflow, respectively, from which the near-optimal relative tower airflow can be determined [10].

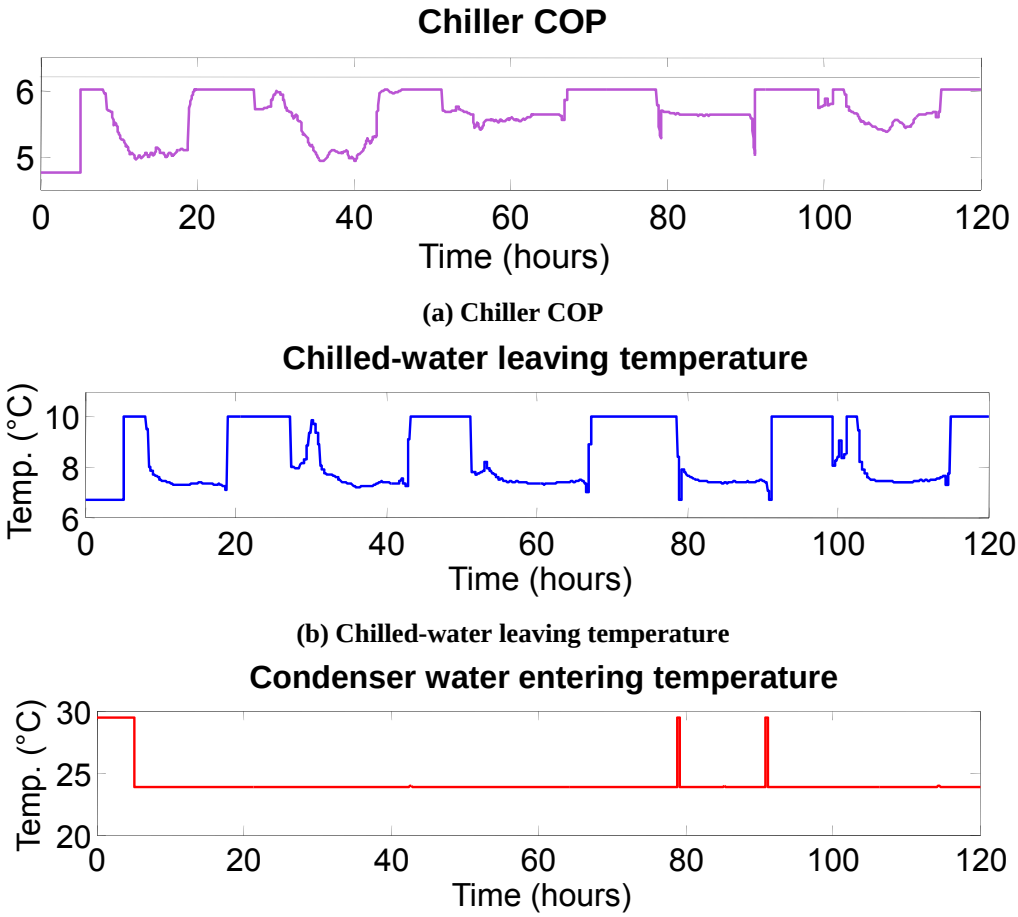

(a) Chiller COP

(b) Chilled-water leaving temperature

(c) Condenser water entering temperature

Figure 6.14. Time evolution of chilled and condenser water temperature and the chiller COP

6.5.3 Potential Energy Savings due to MPC

The energy savings brought by MPC will be presented in two parts. In the first part, we will show the energy savings for MPC by exploiting the trade-offs of control set–points at the AHU level only. The control objective is to obtain the minimum overall energy consumption from the supply fan and the cooling coil in each AHU during the occupied hours. In the second part, we extend our analysis to include the chiller plant optimization and use the advantage of higher chiller efficiency in meeting the thermal loads from these AHUs. Additional savings are achieved by taking advantage of the optimized chiller efficiency through manipulating additional control setpoints of the chilled-water leaving temperature and condenser water entering temperature.

6.5.4 MPC without Chiller Plant Optimization

Figure 6.15 shows comparison of energy consumption for the baseline control and the MPC control without chiller plant optimization. The nearly 6% saving is moderate for the following reasons. When the chiller COP is not optimized it appears as a constant term in the cost function. The only trade-offs being exploited are the supply fan speed setpoint and the supply air temperature setpoint. From the cost function, the supply fan flow rate appears both in the first term (fan power) and the second bilinear term in which it is multiplied by the difference of air temperature after the supply fan and the supply air temperature. Since in the cost function we neglect the effect of latent heat transfer, the second term is underestimated which is a representation of the power consumption for the cooling coil. Thus the first term (fan power) and the second term (cooling coil power) become relatively comparable. Also, the decrease of the latent part of the energy consumption as a function of the supply air temperature is not accounted for. Probably due to these effects, most of the time the MPC determines it is more desirable to minimize the fan flow rate rather than increasing the supply air temperature. Such a behavior gives similar control setpoints in supply air temperature as the baseline except for the first two days. The moderate energy saving in the third to the fifth days are brought by the better zone temperature control from the MPC compared to the baseline.

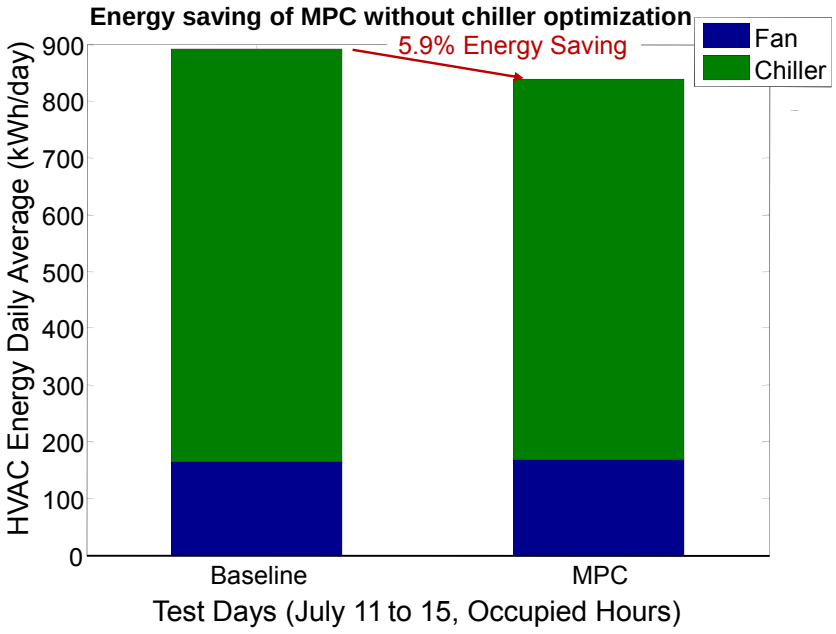

Figure 6.15. Potential energy savings for MPC without chiller plant optimization

6.5.3 MPC with Chiller Plant Optimization

Figure 6.16 shows comparison of energy consumption for the baseline control and the MPC control when chiller plant optimization is included. Promising energy savings at nearly 15% is estimated by manipulating additional setpoints of the chiller-water leaving temperature and condenser water entering temperature. The obtained results indicate significant savings of nearly 9% from the chiller side and comparable energy consumption from the supply fans at the

building level. In particular, the average daily energy consumption in each zone is shown in Figure 6.17; As can be observed, compared to the baseline, the MPC controller in each zone manipulates the ratio of the fan power and the chiller power required for conditioning the zone to satisfy the thermal comfort limits which results in reducing the overall power consumption in each zone, respectively. For example in the NS zone, MPC consumes more fan energy but saves much more energy at the chiller side, which saves the overall energy. For the NN and SW zones, the MPC has comparable fan energy consumption with the baseline but saves overall energy due to chiller savings. For the SE zone, both fan and chiller energy consumption is reduced which results in significant savings in overall energy.

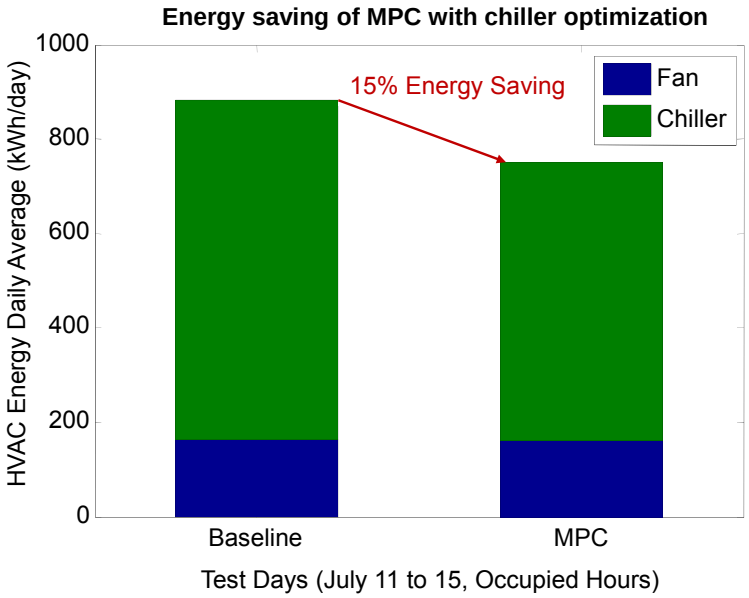

Figure 6.16. Potential energy savings for MPC with chiller plant optimization

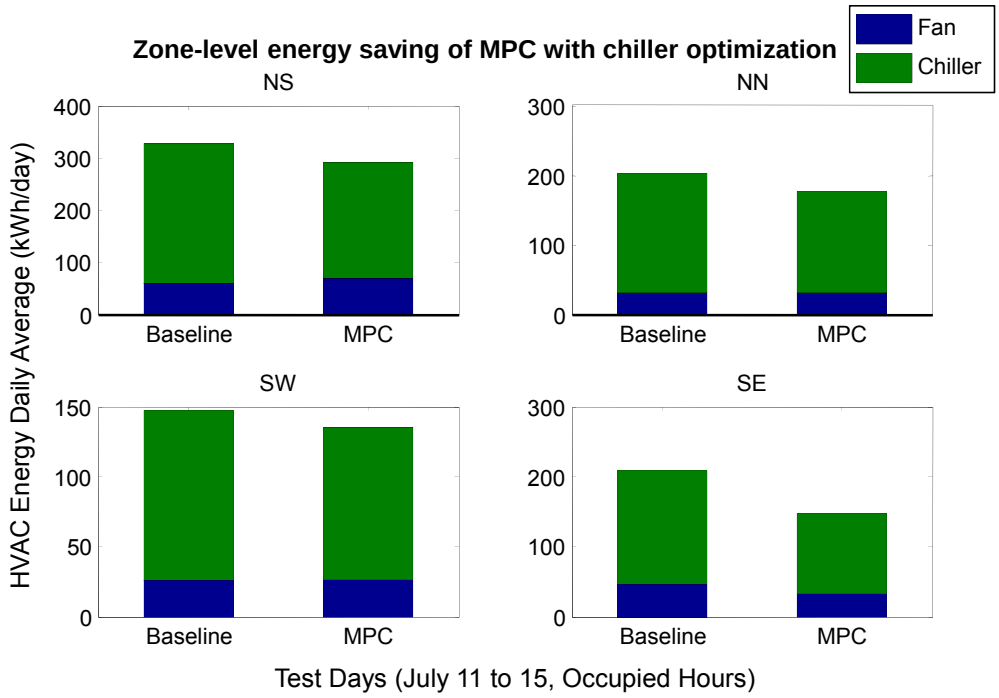

Figure 6.17. Zone-level average daily energy use - HVAC equipment breakdown

6.5 Conclusions

In this study we demonstrated an MPC strategy for HVAC systems based on predictive dynamical models for thermal zones obtained from measured input–output data via system identification. In particular, we have demonstrated the effectiveness of applying a linear ARX model to account for the zone temperature dynamics in the prediction subject to disturbances caused primarily by solar radiation. The usage of linear dynamical models improves computational efficiency of the resulting MPC controller compared to many other approaches. Through a simulation study for a medium-size commercial building, we have demonstrated the promising energy savings potential of nearly 15% by exploiting the trade-offs for control setpoints at the AHU and chiller plant level. However, this study can be further extended at least in the following aspects:

1. *Include optimal outdoor damper control for efficient economizer operation*: In the current study, economizer operation was not included. However, proper use of outdoor air can bring significant energy savings especially in a transition season, e.g., September and October. Future research could be performed to investigate the effectiveness of augmenting this additional decision variable in the MPC cost function.

2. *Include latent heat transfer in the cost function*: The MPC cost function in this study considers only the sensible energy consumption of the cooling coil, which may undermine the relative weights of the cooling coil energy term in the cost function and also neglect the effect of the decrease of latent energy when the supply air temperature at the AHU is increased. Accounting for latent heat would require extension of existing

dynamical models to incorporate inputs such as relative humidity of the fresh air.

3. *Combined cooling tower and chiller optimization*: As described earlier, the combined cooling tower fan and pump energy consumption is nearly negligible when compared to the chiller energy in this study. Future work should consider both the combined energy consumption of the cooling tower fan and pump as well as the chiller energy when determining the optimal condenser entering water setpoint. Also, realistic lower bounds for the condenser temperature should be determined based on the ambient wet–bulb temperature.

4. *Dynamic chiller model for MPC study*: The MPC–based optimal control employed in this study is based on the assumption that the chiller plant and HVAC systems can be treated as steady–state while the dynamics are retained in the building envelope and zones only. The justification is that the dynamics of the chiller and HVAC system are much faster than that of the envelope and zones. Although in the TRNSYS model the local controls are assumed to be ideal, i.e., simultaneously tracking the setpoint, for some practical concerns, we think it is necessary to consider some delays when performing the chiller plant optimization. For example, we perform the chiller optimization every 6 samples (18 min.) and we assume that each temperature setpoint can be met after 4 samples (12 min.)

5. *Better tool–chain for optimization-based control study*: Efficient implementation of an MPC algorithm based on nonlinear optimization requires computations of first and second derivatives of the cost and constraints. For complex models this is a tedious task resulting in an *ad-hoc* code that is difficult to extend. A strong recommendation is to include some of the automatic differentiation software packages, such as [11], into the tool-chain.

6. *Scalability, robustness and stability of the proposed control approach*: Scalability and robustness of the approach needs to be addressed in future studies. Current computational times are sufficiently low for centralized optimization for 4 zones. Inclusion of the second order derivatives would increase the speed of the optimization algorithm and render the presented control algorithm applicable to buildings with larger numbers of thermal zones. The robustness of the proposed MPC controller should be the topic of further investigation. We currently do not encounter such issues since we are performing a simulation–based study in which the local controllers are ideal in the simulation model. However, practical issues such as actuator dead–zone, saturation, and hysteresis as well as controller tuning dynamics, may undermine the effectiveness of the proposed controller. These issue need to be addressed in the control design.

7. *Evaluate new comfort metrics*: New comfort metrics need to be investigated together with the proposed control studies. In this study we consider only the effect of the comfort metric in terms of zone temperature setpoint. However, other environmental variables, such as the relative humidity, need to be accounted for as well. Also, demand–controlled ventilation may be considered when the building zones are partially occupied. Future control studies are expected to leverage the outcomes from the proposed new comfort metrics in order to further reduce the energy consumption of buildings while still

maintaining the comfort conditions.

6.7 References

[1] A. Juditsky, L. Ljung, Q. Zhang, and P. Linskog, *System identification toolbox 7.0-Matlab*, Software MathWorks, March 2007.

[2] S. Yuan, R.D. Taylor, and S. Narayanan, Hierarchical modeling for energy efficient building design. *Technical report*, United Technologies Research Center, Year 1 Final Report in Support of GPIC Energy Efficient Buildings Hub (Subtask 2.2), 2012.

[3] M. Hydeman and K. L. Gillespie. Tools and techniques to calibrate electric chiller component models. *ASHRAE Transactions*, 108(pt. 1), 2002.

[4] L. Ljung. *System Identification: Theory for the User*. Prentice Hall, 2nd edition, 1999.

[5] J.E. Braun. *Methodologies for the Design and Control of Central Cooling Plants*. Ph.D. thesis, University of Wisconsin, Madison, 1988.

[6] R. Cagienard, P. Grieder, E.C. Kerrigan, and M. Morari. Move Blocking Strategies in Receding Horizon Control. In P*roc. 43rd IEEE Conference on Decision and Control* (*CDC'04*), Paradise Island, Bahamas, December 2004.

[7] A. Wächter and L. T. Biegler. On the implementation of an interior-point filter line-search algorithm for large-scale nonlinear programming. *Mathematical Programming*, 106:25-57, 2006.

[8] I.S. Du_ and J.K. Reid. The multifrontal solution of indefinite sparse symmetric linear equations. *ACM Trans. Math. Software*, 9(3):320-325, September, 1983. Implemented as MA27 routine of HSL numerical library as (http://www.hsl.rl.ac.uk/).

[9] P. Carbonetto. MATLAB Interface for IPOPT. Available from: https://projects.coin-or.org/Ipopt/wiki/MatlabInterface , 2011.

[10] J.E. Braun, A general control algorithm for cooling towers in cooling plants with electric and/or gas-driven chillers, *HVAC&R Research*, 13(4):581-598, July 2007.

[11] Robert Fourer, David M. Gay, and Brian W. Kernighan. AMPL: A Modeling Language for Mathematical Programming. The Scientific Press (now an imprint of Boyd & Fraser Publishing Co.), Danvers, MA, USA, 1993.

7. MPC Case Study with Reduced-Order Building Model

This section is focused on utilizing the reduced-order building model developed in section 2 within the MPC structure presented in section 3 for a simple case study. The primary goal is to establish and demonstrate an initial set of tools that can be further developed to enable a tool chain for more complex systems and considerations.

7.1 Overview

Generally speaking, the computational cost of applying model-based predictive control (MPC) grows significantly with the increasing complexity of the system, making it difficult for the real-time implementation of MPC. The objective of the case study outlined in this section is to provide a means for implementing the MPC in multi-zone buildings where there are significant degrees of freedom in terms of HVAC supervisory control variables and multi-zone air temperatures set points. To be realistic, we avoid any assumptions made mainly for reducing the computational load such as constant COP of plant and linear or quadratic form of thermal comfort model. A method which decouples the plant and building analyses is investigated based on the fact that the dynamics of the plant occur on a relatively small time scale compared to the dynamics of the building [1]. Also, a state-space transformation-based technique is applied to determine a reduced-order model that is more amenable for controller design and optimization.

7.2 Nomenclature

R = electric rates [$/kWh]
P = power consumption [kW]
T_z = zone air temperature [C]
T_{MRT} = mean radiant temperature [C]
N_z = number of zones (or rooms)
N_w = number of walls in a zone (or a room)
N_g = the number of heat generation source inside of wall such as radiant heating floor
n = dimension of state
n_o = dimension of output
N = number of steps over prediction horizon
T_{OA} = outdoor air temperature[C]
Q_{vent} = mechanical ventilation at the zone [kW]
m_{OA} = set point for outdoor air mass flow rate[kg/s]
m_{sup} = set point of supply air mass flow rate[kg/s]
m_{CW} = set point of condenser water mass flow rate[kg/s]
m_{CHW} = set point of chilled water mass flow rate[kg/s]
T_{CWS} = set point of condenser water supply temperature[C]

T_{CHWS} = set point of chilled water supply temperature[C]
T_{zone} or T_z = zone air temperature (setpoint) [C]
P = power[kW]
PLR = part load ratio
P_{ref} = reference power consumption[kW]
Q_{ref} = reference capacity[kW]
Q_{CL} = cooling load[kW]
Q_{CCL} = cooling coil load[kW]
Q_{CHL} = chiller load[kW]
Q_{CTL} = cooling tower load[kW]

7.3 Main Assumptions

The main assumptions adopted in this study are summarized as follows.

- We only consider the electrical power consumption from fans, pumps, and chillers, but not from other sources such as lighting and electric heaters.
- Forecasts of weather and internal loads are assumed to be perfect.
- Constant convective heat transfer coefficients at the interior surfaces are assumed.
- Relative humidity and CO_2 level of the zone are not considered.
- Local controllers are ideal such that all feedback controllers follow set-points exactly unless limited by capacity.
- The plant operation is quasi-static and contains no dynamics. For this case study, the plant-side energy storage effects are assumed to be negligible compared to the building thermal mass effects. A careful investigation of the accuracy and validity of this assumption will be considered in the future.
- Only time-of-use energy charges are considered with no demand charges.

7.4 Overview of the Proposed Approach

By neglecting plant dynamics, a method which decouples the plant and building analyses can be applied to reduce the computational cost of testing a supervisory control algorithm. The approach was introduced by Braun [1] and can be found in several works, including [2], [3], [4] and [5]. This approach is advantageous for reducing computational demand for implementation of MPC, because the analysis of plant side can be carried out off-line. However there are many difficulties in obtaining an optimal map, and in determining its validity due to the large number of the variables.

To tackle the computational cost issue, we propose to use the model-order reduction technique described in section 4 to characterize the building dynamics. Most of the previous strategies to handle complex building thermal networks for optimal control are based on system identification methods. Data-driven black box models, which rely on experimental data or simulation results from a physical model, can lead to unrealistic and non-interpretable predictions [6]. Furthermore,

one of the most important and difficult problems in system identification is to choose the "best" model among a set of candidate models, which necessarily requires a "model validation" process. Typically up to 80% of the computation time is spent on this step. The approach presented in section 4 for generating a reduced-order building model is based on a physical description and may lead to a more reliable model that is more easily obtained.

The overall approach is shown in Figure 7.1.

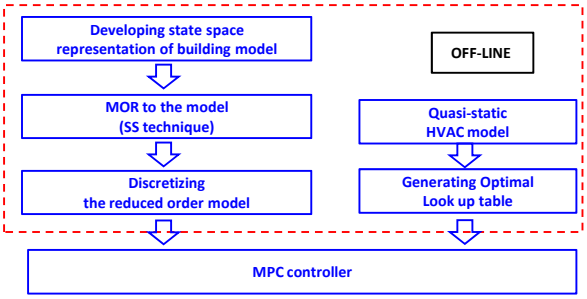

Figure 7.1. Approach to constructing MPC controller for reduction of computational cost

7.5 Objective Function for Model Predictive Control

The objective of MPC method for building systems is to minimize energy costs while maintaining thermal comfort. For this study, the cost of electricity is assumed to vary with time but in the absence of any demand charges. The utility cost is given by

$$Utility = \sum_{k=0}^{N-1} R_k \times P_k \times \Delta t,$$

where $R[k]$ is the electric rate for any interval k [$/kWh] and $P[k]$ is the power consumption for the HVAC system during that time step. An HVAC plant model is described in the subsection on the cooling plant.

Many approaches have been suggested for taking thermal comfort into account for the MPC problem. Examples of comfort level metrics include zone air temperature, relative humidity or CO_2 concentration. Comfort metrics can be either introduced explicitly into the objective function resulting in a multi-objective optimization problem or implicitly in the state/output constraints. One simple approach is to introduce a linear or quadratic form of the thermal comfort model into the objective function in which the discomfort level increases when zone air temperature, relative humidity or CO_2 concentration deviate from given comfort ranges (e.g., [11], [12]) Sometimes the quadratic or linear thermal comfort levels are treated as a state-constraint (e.g., [7], [13]).

Another comfort level metric that incorporates many different indoor environmental parameters is the predicted mean vote (PMV). PMV has been introduced in MPC formulations in the form of state constraints, e.g., PMV value must be kept within the range of -0.5 and 0.5 [8]. Fanger

(1967) developed a PMV model that uses six input variables: zone air temperature, relative humidity, relative air velocity, mean radiant temperature, activity level, and insulation value of the clothing. A zero value of PMV represents the best average thermal comfort condition for occupants. There are seven discrete values corresponding to seven thermal sensations: -3 cold, -2 cool, -1 slightly cool, 0 neutral, 1 slightly warm, 2 warm, and 3 hot. Fanger also related the percent of people dissatisfied (PPD) to PMV with the following formula.

$$PPD = 100\text{-}95\exp[-(0.03353PMV^4 + 0.2179PMV^2)]$$

The PMV-PPD model is widely used and accepted for design and field assessment of comfort conditions [9].

In this study, Fanger's PPD model is used to express the complex nature of thermal discomfort. This model can be included in the objective function or implicitly as a constraint. In the former case, the objective function could be of the form

$$J = \sum_{k=0}^{N-1} R_k P_k \Delta t + \gamma \sum_{k=0}^{N-1} O_k \times PPD_k \Delta t$$

where O_k represents occupancy associated with office hours. For example,

$$O_k = \begin{cases} 1, \; k \in OfficeHour \\ 0, \; else \end{cases}$$

This is a multi-objective optimization problem where selection of the weighting factor, γ, becomes an issue. The factor might vary for different systems. In this study, the PPD model is included as a constraint to avoid the difficulty of determining a weighting factor.

The objective function used in this study is expressed as

$$J = \sum_{k=0}^{N-1} R_k P_k \Delta t \text{ with the constraints } \begin{cases} PPD_k \le 10, \; k \in OfficeHour \\ PPD_k < 30, \; else \end{cases}$$

The value 10 comes from the ASHRAE Fundamentals and corresponds to a PMV range of ± 0.5. The value of 30 is chosen to correspond to "slightly warm" or "slightly cool" according to the PMV index.

7.6 Evaluation of PPD

In the current study, the following assumptions were employed in calculating PPD.

- Relative humidity in a zone is 50%

- Air velocity is less than 0.2 m/s so that the convective heat transfer coefficient is assumed to be 3.1W/m^2-K (Seated with moving air condition) [10]
- The values of 0.5 "clo" and 0.9 "clo" are used for insulation of clothing/ensemble during summer and winter, respectively. Each value approximately represents "Trousers, short-sleeved shirt" and "Trousers, long-sleeved shirt plus suit jacket" respectively [10].
- Unit "Met", i.e., 58.2 W/m^2, is used as the metabolic rate which corresponds to the energy produced per unit surface area of a seated person at rest.

Figures 7.2 and 7.3 show PPD as a function of zone air and mean radiant temperatures for the summer and winter clothing levels with the assumptions given above. For the summer case with 0.5 clo, the comfort range of dry air temperature (within 10% of PPD) is higher than that for the winter case with 0.9 clo for a specific mean radiant temperature. This matches the figure of "Acceptable range of operative temperature and humidity for spaces that meet criteria specified in section 5.2.11" in the ASHRAE standard 55.

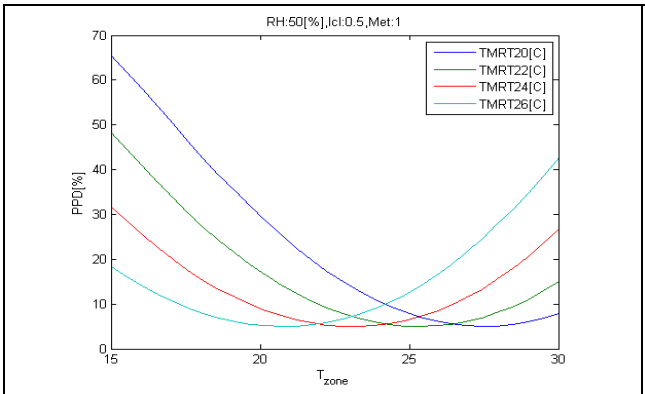

Figure 7.2. Summer PPD with 50% RH, 0.5 clo, unit Met

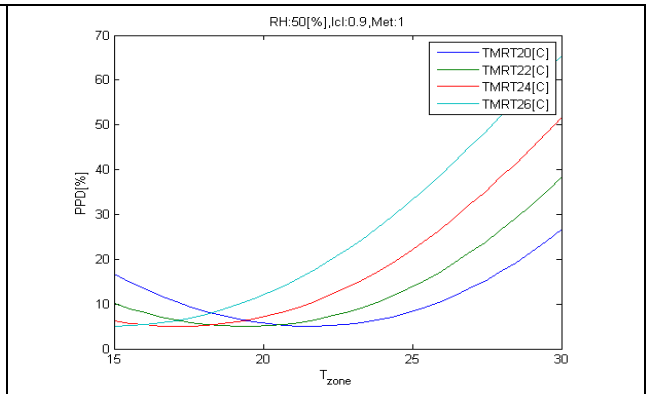

Figure 7.3. Winter PPD with 50% RH, 0.9 clo, unit Met

The evaluation of PPD requires solving nonlinear algebraic equations, which could be a burden for the MPC problem. Therefore, in an effort to reduce computational cost, a regression method is adopted. The independent variables are zone air temperature and mean radiant temperature, which together determine the PPD value for the assumptions previously specified. The regression model is as follows

$$PPD[\%] = \beta_0 + \beta_1 T_z + \beta_2 T_{MRT} + \beta_3 T_z^2 + \beta_4 T_{MRT}^2 + \beta_5 T_z \times T_{MRT} + \beta_6 T_z^3 + \beta_7 T_{MRT}^3 + \beta_8 T_z^2 \times T_{MRT} + \beta_9 T_z \times T_{MRT}^2$$

Separate models were determined for summer and winter clothing. Figures 7.4 and 7.5 show that the regression model tracks the Fanger predictions of PPD over the input range of interest. The scattered points represent the calculated values and the continuous color map indicates the regression-based model.

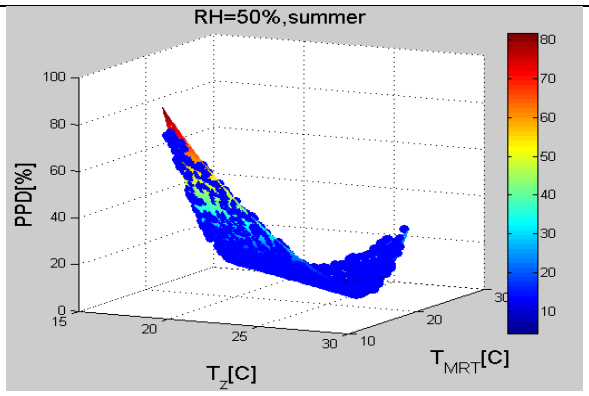

Figure 7.4. Comparison of regression and Fanger model predictions for summer (50% RH, 0.5 clo, unit Met)

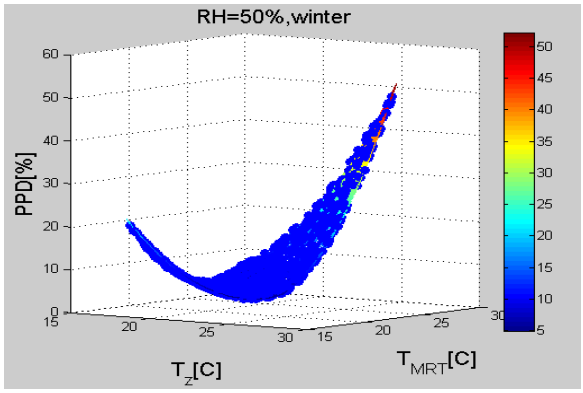

Figure 7.5. Comparison of regression and Fanger model predictions for summer (50% RH, 0.9clo, unit Met)

7.7 Reduced-Order Building Model

A detailed description of the construction of the reduced-order building model is provided in section 4. In this section, the procedure for integrating the MPC and the reduced-order model is discussed. The final form of the reduced order building system, which is linear time invariant, is

$$\dot{x} = Ax + Bu$$
$$y = Cx$$

The input u is given by $u^T = \begin{bmatrix} \vec{q}_{ei}^T & \vec{Q}_z^T & \vec{q}_{gen}^T \end{bmatrix}^T$, where $\vec{q}_{ei}$ is the convective heat flux from outside temperature, long-wave radiation due to sky and ground temperature, absorbed short wave radiation and radiative sources due to internal gains or solar transmission through windows; $(\vec{Q}_Z)_I = \dot{Q}_S^I + \dot{m}_{inf}^I C_p T_a + \dot{Q}_{vent}^I$ is the convective internal source, infiltration and ventilation heat addition; $\vec{q}_{gen}$ is the heat generation inside of a wall due to a radiant heating or cooling.

It is preferable to distinguish the controllable and uncontrollable inputs for MPC purposes. If the infiltration is negligible, then

$$u = \begin{bmatrix} \vec{q}_{ei} \\ \vec{Q}_S \\ \mathbf{0} \end{bmatrix} + \begin{bmatrix} \mathbf{0} \\ \vec{Q}_{vent} \\ \vec{q}_{gen} \end{bmatrix} = \begin{bmatrix} I_{2 \cdot NwNz} & \mathbf{0} \\ \mathbf{0} & I_{Nz} \\ \mathbf{0} & \mathbf{0} \end{bmatrix} \begin{bmatrix} \vec{q}_{ei} \\ \vec{Q}_S \end{bmatrix} + \begin{bmatrix} \mathbf{0} & \mathbf{0} \\ I_{Nz} & \mathbf{0} \\ \mathbf{0} & I_{Ng} \end{bmatrix} \begin{bmatrix} \vec{Q}_{vent} \\ \vec{q}_{gen} \end{bmatrix}$$
$$\equiv \tilde{T}_w \begin{bmatrix} \vec{q}_{ei} \\ \vec{Q}_S \end{bmatrix} + \tilde{T}_u \begin{bmatrix} \vec{Q}_z \\ \vec{q}_{gen} \end{bmatrix}$$

where $\tilde{T}_w \in R^{(2\cdot Nw\cdot Nz+Nz+Ng)\times(2\cdot Nw\cdot Nz+Nz)}$, $\tilde{T}_u \in R^{(2\cdot Nw\cdot Nz+Nz+Ng)\times(Nz+Ng)}$ and I is identity matrix.

By assigning

$$w \equiv \begin{bmatrix} \vec{q}_{ei} \\ \vec{Q}_S \end{bmatrix}, u_c \equiv \begin{bmatrix} \vec{Q}_{vent} \\ \vec{q}_{gen} \end{bmatrix},$$

the following LTI form can be obtained.

$$\dot{x} = Ax + B_w w + B_u u_c$$
$$y = Cx$$

where $B_w = B\tilde{T}_w$ and $B_u = B\tilde{T}_u$.

The controllable input, u_c, includes the heat extraction/addition rate to the zone air and a heat source inside a wall. It could represent mechanical ventilation, an electric heater, chilled beam or radiant heating /cooling. For this case study, it is assumed that only mechanical ventilation is available as the controllable input. w represents several uncontrollable terms, including the heat flow due to solar radiation, long-wave interaction between sky/ground and exterior walls and uncontrollable internal heat gains due to occupants and so on. The output y is chosen to be the zone air and mean radiant temperatures that are inputs to the PPD model. Surface weighted average temperatures are used to approximate the mean radiant temperature.

7.8 MPC Controller Setup

For simplicity,

- the controllable input, u_c, is denoted as u
- the current time within the MPC implementation is set to zero
- Therefore, a predicted sequence of the state is expressed as $x[1], ..., x[N]$ not as $x(k+1|k),...,x(k+N|k)$. A similar sequence is used for the input and output vectors.
- Zero order hold discretization (ZOH) is used for the continuous system and it is denoted as $x[k+1] = Ax[k] + B_w w[k] + B_u u[k]$, although the matrices are different from those for the continuous system.

The states over the prediction horizon are obtained successively by applying the recursion relationship,

$$x[1] = Ax[0] + B_w w[0] + B_u u[0]$$

$$x[2] = A^2 x[0] + AB_w w[0] + B_w w[1] + AB_u w[0] + B_u w[1]$$

.

.

$$x[N] = A^N x[0] + A^{N-1}B_w w[0] + A^{N-2}B_w w[1] .. + B_w w[N-1] + A^{N-1}B_u u[0] + A^{N-2}B_u u[1] .. + B_u u[N-1]$$

or in matrix form,

$$\begin{bmatrix} x[1] \\ x[2] \\ .. \\ x[N] \end{bmatrix} = \begin{bmatrix} A \\ A^2 \\ .. \\ A^N \end{bmatrix} x[0] + \begin{bmatrix} B_w & & & \mathbf{0} \\ AB_w & B_w & & \\ .. & .. & .. & \\ A^{N-1}B_w & A^{N-2}B_w & .. & B_w \end{bmatrix} \begin{bmatrix} w[0] \\ w[1] \\ .. \\ w[N-1] \end{bmatrix} +$$

$$\begin{bmatrix} B_u & & & \mathbf{0} \\ AB_u & B_u & & \\ .. & .. & .. & \\ A^{N-1}B_u & A^{N-2}B_u & .. & B_u \end{bmatrix} \begin{bmatrix} u[0] \\ u[1] \\ .. \\ u[N-1] \end{bmatrix}$$

With the same procedure,

$$\begin{bmatrix} y[1] \\ y[2] \\ .. \\ y[N] \end{bmatrix} = \begin{bmatrix} CA \\ CA^2 \\ .. \\ CA^N \end{bmatrix} x[0] + \begin{bmatrix} CB_w & & & \mathbf{0} \\ CAB_w & CB_w & & \\ .. & .. & .. & \\ CA^{N-1}B_w & CA^{N-2}B_w & .. & CB_w \end{bmatrix} \begin{bmatrix} w[0] \\ w[1] \\ .. \\ w[N-1] \end{bmatrix}$$

$$+ \begin{bmatrix} CB_u & & & \mathbf{0} \\ CAB_u & CB_u & & \\ .. & .. & .. & \\ CA^{N-1}B_u & CA^{N-2}B_u & .. & CB_u \end{bmatrix} \begin{bmatrix} u[0] \\ u[1] \\ .. \\ u[N-1] \end{bmatrix}$$

The above matrix equation can be written in the following compact form,

$$X = A_X x[0] + B_W W + B_U U$$

$$Y = C_Y x[0] + D_W W + D_U U$$

$$B_W \in R^{(n\cdot N)\times((2\cdot Nw\cdot Nz+Nz)\cdot N)}, B_U \in R^{(n\cdot N)\times((Nz+Ng)\cdot N)}$$
$$D_W \in R^{(n_o\cdot N)\times((2\cdot Nw\cdot Nz+Nz)\cdot N)}, D_U \in R^{(n_o\cdot N)\times((Nz+Ng)\cdot N)}$$
$$W \in R^{(2\cdot Nw\cdot Nz+Nz)\cdot N}, U \in R^{(Nz+Ng)\cdot N}, Y \in R^{n_o\cdot N}$$

where X, Y, U, W indicates the sequences of states, outputs, controllable and uncontrollable inputs, respectively and n, n_o and N are the dimensions of the states, outputs and the number of time steps over the prediction time horizon.

The MPC problem for the case study considered here is expressed as

$$u, v = \arg\min \sum_{k=0}^{N-1} R_k P(y_k, w_k, u_k, v_k)\Delta t$$
$$s.t. \begin{cases} x_{k+1} = Ax_k + B_w w_k + B_u u_k \\ y_k = Cx_k \\ PPD(y_k) \le 10,\ k \in OfficeHour \\ PPD(y_k) < 30,\ else \\ f(y_k, w_k, u_k, v_k) = 0 \\ g(v_k) \le 0 \end{cases}$$

where v represents all the set-points in the HVAC system for this study:

- flow rate of supply air and outdoor air
- flow rate and temperature of chilled water
- flow rate and temperature of condenser water

The arguments of the minimum are the vector input sequences of u_c and v, i.e., $\{u[0], u[1], u[2], ..., u[N-1]\}$ and $\{v[0], v[1], v[2], ..., v[N-1]\}$. In order words, the goal is to find the optimal trajectories that minimize the energy costs while keeping the thermal comfort level within specified bounds.

For each prediction time step, $k \in [0, N-1]$, PPD is calculated using the regression model. The power consumption of the plant is a function of the cooling load, room air temperature, and ambient conditions. Therefore, a detailed model that includes these important factors is needed. The plant model is represented as $f(y_k, w_k, u_k, v_k) = 0$ and contains nonlinear algebraic equations.

To handle nonlinearities associated with the plant model, a Sequential Quadratic Programming (SQP) optimization algorithm is used to solve the optimal control problem.

7.8 MPC Case Study Description

The case study considered is simple in order to test initial development of the MPC algorithms. Only a single zone is considered that is served by a dedicated air-handling unit with a chiller plant that is scaled to meet the peak zone load.

7.8.1 Building Description

The building considered in this case study, the Purdue Living Lab #1, is depicted in Figure 7.6. Some parameters employed in the modeling include

- The size of the building: 32[ft] for width and depth and 14.5[ft] height
- The materials for wall construction consist of concrete, insulation board, stucco, gypsum board, and double glazed windows.
- The east wall and floor contact with other rooms and contacting zone air temperatures of adjacent rooms are assumed to be fixed at 22ºC.
- TMY2 weather data in Indianapolis for the summer season (July/1 to July/31)
- 17.77 [W/m2-K] and 3.05[W/m2-K] are used for convective heat transfer coefficient at the outside surface and inside surface, respectively.
- 65 Watt per person, 230 Watt per computer and 20 Watt/m2 are assigned for the internal gains during the office hours (7am ~ 6pm)
- 20 persons with 20 computers during office hours
- Electricity rates of 0.04 [$/kWh] for office hours (7am ~ 6pm) and 0.02 [$/kWh] for other times.

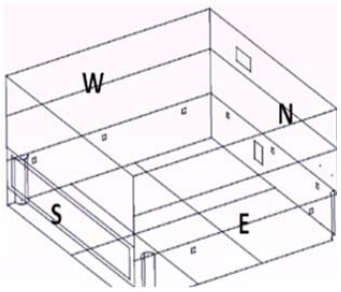

Figure 7.6. Purdue Living Laboratory schematic

Material properties associated with this zone are specified in Tables 7.1 and 7.2

Table 7.1. Material properties used in the simulation for Purdue Living Lab #1

	Concrete	Insul. Bd	Gyp. Bd	Stucco	BR01	IN46	PW04
ρ[kg/m^3]	2242.59	288.33	800.92	1858.14	1121.29	24.028	544.628
k[W/m-K]	1.73	0.055	0.16	0.7211	0.1625	0.0231	0.1156
C_p[J/kg-K]	837	1297.9	837	837	1465	1591	1240

Table 7.2. Layer constructions of walls for Purdue Living Lab #1

Orientation	Outside → Inside			
East Wall	Gyp. Bd 0.015 [m]	IN46 0.018 [m]		Gyp. Bd0.015 [m]
North Wall	″	″		″
South Wall	Stucco 0.025 [m]	InsulBD 0.055[m]	Insul 0.06[m]	GypBd 0.013[m]
West Wall	″	″	″	″
Ceiling	BR01 0.016[m]	IN46 0.066[m]		PW04 0.009[m]
Floor	IN46 0.06 [m]		Concrete 0.2[m]	
Window	Waermeschutzglas,Ar, 1.4 71/59 * the data is extracted from Trnsys window library and window to wall area ratio is 0.2739.			

7.8.2 Plant Description

A schematic of the simple cooling plant considered in this case study is shown in Figure 7.7. It contains an outdoor air (OA) damper, cooling coil, chiller, cooling tower and pumps. The model assumes that the components in the system operate at quasi-steady state. In this study, variable-speed cooling tower fans, pumps and supply air fans were considered. Heat transfer through air duct and pipes are neglected and zone loads are met by control of the supply air to the space (termed mechanical ventilation). The plant equipment models and performance characteristics are based on representations from EnergyPlus and are described in a later section.

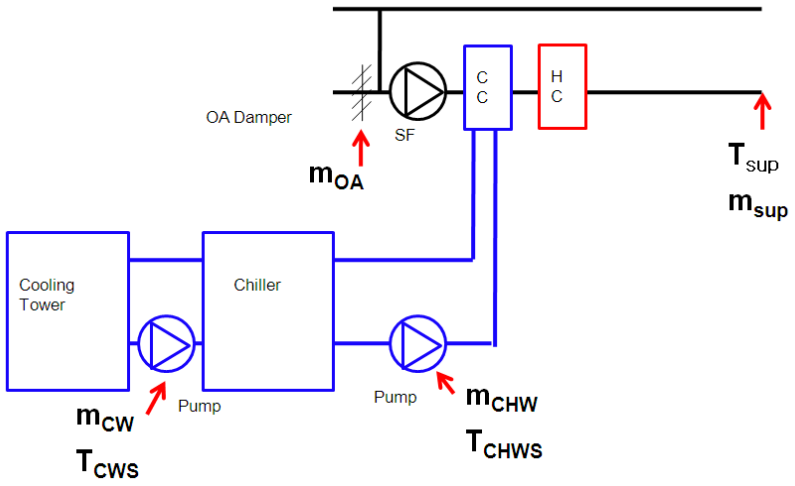

Figure 7.7. Schematic diagram of the considered cooling plant

7.8.3 MPC Description

Figure 7.8 depicts the MPC controller for this case study. The MPC controller provides set points to the local controller of the HVAC system based on zone air temperature, mean radiant temperature and predictions of weather data and internal sources. The number of setpoints that need to be determined by the optimizer of the MPC has a large effect on the computational requirements and feasibility of implementation. The concept employed here to solve this

problem is to decouple the building and plant system. If the dynamic behaviour of the plant is neglected, then the optimal set of cooling plant setpoints is not affected by any past information but only depends on current conditions. Therefore, an optimal plant map can be generated as a function of zone air temperature, T_{OA}, RH, Q_{vent} and used as a lookup table for the MPC algorithm to determined the tracking of zone cooling that takes optimal use of the building dynamics. This is the strategy that is proposed and employed within this case study.

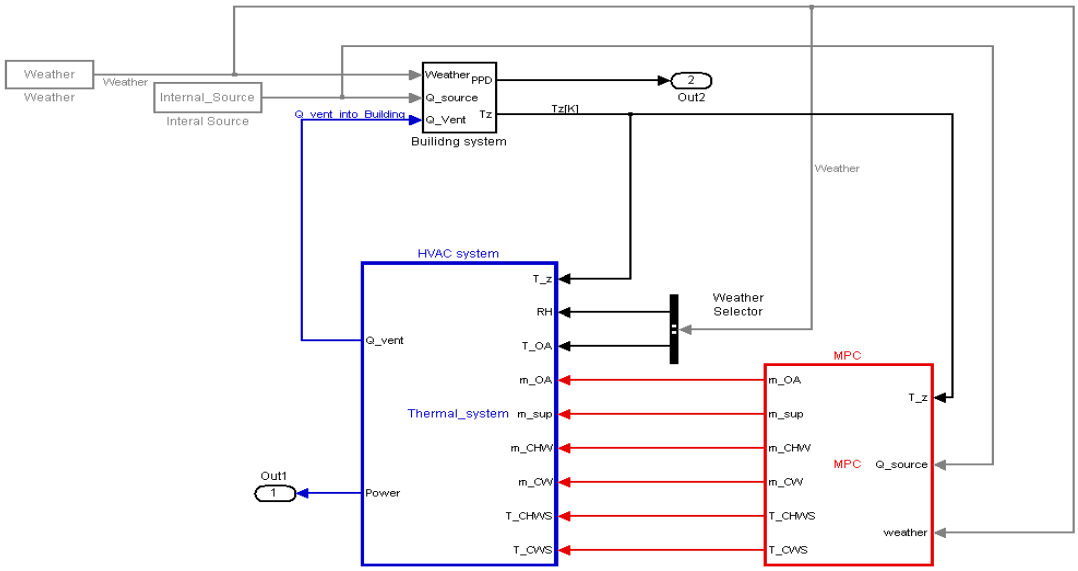

Figure 7.8. Schematic diagram for the MPC controller for this case study

The power consumption of the plant for this case study can be expressed as

$$Power = f(m_{OA}, m_{sup}, m_{CW}, m_{CHWS}, T_{CHWS}, T_{CWS}, T_{OA}, RH, T_{zone}),$$

where Q_{vent} is the mechanical ventilation [kW]; m_{OA} is a set point for outdoor air mass flow rate[kg/s]; m_{sup} is the set point for supply air mass flow rate to the zone [kg/s]; m_{CW} is the set point for condenser water mass flow rate[kg/s]; m_{CHW} is the set point for chilled water mass flow rate[kg/s]; T_{CWS} is the set point for condenser water supply temperature[C]; T_{CHWS} is the set point for chilled water supply temperature[C]; T_{zone} or T_z is the zone air temperature (setpoint) [C].

Because the input variable to the building zone is only Q_{vent}, the total power consumption, P, can be reformulated as a function of the heat extraction/addition rate in the following form,

$$Power = f(m_{OA}, m_{sup}, m_{CW}, T_{CHWS}, T_{CWS}, T_{OA}, RH, T_{zone}, Q_{vent})$$

The plant optimization problem involves finding the optimal set-points that give minimum power consumption for a given heat extraction rate, T_z, T_{OA} and RH at any time or

$$\min \; Power(m_{OA}, m_{sup}, m_{CW}, T_{CHWS}, T_{CWS}, T_{OA}, RH, T_{zone}, Q_{vent})$$

with respect to

$$\begin{bmatrix} m_{OA} \\ m_{sup} \\ m_{CHW} \\ m_{CW} \\ T_{CHWS} \\ T_{CWS} \end{bmatrix} \quad \text{such that} \quad \left\{ \begin{array}{c} A \le m_{OA} \le B \\ C \le m_{sup} \le D \\ E \le m_{CHW} \le F \\ G \le m_{CW} \le H \\ L \le T_{CHWS} \le M \\ \max(T_{CHWS}, T_{wb}) \le T_{CWS} \le N \end{array} \right\}.$$

The optimal plant solution then can be mapped in terms of the input variables according to

$$P^* = P_{min}(T_{OA}, RH, T_{zone}, Q_{vent}).$$

The bounds of A to N are specific to this HVAC system. More generally the problem can be expressed as

$$u^*(w) = \arg\min \; J(u,w) \qquad s.t.\; G(u) \le 0 \quad \& \quad J^*(w) = \min \; J(u,w)$$

$$u \in R^m, w \in R^n, \qquad J : R^m \times R^n \to R$$
$$u^* : R^n \to R^m, \qquad J^* : R^n \to R$$
$$m \,\&\, n \in Z$$

The MPC wants to find a trajectory for Q_{vent} rather than a single point value while the optimal map provides optimal plant setpoints at any time given conditions for $T_{OA}, RH, T_z, Q_{vent}$. There are several difficulties in obtaining an optimal look-up table. The objective function for HVAC plants may be non-convex and contains several nonlinear algebraic equations; it is difficult to generate proper constraints; and there may be several discrete modes of operation that cause discontinuities. In particular, the design variables must be in a feasible region in the optimization process. For example, the supply air temperature must be greater than the chilled water supply temperature by an amount dictated by the capacity of the coil and operating conditions. These types of constraints are difficult to handle without validated models for each of the components.

A global optimization algorithm with an interior barrier method was employed in this study for the plant optimization. The validity of the results were tested by considering limiting cases with known solutions, such as when the only plant power is associated with the chiller.

7.9 Cooling Plant Model

Figure 7.9 shows the MatLab implementation of the cooling plant model used to generate an optimal map for this case study.

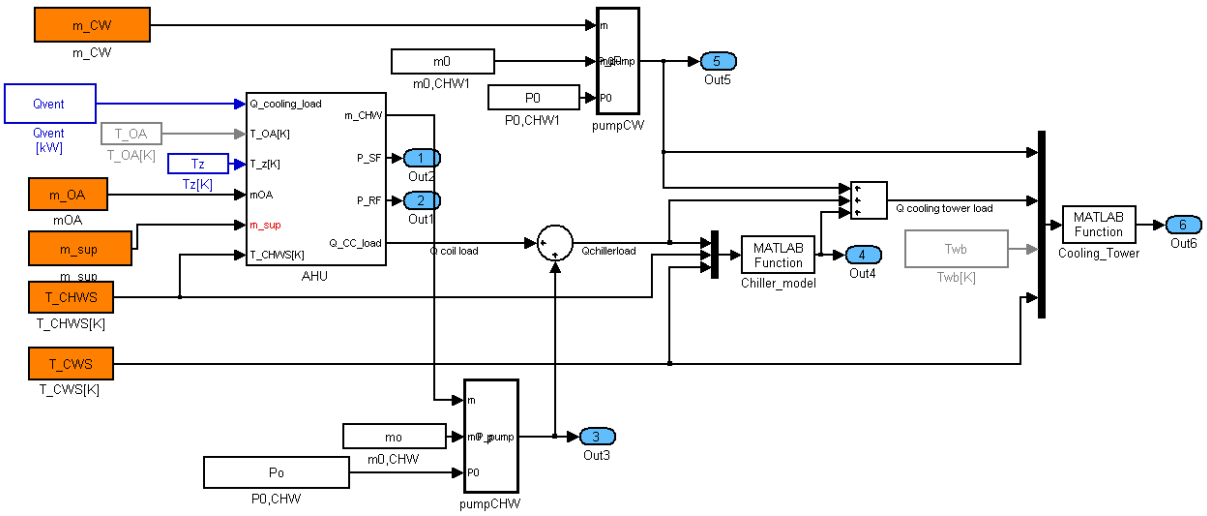

Figure 7.9. Matlab/Simulink HVAC system model to calculate total power consumption (cooling part); Orange: supervisory control variables; Blue: power consumption of fan, pumps, chiller and cooling tower

7.9.1 Pump/Fan Model, Heat Exchanger, AHU

The variable-speed cooling tower fans and pumps are modelled with a cubic relationship between power consumption and flow rate (pump and fan affinity law). For the VAV fan, the fan power is modelled as outlined in ASHRAE 90.1

$$P_{fan} = a_0 + a_1 PLR_{fan} + a_2 PLR_{fan}^2 + a_3 PLR_{fan}^3$$

For now, latent energy removal effects are neglected for the cooling coil. Also, heat gains to air ducts and pipes are neglected. The effectiveness-NTU method is used for the cooling coil to determine the limiting heat transfer rate

$$\epsilon = 1 - \exp[\frac{1}{C_r} NTU^{0.22} \{exp[-C_r NTU^{0.78}] - 1\}]$$

where C_r is the ratio of the minimum to maximum capacity rate ($C_{\min} / C_{max}$) [46]. Energy and mass balance equations are then used to determine temperatures, cooling coil load (Q_{CCL}) and chiller load (Q_{CHL}).

7.9.2 Chiller Model

The empirical model employed in EnergyPlus is used to determine chiller cooling capacity, energy efficiency, and power consumption as a function of chilled water supply temperature, condenser water supply temperature, and part-load ratio [15].

$$\text{CAPFT} = a_1 + b_1 \times T_{CHWS} + c_1 \times T_{CHWS}^2 + d_1 \times T_{CWS} + e_1 \times T_{CWS}^2 + f_1 \times T_{CHWS} \times T_{CWS}$$

$$\text{EIRFT} = a_2 + b_2 \times T_{CHWS} + c_2 \times T_{CHWS}^2 + d_2 \times T_{CWS} + e_2 \times T_{CWS}^2 + f_2 \times T_{CHWS} \times T_{CWS}$$

$$\text{EIRPLR} = a_3 + b_3 \times PLR + c_3 \times PLR^2$$

where CAPFT is maximum cooling capacity relative to capacity at a reference condition, T_{CWS} is condenser water supply temperature to the chiller, T_{CHWS} is temperature supplied by the chiller to the load, EIRFT is energy input ratio at maximum capacity (ratio of power to capacity), and ELRPLT is energy input ratio at part-load divided by the value at full load.

The power consumption of the chiller can be calculated as

$$P_{chiller} = EIRPLR \times EIRFT \times CAPFT \times P_{ref}$$

where P_{ref} is power consumption at a reference condition that corresponds to the reference cooling capacity. For this case study, a specific chiller specification from EnergyPlus was extracted and implemented. It is a centrifugal chiller with continuous inlet guide vane control of capacity. The rated capacity of the chiller is 816 kW, but it was scaled down to match the requirements for the case study. Figure 7.10 shows the effect of the input variables on power consumption for this chiller. These results illustrate that this model produces local minimums for chiller power with changing condenser and chilled water supply temperature that depend on the load. At high loads, the optimal chilled and condenser water temperatures are at their upper and lower bounds, respectively. However, at lower loads the model predicts a local minimum for high condenser water temperature that physically doesn't make sense. This illustrates a potential difficulty in determining an optimal control map for the plant.

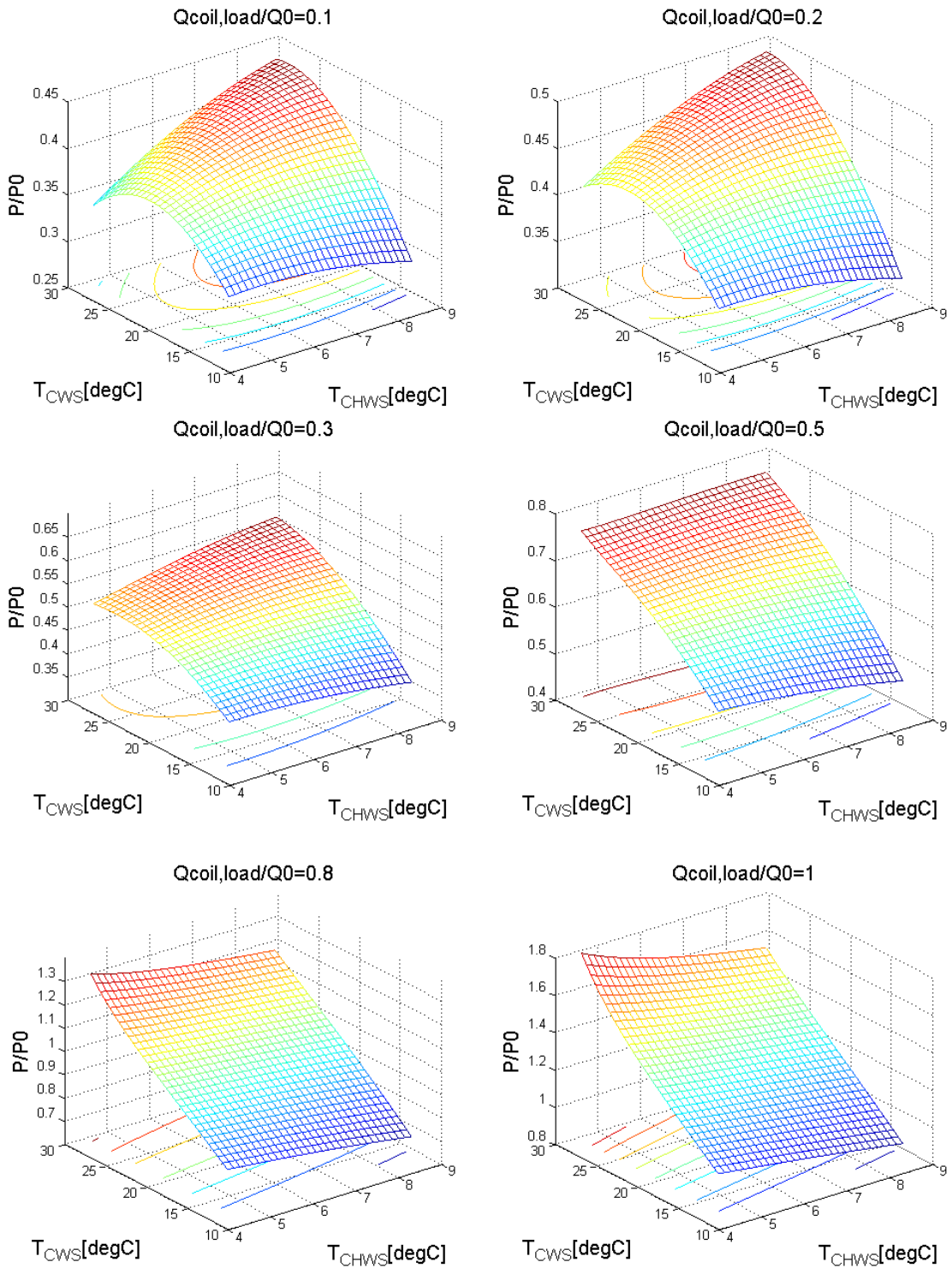

Figure 7.10. Chiller performance trends with operating conditions and load, where nominal capacity (Q0) is 816 kW and nominal COP is 8.11.

7.9.3 Cooling Tower Model

The cooling tower model was also extracted from EnergyPlus and represents a York cooling tower. The model predicts the approach to ambient wet bulb temperature (condenser water supply minus ambient wet bulb temperature) using the following empirical equation.

$$
\begin{aligned}
T_{app} = {} & C_1 + C_2 T_{wb} + C_3 T_{wb}^2 + C_4 T_{range} + C_5 T_{wb} T_{range} + C_6 T_{wb}^2 T_{range} + C_7 T_{range}^2 + \\
& C_8 T_{wb} T_{range}^2 + C_9 T_{wb}^2 T_{range}^2 + C_{10} LG_{ratio} + C_{11} T_{wb} LG_{ratio} + C_{12} T_{wb}^2 LG_{ratio} + \\
& C_{13} T_{range} LG_{ratio} + C_{14} T_{wb} T_{range} LG_{ratio} + C_{15} T_{wb}^2 T_{range} LG_{ratio} + C_{16} T_{range}^2 LG_{ratio} + \\
& C_{17} T_{wb} T_{range}^2 LG_{ratio} + C_{18} T_{wb}^2 T_{range}^2 LG_{ratio} + C_{19} LG_{ratio}^2 + C_{20} T_{wb} LG_{ratio}^2 + C_{21} T_{wb}^2 LG_{ratio}^2 + \\
& C_{22} T_{range} LG_{ratio}^2 + C_{23} T_{wb} T_{range} LG_{ratio}^2 + C_{24} T_{wb}^2 T_{range} LG_{ratio}^2 + C_{25} T_{range}^2 LG_{ratio}^2 + \\
& C_{26} T_{wb} T_{range}^2 LG_{ratio}^2 + C_{27} T_{wb}^2 Tr^2 LG_{ratio}^2
\end{aligned}
$$

where

$$LG_{ratio} = \frac{\dot{m}_{CW} / \dot{m}_{CW,o}}{\dot{m}_{air} / \dot{m}_{air,o}}.$$

and where T_{WB} is ambient wet bulb temperature, T_{range} tower range (temperature difference between condenser water return and supply), and T_{CHWS} is the tower mass flow rate of air. The nominal tower air flow rate and fan power are determined as outlined in [17]

7.10 Initial Case Study Results

The baseline state-space model was applied to the Living Laboratory zone described in section 7.8 and then model-order reduction was performed. The baseline model employed 201 states and the model order was reduced to 10 states with about a factor of four reduction in the computational requirements. Figure 7.11 shows a comparison of zone temperature variation with a PID controller in place for the baseline and reduced-order model. The zone temperature responses are very similar and lead to near identical time variations in zone loads. More detailed analyses will be performed in future work to better understand any limitations of the reduced-order model for this case study.

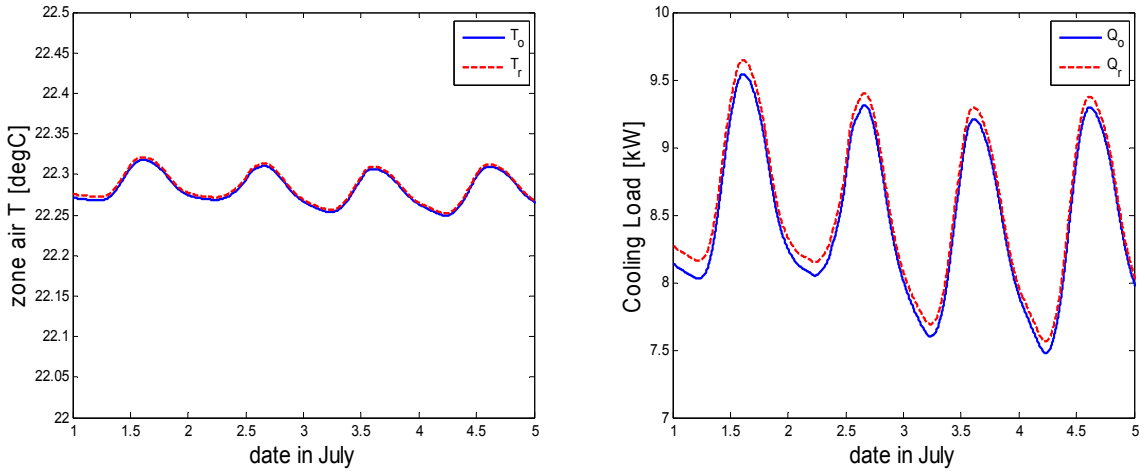

Figure 7.10. Example model comparisons between baseline state-space and reduced-order models under PID control (T_o = zone air temperature profile for baseline state-space model, T_r = zone air temperature for reduced-order model)

The cooling plant described in section 7.9 was scaled to meet the peak load requirements for the Living Laboratory zone and an optimal cooling plant model was generated which was used within the MPC formulation described in section 7.8 for a simple case study. The MPC optimization algorithm generates an optimal sequence of {u[k],u[k+1]..u[k+Np-1]} over a prediction horizon [k, k+Np] and only the first part of the sequence, u[k], is applied to the building model. For the next time k+1, the same procedure is applied with the initial guesses of the pre-calculated {u[k+1],u[k+2],.., u[k+Np-1]}. A 24-hour prediction horizon was used to capture the usage of thermal mass in the building structure and a 15-minute prediction time step was adopted.

Figure 7.11 shows sample MPC results for a day in July. The time-of-use energy charges provide incentive for the MPC to apply precooling prior to the occupied period. The optimal trajectory satisfies the constraints of PPD within 10% during occupied hours and 30% during unoccupied hours. After precooling prior to occupancy, the PPD is maintained at the upper limit of 10% to minimize energy consumption since the high energy rates are coincident with the occupied period. This level of PPD corresponds to a zone air temperature setpoint during occupancy of around 25 C for summer clothing levels. It is interesting to note that the difference between the zone air and mean radiant surface temperatures reaches a maximum at the occupied period due to precooling. Further, the mean radiant temperature is always lower than the zone air temperature during occupancy implying that energy storage in the wall surfaces is acting to reduce the load. This difference tends towards zero by the end of occupancy implying that the MPC is attempting to make full utilization of the energy storage. Another interesting point is that the optimal zone air temperature peaks at the beginning of the occupied period and decreases over time. This is a result of the use of PPD as the cost constraint. The lower mean radiant temperature at the beginning of occupancy allows use of a higher zone temperature to achieve

the same comfort level as compared with the higher mean radiant temperatures experience later in the day. Higher zone air temperature setpoints lead to energy savings because of reduced loads.

It is also interesting to note that precooling includes both mechanical and ventilation precooling because the ambient temperature is lower than the zone temperature prior to occupancy but not cool enough to provide the level of cooling needed to minimize total daily operating costs. Plant power consumption peaks near the end of occupancy because of the higher ambient temperature.

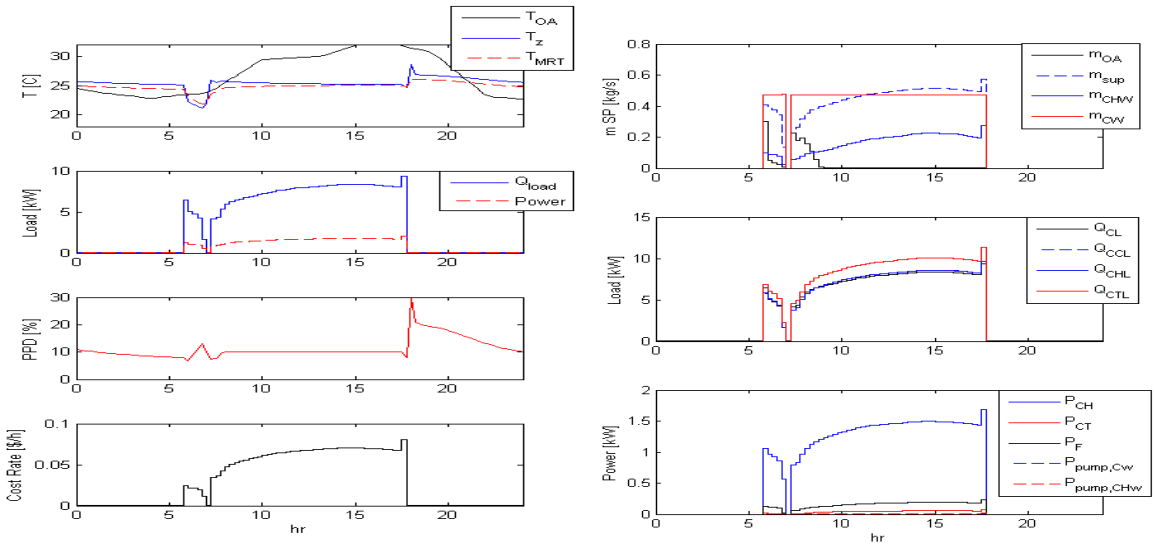

Figure 7.11 Example MPC results for July 22

These results are preliminary. Much more work is needed to evaluate the MPC in terms of benefits compared to a baseline control, robustness, and computational requirements.

7.11 References

1. J.E. Braun , "A Reducing energy costs and peak electrical demand through optimal control of building thermal mass", *ASHRAE Transactions* , 1990
2. M. Krarti1, M.J. Brandemuehl, G.P. Henze, "Evaluation of optimal control for ice storage systems", Final Project Report for ASHRAE 809-RP, 1995
3. A. Kusiak, M. Li, F. Tang, "Modeling and optimization of HVAC energy consumption", *Applied Energy*, 87, 3092-3102, 2010
4. K.F. Fong, V.L. Hanby, T.T. Chow, "HVAC system optimization for energy management by evolutionary programming", *Enegy Build*, 38(3): 220-31, 2006
5. L. Lu, W. Cai, L Xie, S. Li, Y.C. Soh, "HVAC system optimization in building section". *Energy Build*; 37(1):11-22, 2005
6. J. Casillas, O. Cordón, F. Herrera, L. Magdalena, "interpretability issues in fuzzy modeling", Vol. 128 of Studies in Fuzziness and Soft Computing, Springer, 2003

7. Y. Ma, G. Anderson, F. Borrelli, "A distributed predictive control approach to building temperature regulation", *American Control*, 2011
8. F.B. Morris, J.E.Braun, S.J.Treado, "Experimental and simulated perforamce of optimal control of building thermal storage.", *ASHRAE Transactions*, Vol.100, No.1, 1994
9. ASHRAE Fundamentals, 29.22, 1997
10. ASHRAE Handbook-Fundamental,8.8, 2005
11. V. M. Zavala, "Real-time optimization strategies for building systems", Preprint ANL/MCS-P1911-0611, 2011
12. V. M. Zavala, D. Skow, T. Celinski, and P. Dickinson, "Techno-economic evaluation of a next-generation building energy management system," Technical Memorandum ANL/MCS-TM-313, 2011
13. A. Kelman, F. Borrelli, "bilinear model predictive control of a hvac system using sequential quadratic programming", *18th IFAC World Congress*
14. S. Wang, " dynamic simulation of a building central chilling system and evaluation of emcson-line control strategies", *Building and Environment*, Vol. 33, No. 1, pp. I-20, 1998
15. M. Hydeman, K.L. Gillespie. "tools and techniques to calibrate electric chiller component models". *ASHRAE Transactions*, AC-02-9-1, 2002
16. F.P. Incropera, D.P. DeWitt , "Fundamentals of heat and mass transfer", John Wiley & Sons, Aug 3, 2001
17. Energy Plus Engineering reference Version 6.0 Documentation, October 2010

ASHRAE standard 55, p9, figure 5.2.1.1-1, 2003

8. High Fidelity Indoor Environmental Modeling

This section describes progress of Lawrence Livermore National Laboratories (LLNL) in developing high-fidelity indoor environmental modeling of the Purdue Living Laboratory for the purpose of providing detailed validation of reduced-order indoor environmental models.

The primary objective of the CFD-based effort at LLNL is to develop an open source tool that can be used to perform medium and high fidelity simulations of the airflow and heat transfer in buildings and that can be used in the development and design of reduced order models and building energy control systems. The open source tool will be based on LLNL's Cgins incompressible Navier-Stokes solver and the grid generation and CAD capabilities in the Overture object-oriented simulation framework that has been developed at LLNL.

Our work in the first year has been focused on developing enhancements to our open-source high-fidelity CFD solver Cgins so that it can be applied to building energy modeling and simulation. Cgins is a high- performance parallel program for the coupled simulation of airflow and heat transfer (solving the incompressible Navier-Stokes equations with Boussinesq approximation for heat transfer and buoyancy). The main project tasks are (1) evaluate approaches for generating grids for the interior and exterior of buildings, (2) development and specification of boundary conditions, (3) development and specification of body forcings (e.g. heat sources and sinks) (3) addition of appropriate LES turbulence models for building simulations, (4) addition of capabilities to simulate passive scalars (e.g. humidity, aerosols), (5) adding support for performing closed loop control simulations, (6) developing capabilities to construct reduced order models from solution snapshots through the use of proper orthogonal decompositions (POD) and Galerkin projection of the full order equations, (7) verification and validation of the approach.

The funding for this work began in July 2011 and thus we are at approximately the half year point of the first year's effort.

Grid Generation: Cgins uses overlapping grids to represent the geometry. This flexible approach is based on the use of local structured component grids. Grids are generated for typical building components such as desks and cabinets, HVAC inlets and outlets, etc. These component grids can then be used to build up a given room. We have been constructing a library of parameterized component grids for building geometries. The parameters define the various dimensions of the component. One of our target applications is a room in the Purdue Living Lab and we have been also developing the grids for this room.

Body forces and boundary conditions: we are adding capabilities to make it easy to specify volume forces to the equations (e.g. heat sources and sinks) along with boundary conditions that vary over surfaces (e.g. varying the temperature or heat flux on different portions of a wall or floor). To specify locally varying boundary conditions and body forces we have designed a flexible approach and user interface that allows one to specify the forced region through the

union of simpler domains (box, cylinder, sphere ...). More generally we will also allow (although this is not yet implemented) the forcing domain to be specified by a general triangulated surface; this will allow representations of complex objects in the flow (e.g. occupants in a room). Once a forcing domain has been specified, one can then define the various parameters that apply to that domain, (e.g. inflow velocity or heat flux on a boundary). In addition one can define a spatial profile for the force (e.g. parabolic profile) along with the time variation of the forcing. We have implemented a quadratic drag law that can be used to remove momentum from a given forcing region. We have also been adding some immersed boundary (IB) capabilities so that solid regions in the flow can be more easily specified without the need to build a full CFD mesh. We envision that the IB approach will allow nearly automatic generation of grids from architectural design programs and thus enable the rapid setup for medium fidelity CFD simulations (although further work is required to interface to the architectural design programs and extract the relevant geometry and material properties). We have used the IB approach as a model for a chilled beam in a suspended ceiling and compared this to a more detailed mesh-based approached.

Control systems: We are working with Virginia Tech, Purdue and UTRC to develop building control systems. The control system is usually designed using a reduced order model. The resulting controller can be evaluated by performing closed loop simulations with the full order model (i.e. the high fidelity CFD simulations). We have been adding the capabilities needed to couple a controller to the Cgins flow solver. This requires one to evaluate the output from one or more sensors (e.g. thermostats or flow meters). This sensor output is fed through the control system which then adjusts the simulation by, for example, changing the flow rate or inflow temperature on a boundary. As a first step in this process we have coupled a PID controller to the flow simulation and used this to control the temperature of the incoming flow so as to drive the average temperature of the room to a given desired value.

Reduced Order Models: A reduced order model can be developed from a set of snap-shots from a high-fidelity CFD model. These snapshots can, for example, represent the solution at different times from a time-dependent simulation. A proper orthogonal decomposition of the snapshots is used to determine a reduced order basis for the solution. This reduced order basis can be used to develop reduced order equations (through a Galerkin projection) that can be used in place of solving the full order equations. We have begun work on developing the capabilities to take the high fidelity flow simulations from Cgins and use these to construct the reduced order basis (through the computation of a singular value decomposition) and the construction of the reduced order model for the Navier-Stokes equations.

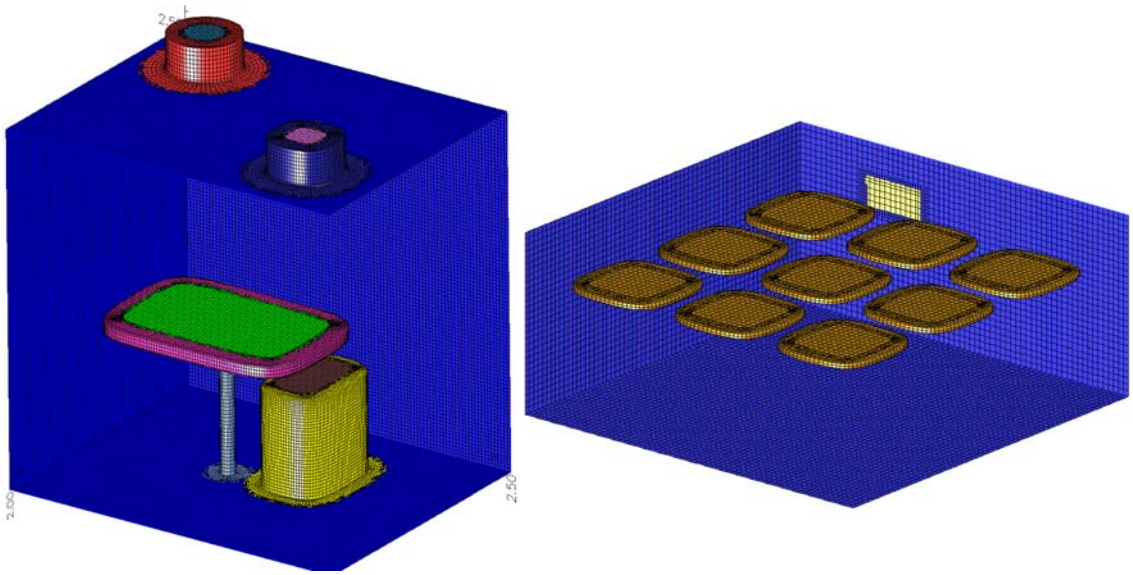

Figure 8.1. Left: overlapping component grids constructed to model features in a room. Right: overlapping grid for the Purdue Living Lab showing the suspended ceiling “clouds”.

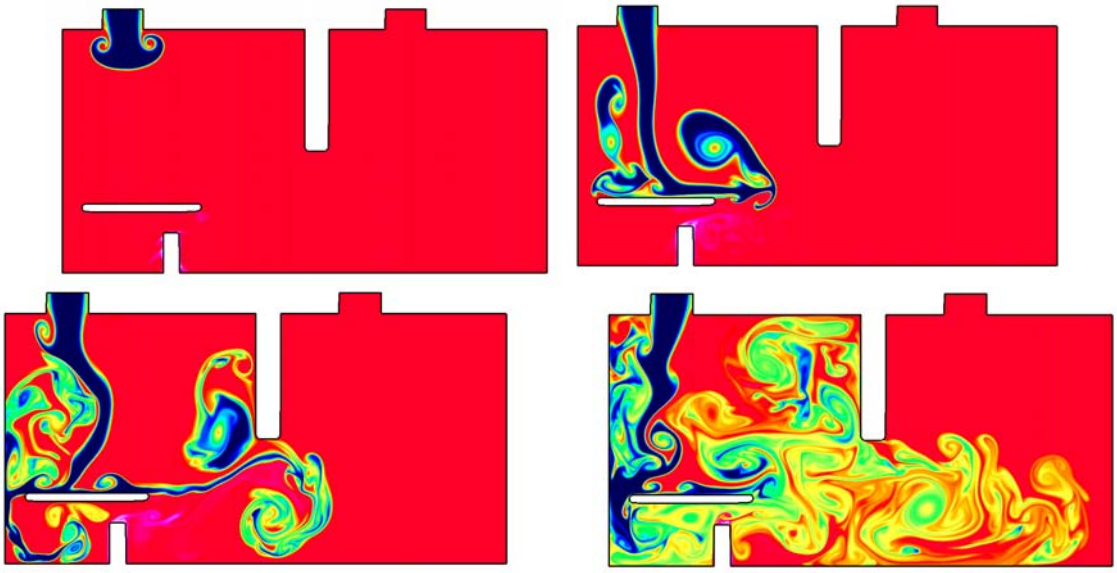

Figure 8.2. Results of a sample high-fidelity simulation from LLN:’s Cgins CFD solver: temperature of air entering a room.

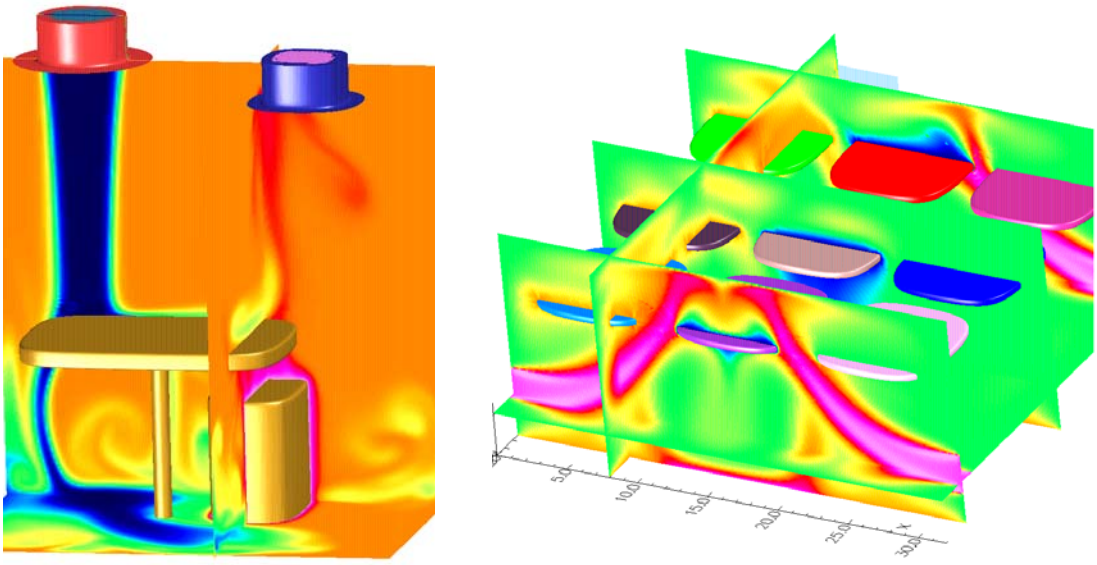

Figure 8.3. Sample flow simulations using LLNL's Cgins CFD solver. Left: temperature of the air entering a room. Right: temperature of the air flowing into the Purdue Living Lab.

9. Summary and Future Work

Significant progress was made in developing and demonstrating tools that could be used to provide a scalable and cost effective platform for generation of site-specific optimized controls for buildings. Progress in the first year has included 1) a literature review of existing tools and models that could be used as part of the envisioned control system design platform, 2) initial formulation of the MPC problem, 3) initial tools to generate reduced-order models for building envelopes from detailed physics-based models along with case study results, 4) initial tools to generate models for indoor environments using CFD along with case study results, and 5) initial case studies to illustrate issues and opportunities for MPC applied to buildings.

This collaborative effort will continue in the next year and will involve further development and application of the tools. Approaches for generating reduced-order building and indoor air models need to be generalized and further validated. Coupling of the building and indoor air models will be carried out and integrated within MPC framework for the Purdue Living Laboratories, including rooms that have radiant and air comfort delivery. Inverse modeling approaches will be investigated for both the Living Laboratories and Building 101. Finally, the benefits and implementation requirements for MPC will be evaluated for both the Purdue Living Laboratories and Building 101.